bio-techne®

ACD™
a bio-techne brand

Spatial RNA Profiling in the Nervous System with the RNAscope™ Technology

Applications of the RNAscope and BaseScope™ Assays for Neuroscience

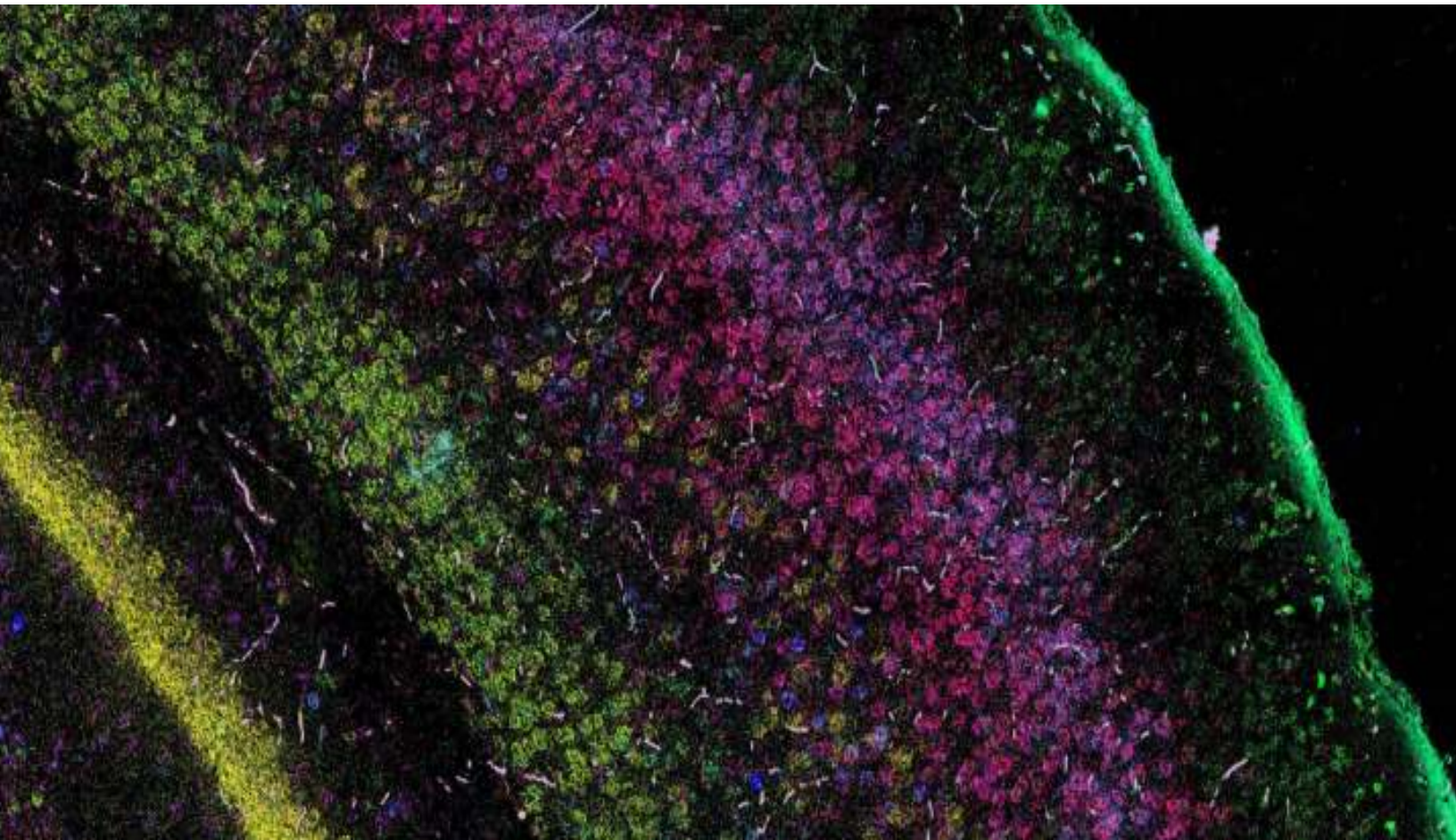

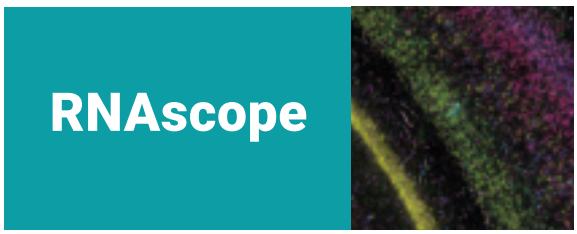

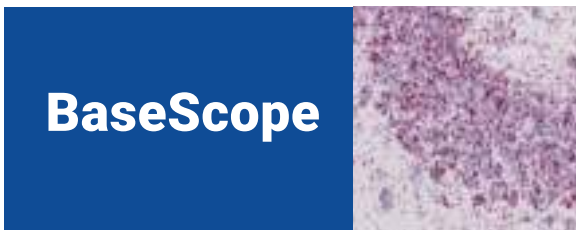

Dual ISH-IHC

Axons & Astrocyte Processes

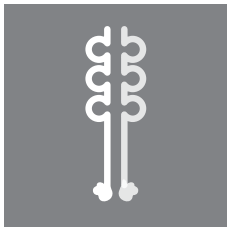

Soluble Factors

Post Mortem Brains

Whole Mount Samples

GPCR

Ion Channels

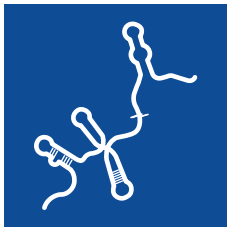

LncRNA

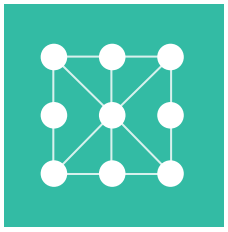

Neuronal Activity

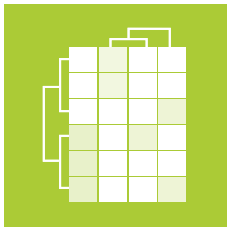

RNAseq Validation

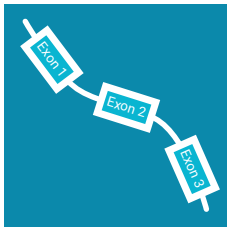

Splice Variants

Get Started

Validate

Optimize

Troubleshoot

Analyze

Explore neuroscience with RNAscope and BaseScope

Table of Contents

Introduction

The nervous system is one of the most complex tissues composed of numerous cell types and subtypes organized with delicate topological characteristics, presenting unique challenges to traditional gene expression analysis techniques. Interrogation of the complex nervous system, especially the brain, requires a highly sensitive, specific, and multiplexed spatial approach with single-cell resolution.

The RNAscope *in situ* hybridization (ISH) technology provides a powerful method to detect gene expression within the spatial and morphological tissue context. The proprietary "double Z" probe design in combination with the advanced signal amplification enables highly specific and sensitive detection of the target RNA with each dot visualizing a single RNA transcript[1]. This robust signal-to-noise technology allows for the detection of gene transcripts at the single molecule level with single-cell resolution and can further expand our understanding of gene expression in cell lines and tissues samples. Furthermore, the multiplexing capabilities of the RNAscope assays, with the power to spatially map up to 12 targets simultaneously, enables thorough characterization of cell populations within the nervous system. In summary, the RNAscope technology allows the visualization and quantification of virtually any gene from any genome in any tissue with unprecedented specificity and sensitivity.

With more than 2,500 publications to date* and 1/3 of them in the field of neuroscience, the RNAscope technology has become a key method for detecting gene expression within the nervous sytem. In this book, we will highlight the use of the RNAscope technology in the neuroscience field with several examples from studies performed at ACD as well as recent peer-reviewed publications showing how researchers have taken advantage of the RNAscope technology to complement their neuroscience research with spatial genomics.

* As of September 2019.

RNAscope and BaseScope Assays

The RNAscope and BaseScope assays are based on the proprietary RNAscope ISH technology, enabling multiplexed spatial analysis and single RNA molecule detection with high sensitivity and specificity and at single-cell resolution.

RNAscope Assay

The innovative RNAscope assay was launched in 2011 and marks the foundation of the ACD product portfolio. Its signature "double Z" probe design allows for the spatial interrogation of mRNA and long non-coding RNA (lncRNA) targets longer than 300 nucleotides in any tissue and any species.

BaseScope Assay

The BaseScope assay is a recent addition to the ACD product portfolio, launched in early 2016. Using the same innovative technology and proprietary probe design as employed by the RNAscope assay, the BaseScope assay has been developed to spatially map RNA molecules that have previously been unable to be detected in the tissue context. This powerful ISH assay enables the specific detection of exon junctions, splice variants, highly homologous sequences, short targets (~50 to 300 nucleotides), and point mutations, all with single molecule detection sensitivity at single cell resolution in a broad range of tissues, samples and species.

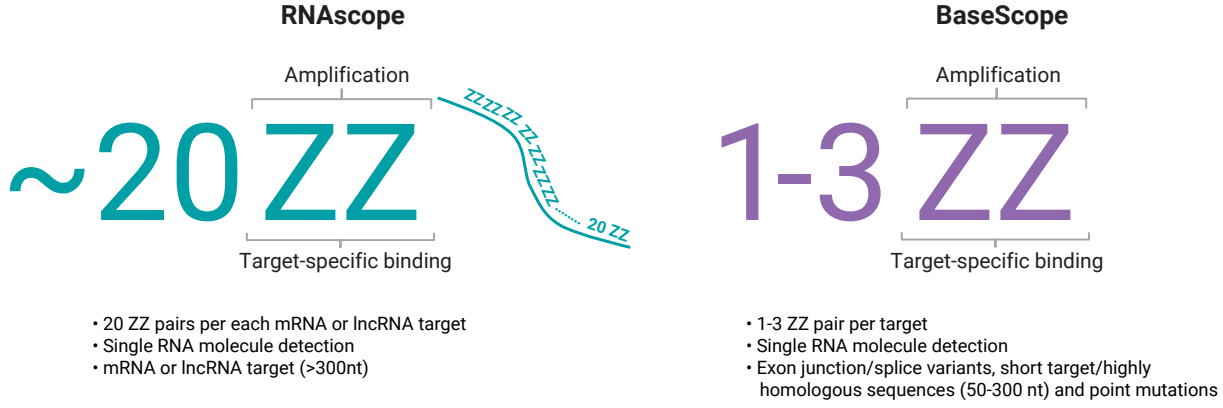

FIGURE 1. Comparison of the RNAscope and BaseScope assays.

Benefits of the RNAscope Technology

- **High sensitivity:** The serial signal amplification design increases sensitivity such that a single RNA molecule can be detected.
- **High specificity:** Proprietary probe design ensures target-specific binding while the double Z probe design prevents signal amplification of non-specific hybridization.
- **Morphological context:** Spatial resolution of gene expression in the complex tissue environment allows spatial mapping.
- **Single-cell resolution:** High sensitivity combined with morphological context results in single-molecule detection at single-cell resolution and allows for quantification.
- **Universal:** Works for virtually ANY gene from ANY species in ANY tissue.
- **Multiplexing:** Ability to detect up to 12 targets simultaneously in the tissue enables thorough characterization of cell populations.

	RNAscope Assay	RNAscope HiPlex Assay	BaseScope Assay
Number of ZZ Pair per target	• Standard probe design is 20 ZZ probes (minimum of 6 ZZ probes)	• Standard probe design is 20 ZZ probes (minimum of 6 ZZ probes)	• 1 to 3 ZZ probes based on the application
Target	• mRNA >300 bases • lncRNA >300 bases	• mRNA >300 bases • lncRNA >300 bases	• Exon junctions/ splice variants • RNA targets between 50 to 300 nucleotides • Validated point mutations
Application	• lncRNA and mRNA >300 bases	• lncRNA and mRNA >300 bases	• Exon junctions/splice variants, circular RNA, gene fusion, gene knockout • Short/highly homologous sequences, TCRs and CDR sequence for T cell clones, pre-miRNA, gene editing/CRISPR, CAR-T cell validation and detection • Point mutation, short InDel, homologues
Multiplex capability	Single to up to 4-plex	8 to 12-plex	Single to duplex
Detection	Chromogenic or fluorescent	Fluorescent	Chromogenic
Sample type	FFPE cells and tissues Fresh frozen tissues Fixed frozen tissues Cultured cells Whole mount	Fresh frozen tissues Fixed frozen tissues	FFPE cells and tissues Fresh frozen tissues Fixed frozen tissues Cultured cells
Pretreatment kit	Reagent Kit includes Universal Pretreatment Kit	Reagent Kit includes Universal Pretreatment Kit	Reagent Kit includes Universal Pretreatment Kit
Reagent kit	RNAscope Kit*	HiPlex Kit*	BaseScope Kit*
Probe type	RNAscope probe*	HiPlex probe*	BaseScope probe*
Automation capability	Available on Leica Bond Rx and Ventana Discovery ULTRA	—	Single-plex available on Leica Bond Rx and Ventana Discovery ULTRA

*RNAscope, HiPlex and BaseScope assay products components cannot be interchanged.

TABLE 1. Comparison of the product offerings for the RNAscope and BaseScope assays.

RNAscope and BaseScope Product Portfolio

The RNAscope and BaseScope assays can be performed manually or on fully automated staining systems, including the Discovery Ultra Automated IHC/ISH slide staining systems from Roche Tissue Diagnostics and Leica Biosystems' BOND RX Research Advanced Staining System.

ACD also offers Pharma Assay Services to make this technology available for customers preferring to outsource tissue-based projects.

		Chromogenic Single-plex Brown	Chromogenic Single-plex Red	Chromogenic Duplex	Multiplex Fluorescent	Hi-Plex Up to 12-plex
RNAscope Assay	Manual assays	●	●	●	●	●
	Automated on Leica BOND RX System	●	●	●	●	
	Automated on DISCOVERY ULTRA automated tissue staining systems by Roche Tissue Diagnostics	●	●	●	●	
BaseScope Assay	Manual assays		●	●		
	Automated on Leica BOND RX System		●			
	Automated on DISCOVERY ULTRA automated tissue staining systems by Roche Tissue Diagnostics		●			
Pharma Assay Services	Manual assays	●	●	●	●	
	Automated on Leica BOND RX System	●	●	●	●	
	Automated on DISCOVERY ULTRA automated tissue staining systems by Roche Tissue Diagnostics	●	●	●	●	
	Whole slide high resolution (40x) imaging	●	●	●	●	
	Visual semi-quantitative scoring or quantitative digital image analysis	●	●	●	●	

TABLE 2. Overview of the RNAscope and BaseScope product portfolio.

Principle and Features of the RNAscope Technology

Innovative solution for single RNA molecule detection in tissues with high signal and low background

RNAscope probe design

In order to substantially improve the signal-to-noise ratio that hinders traditional RNA ISH, the RNAscope technology employs a probe design strategy much akin to fluorescence resonance energy transfer (FRET), in which two independent probes (referred to as "double Z" probes) must hybridize to the target sequence in tandem for signal amplification to occur. As it is highly unlikely that two independent probes will hybridize to a non-specific target right next to each other, this design concept ensures selective amplification of target-specific signals.

For each target RNA species, ~20 double Z target probe pairs targeting a region of ~1,000 nucleotides are designed to specifically hybridize to the target molecule, but not to non-targeted molecules.

Each target Z probe contains three elements (Figure 2):

1. The lower region of the Z is an 18- to 25-base region that is complementary to the target RNA. This sequence is selected for target specific hybridization and uniform hybridization properties.

2. A spacer sequence that links the two components of the probe.

3. The upper region of the Z is a 14-base tail sequence.

The two tails from a double Z probe pair form a 28-base binding site for the pre-amplifier.

Subsequently, signal amplification is achieved by a cascade of hybridization events.

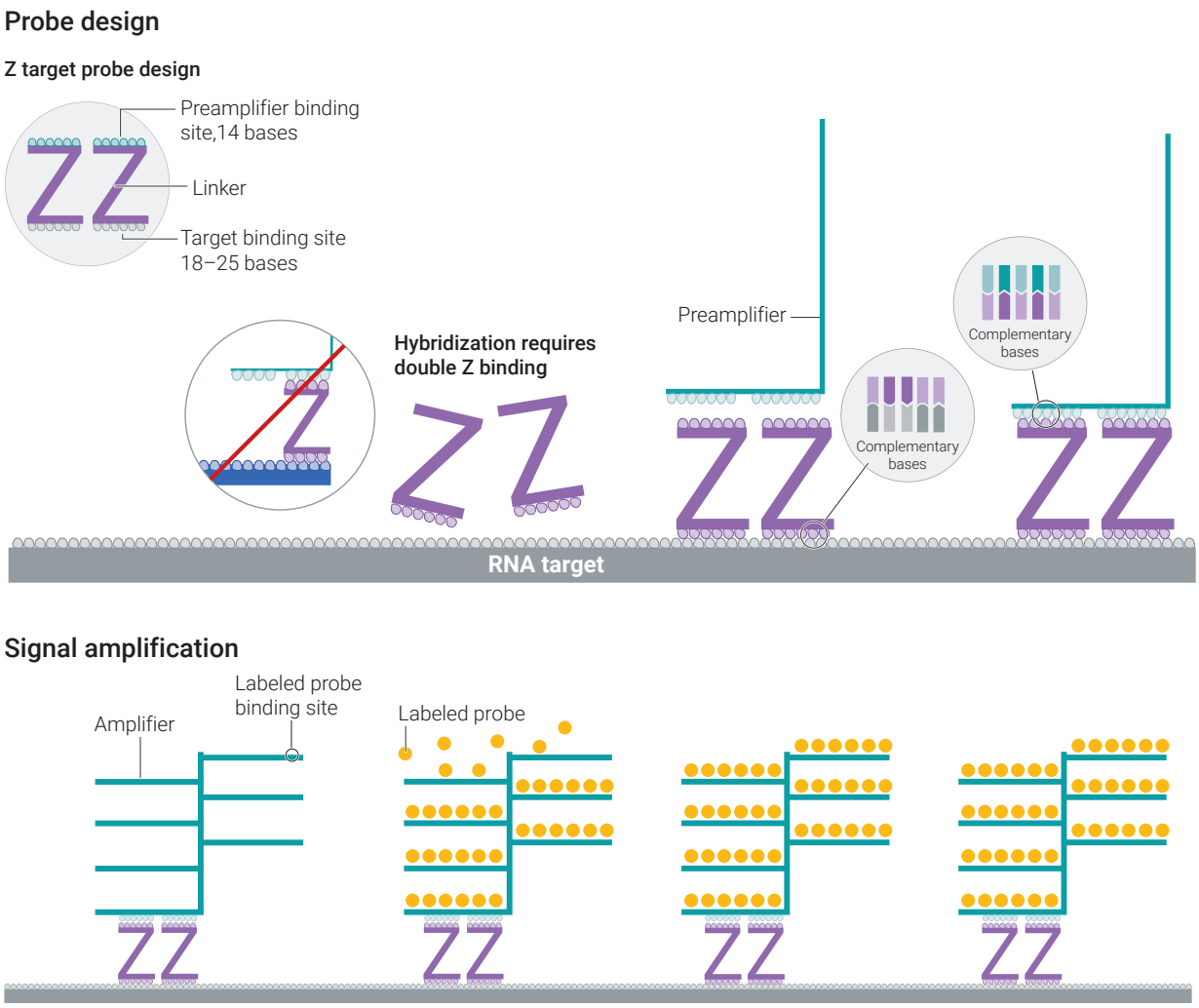

FIGURE 2. RNAscope probe design and signal amplification principles.

Taken together, the probe design coupled with the amplification strategy ensures low background with high sensitivity, resulting in a high signal-to-noise ratio.

Using the proprietary ACD RNAscope Probe Design algorithm, ACD designs double-Z oligonucleotide probe pools that hybridize to a specific RNA target of interest. ACD can design probe pools for virtually ***any*** gene in ***any*** genome for interrogation in ***any*** tissue. The probe pools consist of proprietary oligonucleotides designed for detecting specific RNA sequences.

Researchers can select from a growing catalogue of over 20,000 target probes for mRNA and lncRNA. The RNAscope and BaseScope probes span a variety of species including human, mouse, rat, dog, cow, zebrafish, rabbit, pig, chicken, monkeys, viral species, and many others.

If catalogue probes are not available for a gene of interest, ACD can create new probes within two weeks using public or proprietary sequences. Probes can be designed for use with any of our RNAscope or BaseScope Reagent Kits.

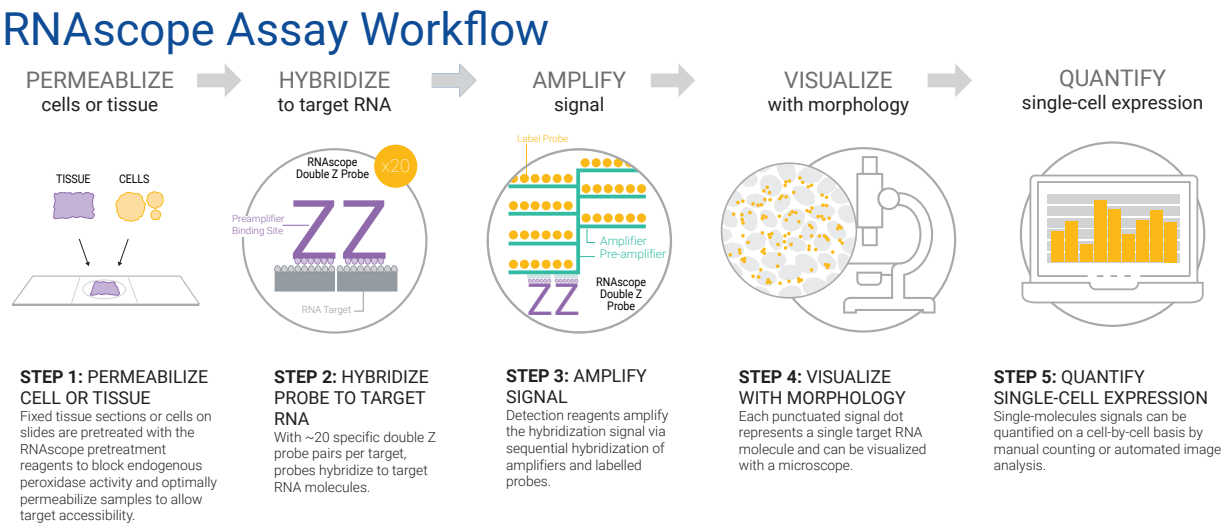

FIGURE 3. The RNAscope assay workflow and description of critical steps of the assay.

STEP 1: Pretreatment of samples

In order to perform the RNAscope assay, samples first need to be optimally prepared and pre-treated with the RNAscope Pretreatment Reagents for target accessibility.

Sample preparation and pretreatment include the following steps:

- Fixation of cells or tissues if needed (fresh-frozen, cultured cells)
- Deparaffinization if needed (FFPE)
- Pretreatment of samples with Hydrogen Peroxide, Target Retrieval and Protease

RNAscope 2.5 Pretreatment Reagents provide improved accessibility to target RNA, reducing the time and effort in assay optimization. The pretreatment reagents allow the RNAscope probes to access the target RNA, breaking cross links that occur during fixation and permeabilizing cells to allow target accessibility.

STEP 2: Hybridization of the RNAscope Target Probes to the target RNA

A hybridization-based signal amplification system with a unique probe design provides simultaneous signal amplification together with background suppression. Probes designed and provided by ACD are hybridized to the target RNA.

STEP 3: RNAscope signal amplification

After probe hybridization, a cascade of hybridization events occurs, to form the signal amplification system. These serial hybridization events result in the hybridization of thousands of labeled probes per RNA target:

1. Double Z target probes hybridize to the RNA target (~1kb)
2. Pre-amplifiers hybridize to the 28-base binding site formed by each double Z probe
3. Amplifiers are then binding to the multiple binding sites on each preamplifier.
4. Labeled probes, containing a fluorescent molecule or chromogenic enzyme, bind to the numerous binding sites on each amplifier.

STEP 4: Visualizing the RNAscope signal

The last step of the signal amplification, the labeled probes, contain either an enzyme or a fluorophore generating one punctate dot per RNA target. While most RNAscope probes contain ~20 Z probe pairs, hybridization of only three Z probe pairs is enough to obtain a detectable signal by a standard microscope.

STEP 5: Quantifying the RNAscope signal

The assay provides visualization of each individual RNA molecule as a punctate dot under a standard bright-field microscope or fluorescent microscope. These dots can be quantified by counting the number of signal dots in individual cells, either manually or by using image analysis tools.

Applications of the RNAscope Technology in Neuroscience

Identification, Characterization, and (Co-)Localization of mRNA and lncRNA in the Nervous System

The RNAscope assay can be used to detect up to 12 targets simultaneously and visualize co-expression or co-localization of specific transcripts in microglia, astrocytes and neuronal cells. In Figure 4, RNAscope probes targeting commonly used cell type markers have been used to distinguish microglia, astrocytes and neurons in normal mouse brain tissue samples.

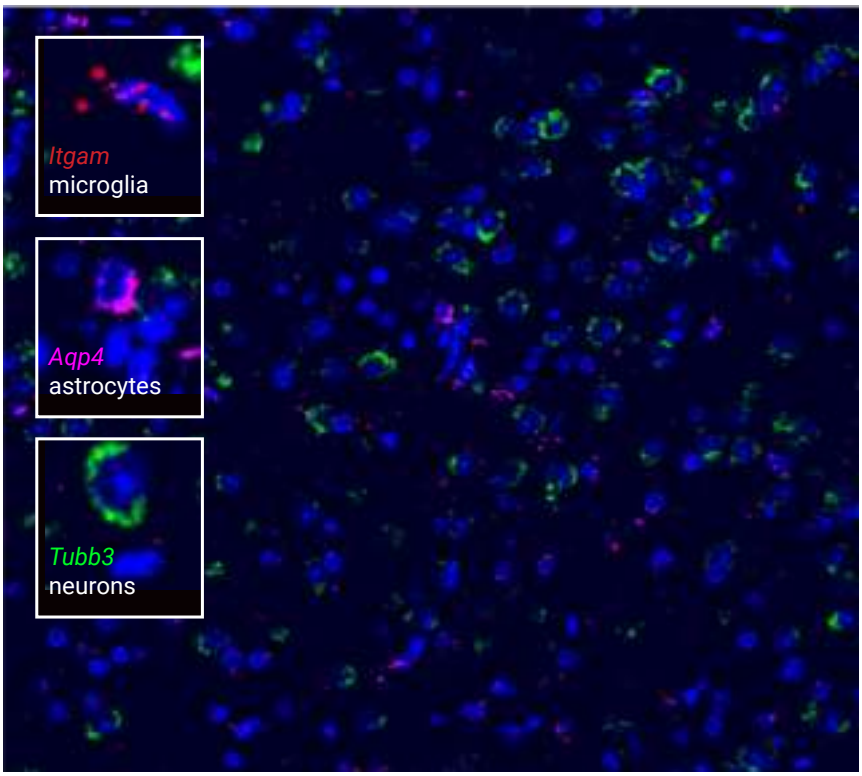

FIGURE 4. Identification of microglia, astrocytes and neurons with RNAscope probes for ***Itgam*** (red), ***Aqp4*** (magenta) and ***Tubb3*** (green) using the RNAscope Multiplex Fluorescent v2 assay on FFPE mouse brain sample. Pictures at 20X magnification. Cells are counterstained with DAPI. Panels A, B and C show higher magnification of single channels.

Further information about the applications of the RNAscope and BaseScope assays in Neuroscience:
acdbio.com/science/applications/research-areas/neuroscience

The different cell types from the nervous system can be accurately detected and visualized using the RNAscope technology. Commonly used cell types markers can be found in the table below:

Cell Type	Markers*
Neuroepithelial cells	*Nestin (Nes), Sox2, Notch1, Hes1, Hes3, E-cadherin (Cdh1), Occludin (Ocl)*
Radial glia	*Vimentin (Vim) , Nestin (Nes), Pax6, Hes1, Hes5, Gfap, Glast (Slc1a3), Blbp (Fabp7), Tnc, N-cadherin (Cdh2), Sox2*
Intermediate progenitors	*Tbr2 (Eoms), Mash1 (Ascl1)*
Immature neurons	*Doublecortin (Dcx), ß III tubulin (Tubb3), NeuroD1, Tbr1, Stathmin 1 (Stmn)*
Oligodendrocyte precursor cells	*Pdgfr alpha (Pdgfra), Ng2 (Cspg4)*
Mature oligodendrocytes	*Olig1, Olig2, Olig3, Mbp, Osp (Spp1), Mog, Sox10*
Schwann cells	*Mpz, Ncam, Gap43, S100*
Astrocytes	*Gfap, Eaat1 (Slc1a3), Eaat2 (Slc1a2), Glutamine synthetase (Glul), S100-beta (S100b), Aldh1l1*
Microglia	*Cd11b, Cd45, Iba1 (Aif1), F4/80 (Emr1), Cd68, Cd40*
Mature neurons	*NeuN (RbFox3), Map2, 160kDa neurofilament medium (Nefm), 200kDA neurofilament heavy (Nefh), Synaptophysin (Syn), Psd95*
Glutamatergic neurons	*Vglut1 (Slc17a7), Vglut2 (Slc17a6), Nmdar1 (Grin1), Nmdar2b (Grin2b), Glutaminase (Gls), Glutamine synthetase (Glul)*
GABAergic neurons	*Gaba Transporter 1 (Slc6a1), Gaba Receptor 1 (Gabra1), Gaba Receptor 2 (Gabra2), Gad 65 (Gad2), Gas67 (Gad1)*
Dopaminergic neurons	*Tyrosine Hydroxylase (Th), Dopamine Transporter (Chat), FoxA2, Girk2 (Kcnj6), Nurr1 (Nr4a2), Lmx1b*
Serotonergic neurons	*Tryptophan Hydroxylase (Tph), Serotonin Transporter (Slc6a4), Pet1*
Cholinergic neurons	*Choline Acetyltransferase (Chat), Vesicular Acetylcholine Transporter (Slc18a3), Acetylcholinesterase (Ache)*

* Cell markers may not have been tested and confirmed internally by ACD; recommendations may be based on literature searches and protein detection by IHC therefore RNA levels may vary from protein levels

Different neuronal cell sub-types can also be accurately detected and visualized using the RNAscope technology (Figure 5 and Figure 6). For example, the striatum harbours two distinct neuronal populations that are involved in action selection. These medium spiny neurons either express Dopamine Receptor D1 (*Drd1*) — the striatonigral pathway — or Dopamine Receptor D2 (*Drd2*) — the striatopallidal pathway.

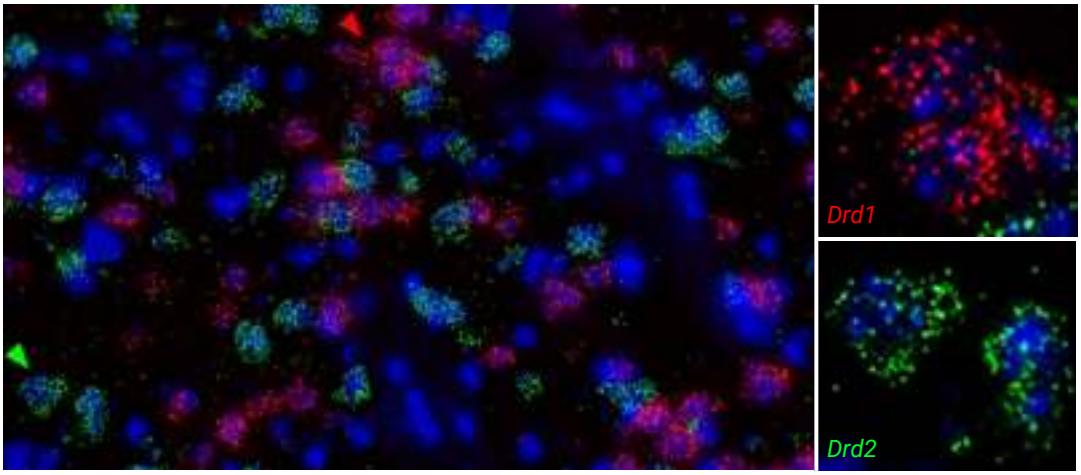

FIGURE 5. Detection of two distinct striatal neuronal populations expressing either Dopamine Receptor D1 (*Drd1*, red) or Dopamine Receptor D2 (*Drd2*, green) using the RNAscope Multiplex Fluorescent assay on Fresh Frozen tissue samples. Areas indicated by green and red arrows are shown as higher magnification images in the right panels. Cells are counterstained with DAPI.

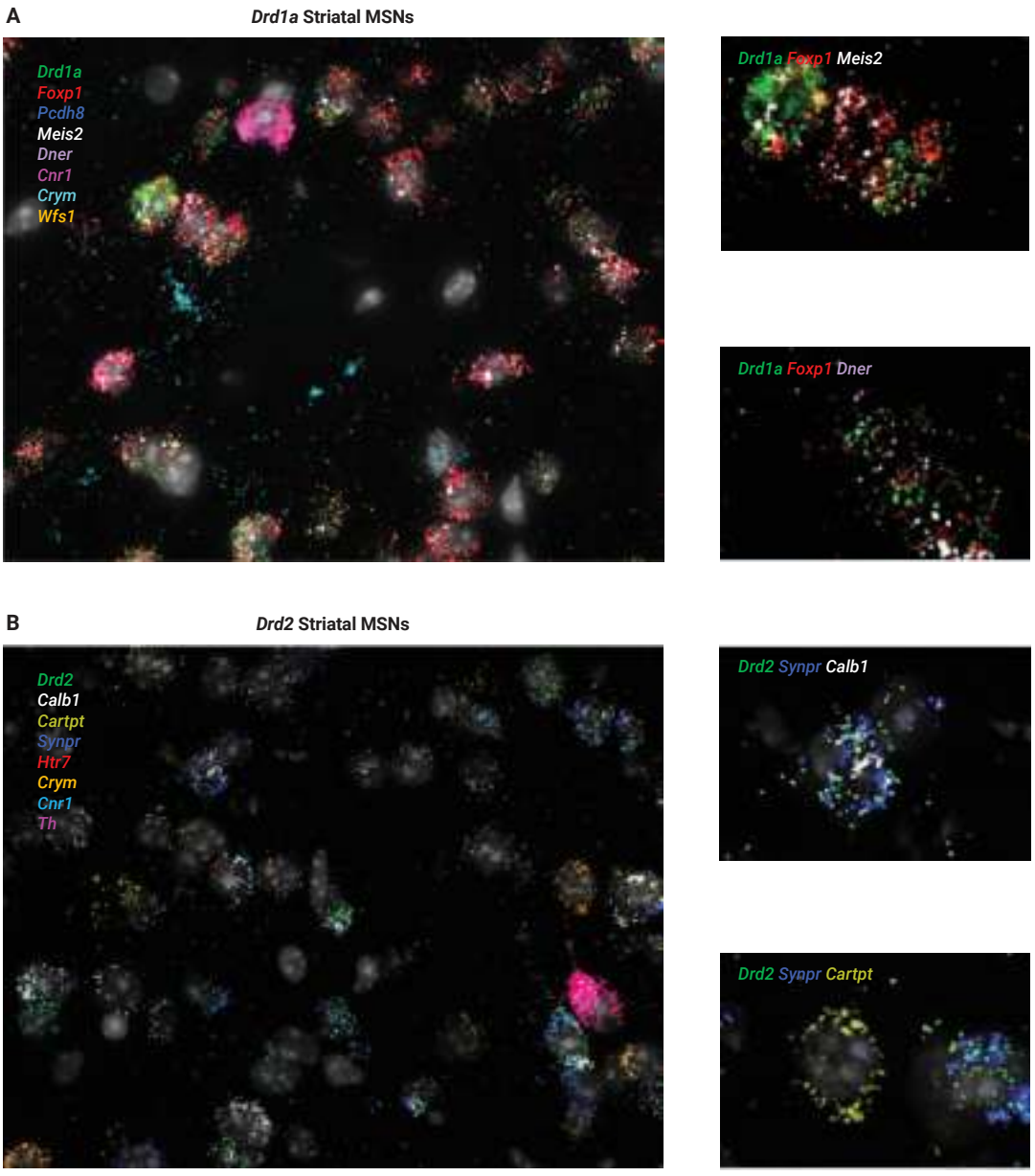

FIGURE 6. Simultaneous visualization and characterization of D1 and D2 subtypes in the mouse striatum with the RNAscope HiPlex assay. The D1 subtypes are characterized by *Drd1a*, *Foxp1*, *Pcdh8*, *Meis2*, *Dner*, *Cnr1*, *Crym*, and *Wfs1* (A), whereas the D2 subtypes are characterized by *Drd2*, *Calb1*, *Cartpt*, *Synpr*, *Htr7*, *Crym*, *Cnr1*, and *Th* (B). Insets show cells expressing markers indicative of the major D1 (A) and D2 (B) subtypes.

Related publications

Below are a few examples of recent peer-reviewed publications illustrating how researchers have taken advantage of the RNAscope technology to complement their neuroscience research and combine cell type-specific markers with their genes of interest to spatially map their cell populations.

Perineuronal Nets Suppress Plasticity of Excitatory Synapses on CA2 Pyramidal Neurons[2]

Reported by Carstens et al., J Neurosci, 2016

In their study of perineuronal nets in hippocampal CA2 neurons, Carstens *et al.* used the RNAscope assay (Figure 7) to demonstrate the co-localization of *Aggrecan* mRNA, a perineuronal net component; and *Pcp4* mRNA, a marker of hippocampal CA2 neurons.

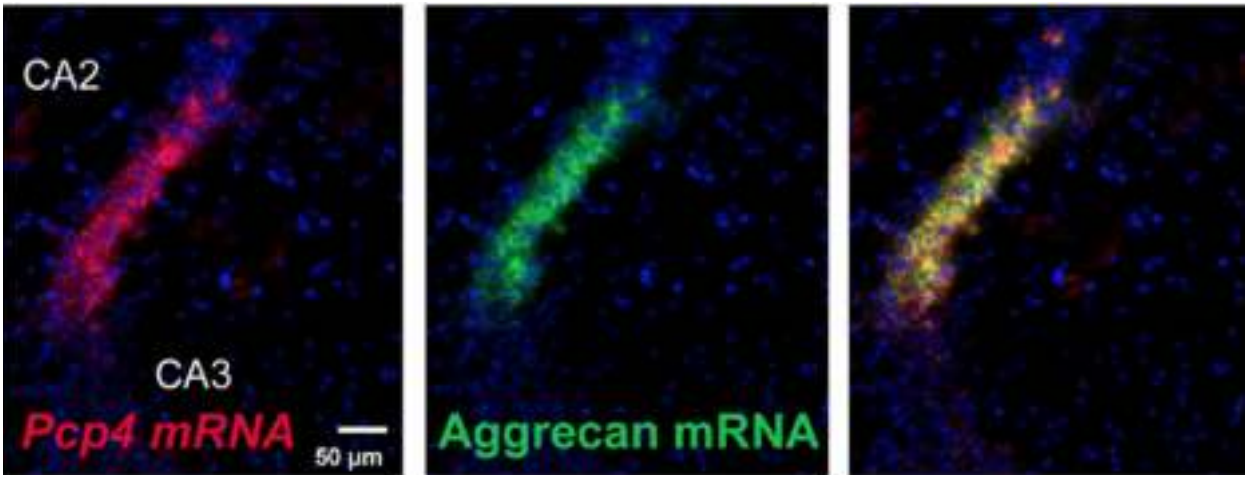

FIGURE 7. RNAscope Multiplex Fluorescent Assay shows that *Aggrecan* mRNA (green) and *Pcp4* mRNA (red), a marker of the CA2 hippocampal region, colocalize to the CA2 pyramidal cell layer. Images from Carstens *et al.*, *J Neurosci*, 2016.

Differential maturation of vesicular glutamate and GABA transporter expression in the mouse auditory forebrain during the first weeks of hearing[3]

Reported by Hackett et al., Brain Structure Function, 2016

Vesicular transporters are packaging neurotransmitters into synaptic vesicles and therefore play important roles in the release machinery of the central nervous system. Among numerous vesicular transporters, Hackett *et al.* have studied the expression of glutamate (*Vglut1*, *Vglut2,* and *Vglut3*) and glycine (*Vgat*) transporters in the primary auditory cortex (A1) and medial geniculate body (MGB) of developing mice. To track the changes in transporter expression during development, they used RNA sequencing, immunohistochemistry (IHC) and ISH using the RNAscope Fluorescent Multiplex Assay (Figure 8 and Figure 9). The study from Hackett *et al.* shows the powerful impact of the RNAscope assay on the identification of target genes from the sequencing data by providing a detailed evaluation of the co-expression and co-localization of several genes in intact tissue sections, where natural anatomical features are preserved.

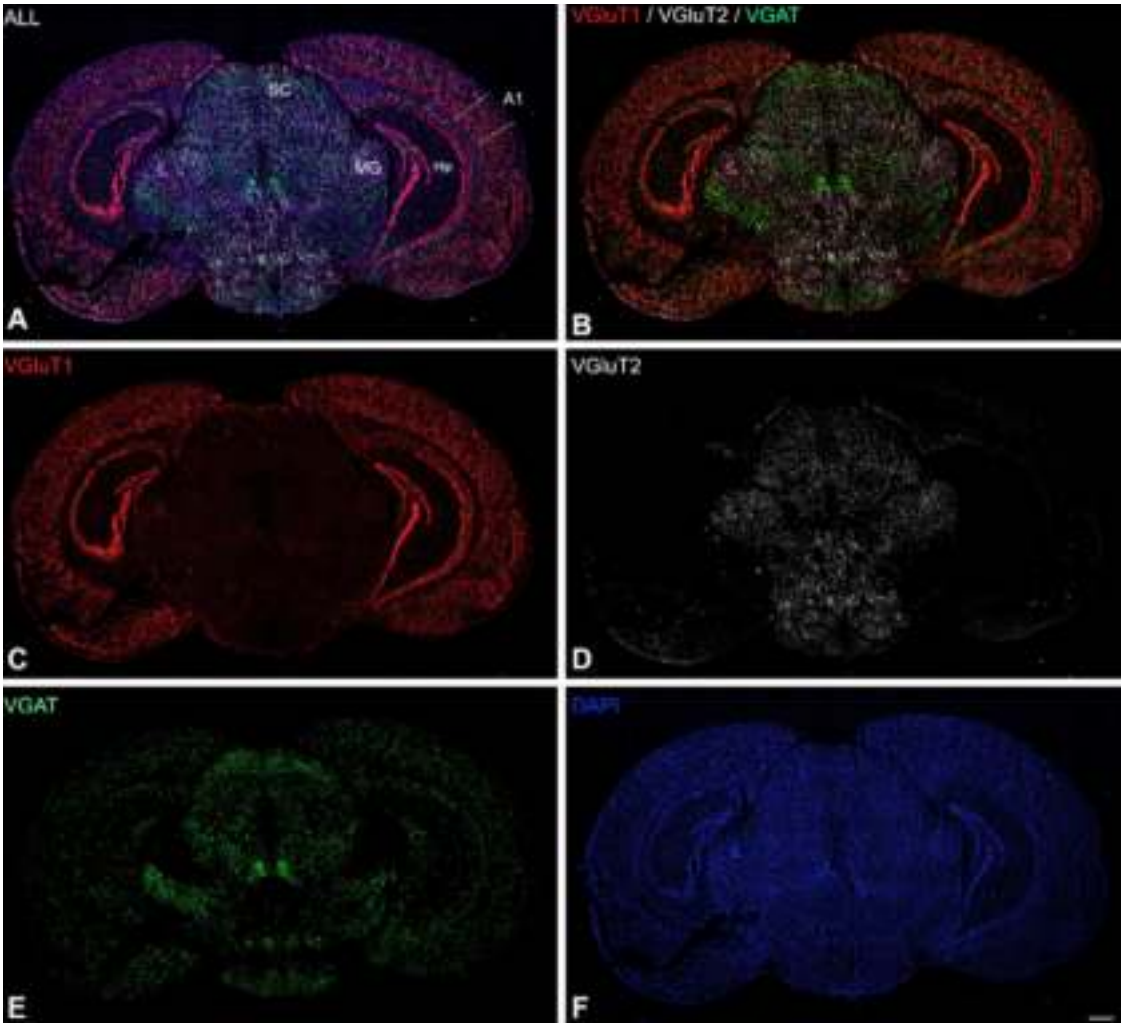

FIGURE 8. A. Multiplex staining of *Vgat*, *Vglut1* and *Vglut2* mRNA, counterstained by DAPI in fresh frozen coronal sections of adult mouse at the level of A1 and MGB using the RNAscope Multiplex Fluorescent assay. B–F, Single channel expression for *Vglut1* (C), *Vglut2* (D), *Vgat* (E), *DAPI* (F), and merged *Vglut1*/*Vglut2*/*Vgat* (B). Images from Hackett *et al.*, *Brain Structure Function*, 2016.

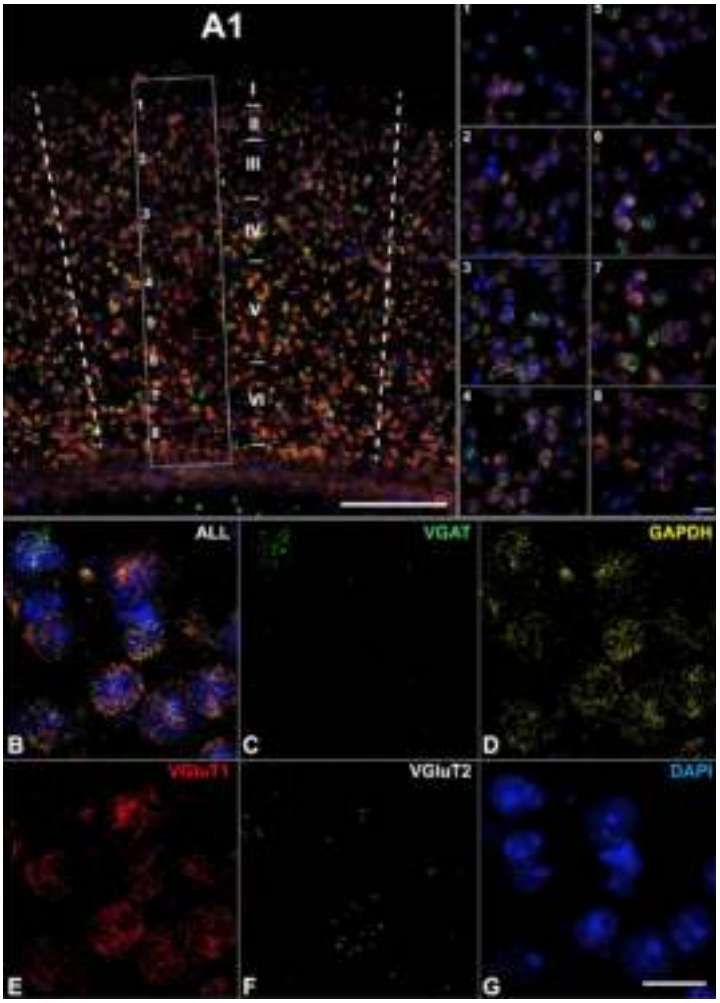

FIGURE 9. Quadruple staining of *Vgat, Gapdh, Vglut1* and *Vglut2* mRNA, counterstained by DAPI in fresh frozen coronal sections of adult mouse centered on A1 using the RNAscope Multiplex Fluorescent assay. Image montage obtained at 40x magnification showing combined expression for *Vgat, Gapdh*, *Vglut1* and *Vglut2* mRNA, counterstained with DAPI. Subpanels 1–8 show 100X magnification image stacks taken at sites in different layers of (A1). B-G. Higher resolution examples of transcript labelling from subpanel 4 shown separately for each gene. Images from Hackett *et al.*, *Brain Structure Function*, 2016.

Identification of a Brainstem Circuit Controlling Feeding[4]

Reported by Nectow et al., Cell, 2017

In mammals, energy balance and food intake are tightly regulated by neurons in several brain areas. Nectow *et al.* have expanded the view beyond the hypothalamus to two molecularly and anatomically distinct cell types within the dorsal raphe nucleus (DRN), characterized by the expression of *Vgat* and *Vglut3*. The RNAscope Multiplex Fluorescent assay demonstrated the colocalization of cell type-specific markers (*Vgat*, *Vglut3*) and receptors (*Mc4r, Htr1a*, *Npy2r*) and established the expression of each of these receptors in DRN^{Vgat} or DRN^{Vglut3} neurons (Figure 10).

By studying these cell types in normal and obese mice, the authors identified a possible pharmacological approach that could modulate food intake, body weight and locomotor activity.

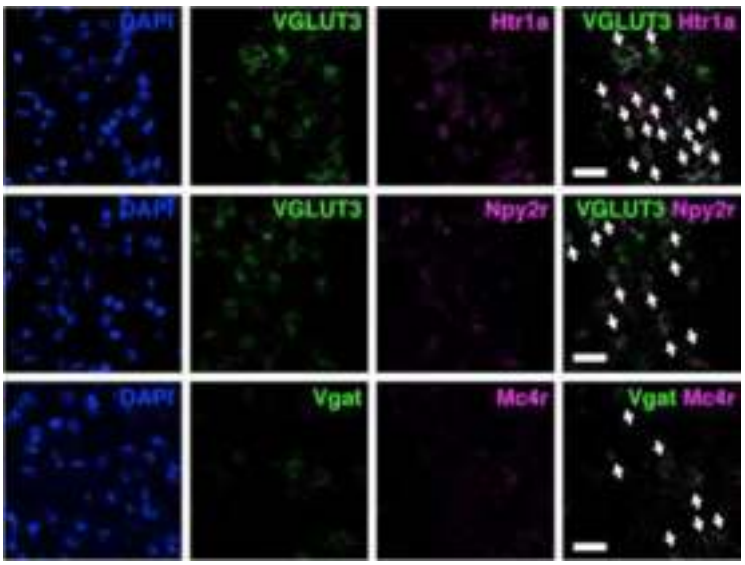

FIGURE 10. Colocalization between cell-type-specific marker genes (*Vgat* or *Vglut3*) and receptors (*Mc4r*, *Htr1a*, *Npy2r*) using the RNAscope Multiplex Fluorescent assay. White arrows designate double-labeled cells. Images from Nectow *et al.*, *Cell*, 2017.

The Fat Mass and Obesity-Associated Protein (FTO) Regulates Locomotor Responses to Novelty via D2R Medium Spiny Neurons[5]

Reported by Ruud et al., Cell Reports, 2019

The fat mass and obesity-associated gene *Fto* is an obesity-risk gene associated with locomotor activity regulation. However, the specific role of *Fto* in the neurons that control voluntary movements, the medium spiny neurons (MSNs), remains unclear. MSNs are comprised of two dopaminoceptive neuron types:

- D1 (Dopamine Receptor 1a, *Drd1a*) MSNs are the direct pathway and facilitate movement activation
- D2 (Dopamine Receptor 2, *Drd2*) MSNs are the indirect pathway and suppress movement initiation

Ruud *et al.* found that *Fto* regulates physical activity via D2 MSNs in the brain. They used the RNAscope Multiplex Fluorescent v2 assay (Figure 11) to confirm the expression of *Fto* expression in D1 and D2 MSNs and deletion of *Fto* in these cell populations.

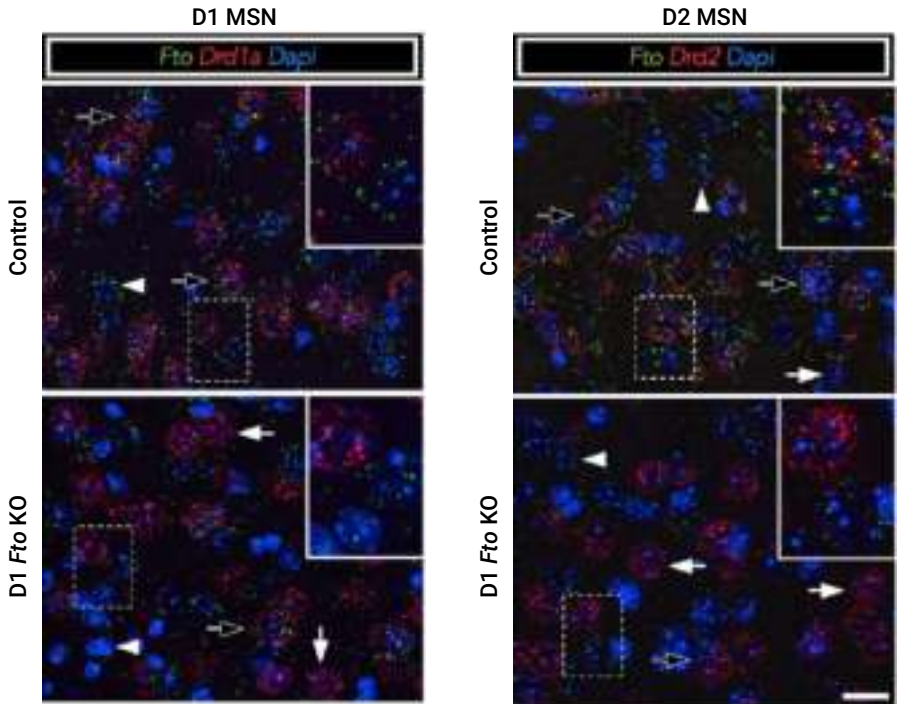

FIGURE 11. Detection of *Fto* mRNA (green) in the striatum of representative control (top) and *Fto* knockout mice (bottom) using the RNAscope Multiplex Fluorescent v2 assay. Left: *Drd1a* mRNA (red) in the same field of view. Right: *Drd2* mRNA (red) in the same field of view. Nuclei are counterstained with DAPI (blue). Images from Ruud *et al.*, *Cell Reports*, 2019.

Combining the RNAscope ISH assay with IHC/IF for cell type-specific spatial analysis

Visualization of gene expression with spatial context can be critical when interrogating heterogenous tissues like the brain or the spinal cord. To understand the cellular crosstalk between different cell populations, it can be essential to simultaneously study gene and protein expression within a complex tissue. By detecting both RNA and protein in the same tissue sample in a spatially resolved manner, researchers can leverage the best of transcriptomic and proteomic features to reveal cell-type specific gene expression[6,7], identify the cellular sources of secreted proteins[8] and visualize the spatial organization of the various cell types and their interactions (Figure 12 and Figure 13).

This can be achieved by combining the highly sensitive and specific RNAscope ISH assay with immunohistochemistry/immunofluorescence (IHC/IF) into one protocol due to the similarities in their workflows. Researchers have used this technique (Figure 12), referred to as dual ISH-IHC/IF, in neurobiology applications to accurately identify areas of the brain and differentiate between various cell types. [6,9–13]

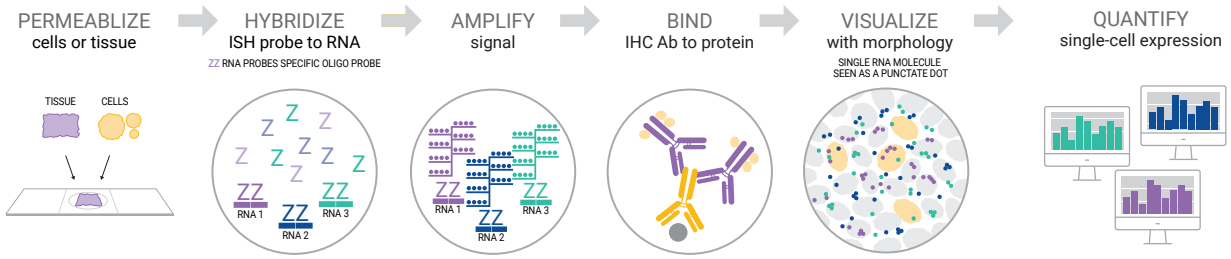

FIGURE 12. Schematic of the dual ISH-IHC/IF workflow with the RNAscope and BaseScope assays.

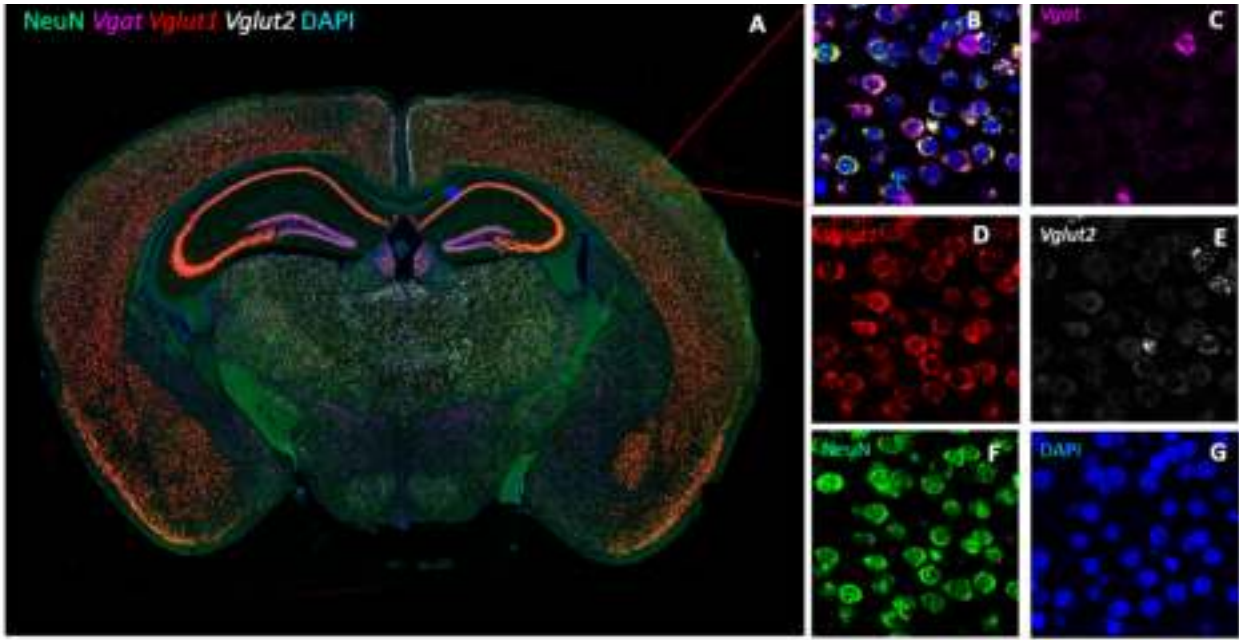

FIGURE 13. Dual ISH-IF on FFPE coronal section of mouse brain using the RNAscope Multiplex Fluorescent v2 ISH assay combined with IF. A. Low magnification image showing the spatial expression of NeuN protein (green) and *Vglut1* (Mm-Slc17a7; red), *Vglut2* (Mm-Slc17a6; white) and *Vgat* (Mm-Slc17a1; pink) mRNA in the coronal section of a mouse brain. B. High magnification (40X) images showing mRNA expression of the neuronal membrane transporters *Vglut1*, *Vglut2*, and *Vgat* and protein expression of the neuronal marker NeuN in the brain cortex. C–F. High magnification (40x) individual images for *Vgat*, *Vglut1*, *Vglut2*, and NeuN, in the same cortical region of the brain. G. nuclear staining using DAPI (blue).

Related publications

Below are a few examples of recent peer-reviewed publications illustrating how researchers have taken advantage of the dual ISH-IHC/IF technique for cell type-specific gene expression analysis in the tissue.

Glial- and Neuronal-Specific Expression of *CCL5* mRNA in the Rat Brain[14]

Reported by Lanfranco et al., Frontiers in Neuroanatomy, 2018

The chemokine Ccl5 and its receptors promote neuroinflammation in the CNS. Lanfranco *et al.* have examined the expression profile of *Ccl5* in the adult rat brain and provide evidence of its cellular localization. The RNAscope ISH assay combined with IF was used to thoroughly characterize the cellular expression profile of *Ccl5* in the brain (Figure 14).

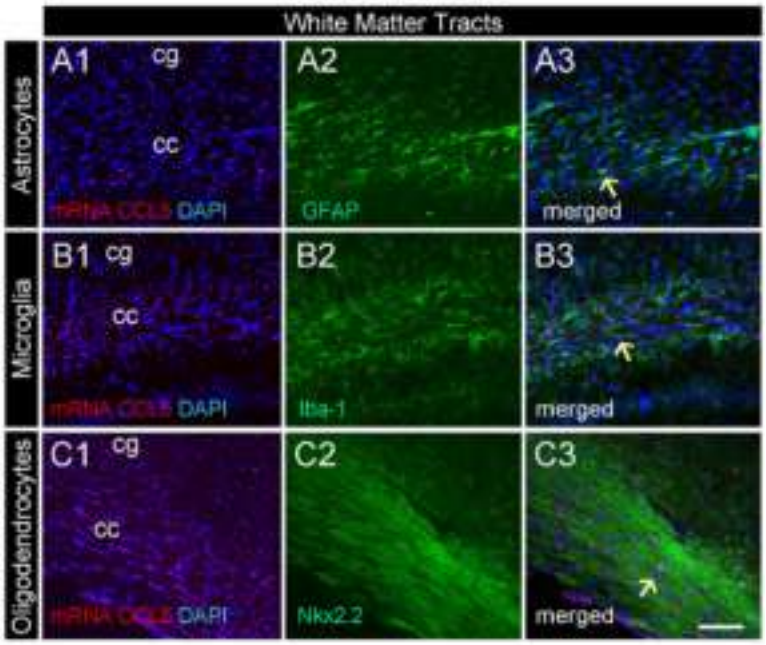

FIGURE 14. Detection of inflammatory marker *Ccl5* (red) in different CNS cell types using the RNAscope Multiplex Fluorescent assay on rat fresh frozen brain sample combined with IF staining (green) of neuronal cells (NeuN antibody, A1, A2, A3), microglia (Iba-1 antibody, B1, B2, B3), astrocytes (GFAP antibody, C1, C2, C3) and oligodendrocyte progenitors (Nkx2.2 antibody, D1, D2, D3). Images from Lanfranco *et al., Bio Protoc*, 2017.

Mechanically activated Piezo channels mediate touch and suppress acute mechanical pain response in mice[15]

Reported by Zhang M et al, Cell Reports, 2019

The molecular mechanisms underlying the mechano-transduction processes of touch and mechanical pain remain poorly understood. Zhang *et al.* have shown that deletion of the mechanically activated and rapidly adapting Piezo2 channel in a portion of the low-threshold mechanoreceptors and most of the IB4-positive nociceptors impairs touch but sensitizes mechanical pain in mice. Using the dual RNAscope ISH-IF workflow to validate scRNA-seq data and identify cell-type specific expression of Piezo2, they found that *Piezo2* is widely expressed in molecularly-defined subsets of DRG neurons, including LTMRs, marked by tropomyosin-receptor kinase (Trk) B, calbindin 1 (Calb1), or TrkC LTMRs and proprioceptors by neural filament heavy chain (NFH), non-peptidergic nociceptors by IB4, and peptidergic nociceptors by calcitonin gene-related peptide (CGRP) (Figure 15).

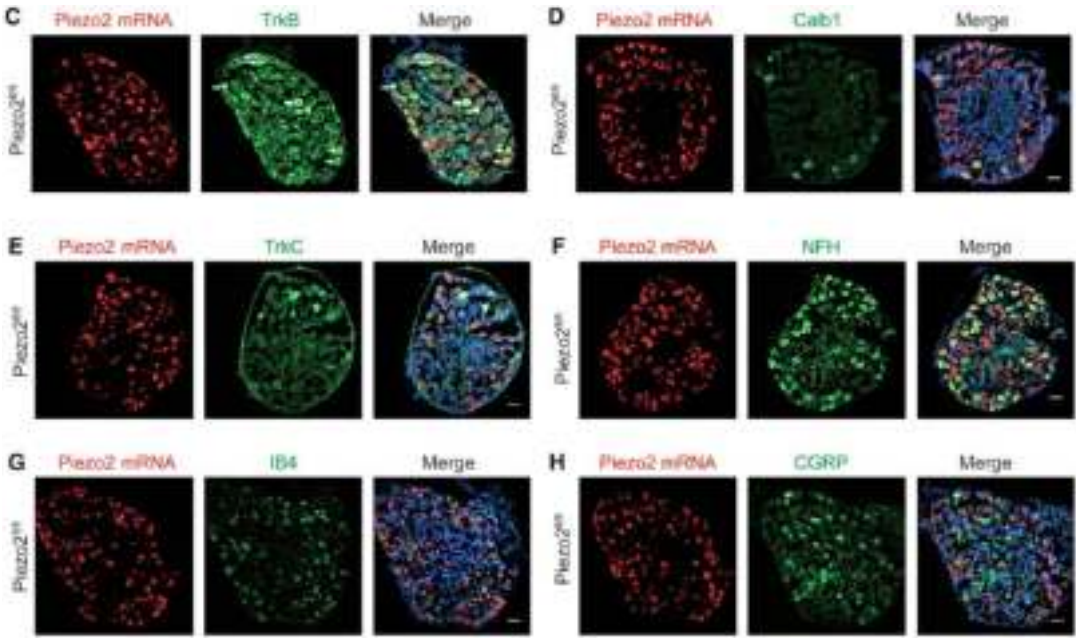

FIGURE 15. Representative images showing staining of DRG sections from Piezo2$^{fl/fl}$ mice with the RNAscope probe for *Piezo2* mRNA and antibodies against TrkB (C), Calb1 (D), TrkC (E), NFH (F), and CGRP (H) or IB4-biotin (G) to identify the distinct subsets of DRG neurons expressing *Piezo2*. In (C), the arrows indicate TrkB positive neurons. Scale bars, 50 mm. Images from Zhang M *et al.*, *Cell Reports*, 2019.

Detection of mRNA in axons or in astrocyte processes

The unique morphology of neurons and astrocytes raises the question of how the molecules required for the structure and function are supplied at the axon's terminals or the astrocytes processes. The discovery of protein synthesis machinery in the growth cones and astrocytes processes of mammalian cells and the subsequent identification of various mRNAs specifically localized suggested that mRNA can be transported along the axon or astrocytes processes and locally translated. In addition, local translation may give autonomy to respond quickly to signals without waiting for input from the cell body. It has been suggested that local protein synthesis is required, for example, for axon growth as well as retrograde signalling from the tip of the axon to the cell body.

Related publications

In the selected publications below, we highlight how researchers have used the RNAscope assay to track RNA expression along the axon or astrocyte processes.

ALS along the axons — Expression of coding and noncoding RNA differs in axons of ALS models[16]

Reported by Rotem et al. Scientific Reports, 2017

Amyotrophic lateral sclerosis (ALS) is a lethal motor neuron disease with no current treatment. Rotem *et al.* were the first to investigate the somatic- and axonal-specific subcellular expression profiles and localization of coding and noncoding RNAs in two ALS models, providing crucial new data on potential drug targets. They used the RNAscope Multiplex Fluorescent assay to detect the key target Elavl2 combined with IHC for MAP2 in cultured primary motor and confirmed the predicted Elavl2 expression in axons of motor neurons (Figure 16).

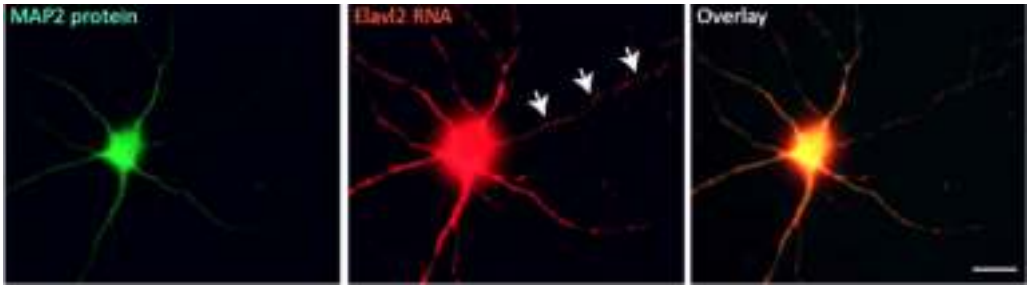

FIGURE 16. Visualization of *Elavl2* mRNA by the RNAscope assay combined with MAP2 protein by IF in cultured primary motor neurons from wild-type mice shows abundant mRNA in the soma and MAP2+ dendrites. In addition, distinct puncta are present along the MAP2- axon shaft (arrows). Scale bar: 20 µm. Images from Rotem *et al., Scientific Reports,* 2017.

Translation in astrocyte distal processes sets molecular heterogeneity at the gliovascular interface[17]

Reported by Boulay et al., Cell Discovery, 2017

Astrocytes also send out long processes terminated by end feet, to regulate vascular functions as well as homeostasis at the vascular interface. To date, the astroglial mechanisms

underlying these functions have been poorly addressed. Using the RNAscope assay (Figure 17), Boulay *et al.* have demonstrated that a subset of messenger RNAs is distributed in astrocyte endfeet and identified a pool of messenger RNAs bound to ribosomes, termed the "endfeetome", that primarily encodes for secreted and membrane proteins.

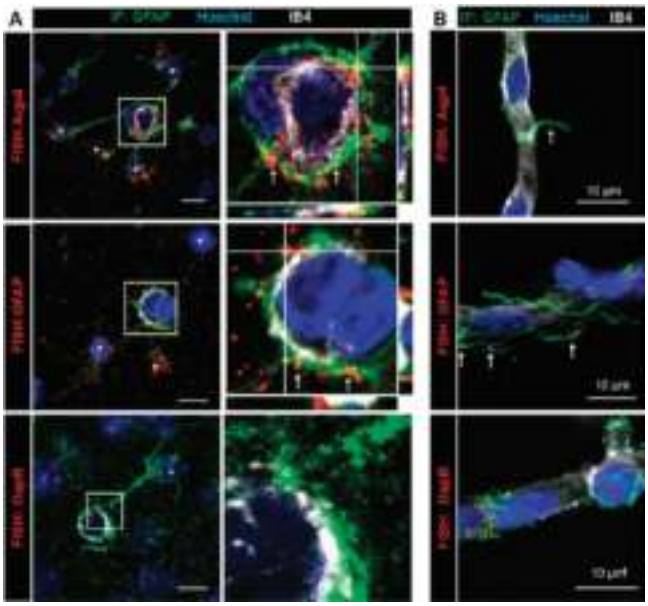

FIGURE 17. A. Representative confocal images of astrocyte-specific mRNAs encoding *Aqp4*, *Gfap* and *dapB* (negative probe) detected by the RNAscope Multiplex Fluorescent ISH assay on brain sections of 2-month-old C57BL6 mice. Astrocytes (here in the hippocampus) are immunostained for GFAP (green). *Aqp4* or *Gfap* mRNAs are mostly detected in perivascular astrocyte processes and endfeet (red) (white arrows). Enlarged views of boxed areas show details of the FISH signals in PVAPs and endfeet. Images from Boulay *et al., Cell Discovery*, 2017.

Subcellular transcriptomes and proteomes of developing axon projections in the cerebral cortex[18]

Reported by Poulopoulos et al., Nature, 2019

The development of neural circuits relies on axon projections, formed by growth cones, establishing diverse connections between areas of the nervous system. To investigate the set of molecules within native growth cones Poulopoulos *et al*. developed an approach that identifies and quantifies local transcriptomes and proteomes from labeled growth cones of single projections *in vivo*. Using this approach on the developing callosal projection of the mouse cerebral cortex, they mapped molecular enrichments in growth cones from single neuron subtypes directly from the brain. They used the RNAscope 2.5 HD Chromogenic assay (Figure 18) to detect axonally transported mRNA in cultured callosal projection neurons.

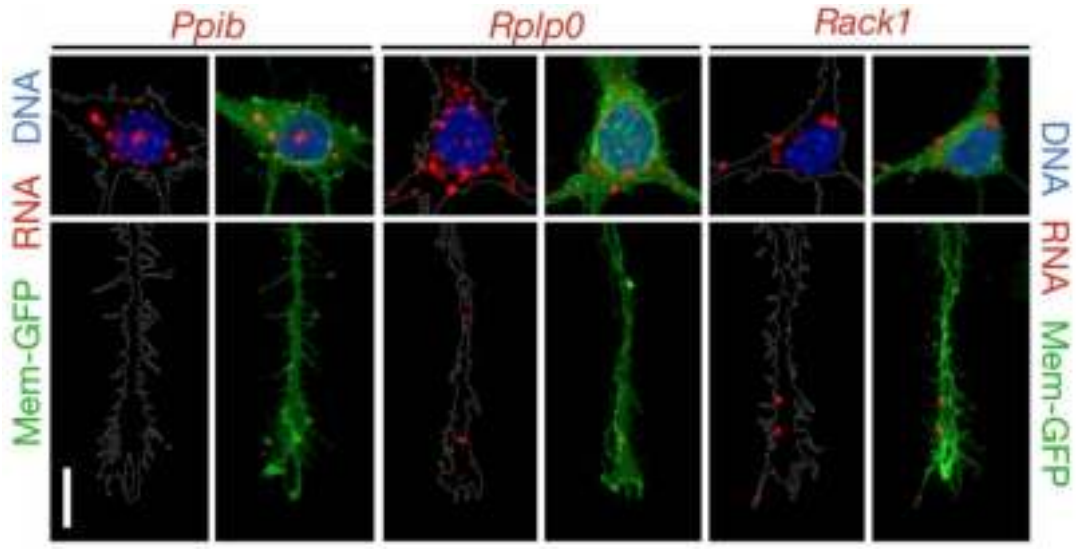

FIGURE 18. Single-molecule RNA *in situ* hybridization using the RNAscope 2.5 HD Chromogenic RED assay (red) for *Rack1*, *Rplp0*, and control transcript *Ppib* on cultured callosal projection neurons labeled with membrane-GFP (green). Nuclei were stained with DAPI (blue). Images from Poulopoulos *et al., Nature*, 2019.

Detection of soluble factors in the nervous system

As secreted proteins (such as growth factors, cytokines, or chemokines) are released from the producing cell, IHC/IF will provide the localization of the protein in the tissue matrix but will not provide information for the cell that secreted the protein. To overcome this issue, ISH can be used to identify the cell producing the secreted protein by targeting the mRNA precursor. Combination of ISH and IHC/IF can also provide the unique opportunity to both identify the original cell producing the protein and localize where the protein goes in the tissue sample.

Related publications

Below are a few examples of recent peer-reviewed publications illustrating how researchers have taken advantage of the RNAscope assay to detect soluble factors within the nervous system.

Loss of adaptive myelination contributes to methotrexate chemotherapy-related cognitive impairment[19]

Reported by Geraghty et al., Neuron, 2019

Methotrexate (MTX) chemotherapy results in a microglial-dependent reduction of Bdnf expression and loss of activity-regulated myelination, which requires Bdnf to TrkB signalling. Oligodendrocyte precursor cell (OPC)-specific loss of TrkB results in impaired cognitive behavioural performance. Geraghty *et al.* have shown that the stimulation of the OPC TrkB signalling, using a small-molecule TrkB agonist, can restore myelination and rescue cognition after MTX. They used the RNAscope assay to detect the depletion of the expression of *Bdnf* after exposure to MTX in mouse brain (Figure 19).

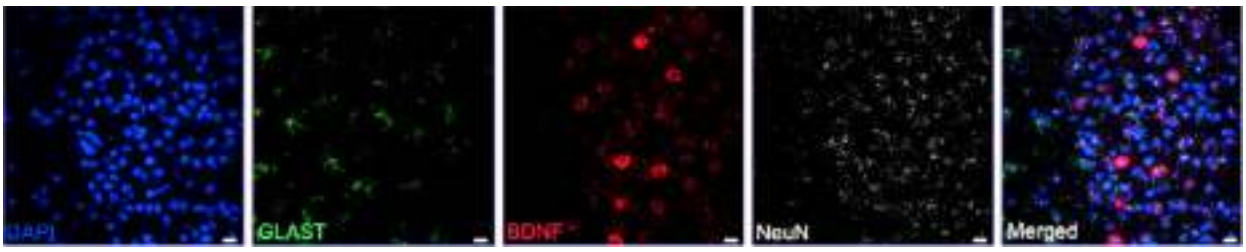

FIGURE 19. Representative image demonstrating RNAscope visualization of frontal cortex deep-layer neurons (*NeuN*, white), astrocytes (*Glast*, green), and *Bdnf* mRNA (red). DAPI, blue. Scale bar, 20 mm. Images from Geraghty *et al., Neuron*, 2019.

Parabrachial interleukin-6 reduces body weight and food intake and Increases thermogenesis to regulate energy metabolism[20]

Reported by Mishra et al., Cell Reports, 2019

Using the RNAscope Multiplex Fluorescent assay, Mishra *et al.* demonstrated that *Il-6* is produced by lateral parabrachial nucleus (lPBN) neurons, astrocytes, and microglia (Figure 20). They also showed that IL-6 acts in the lPBN to reduce body weight by increasing thermogenesis and reducing food intake.

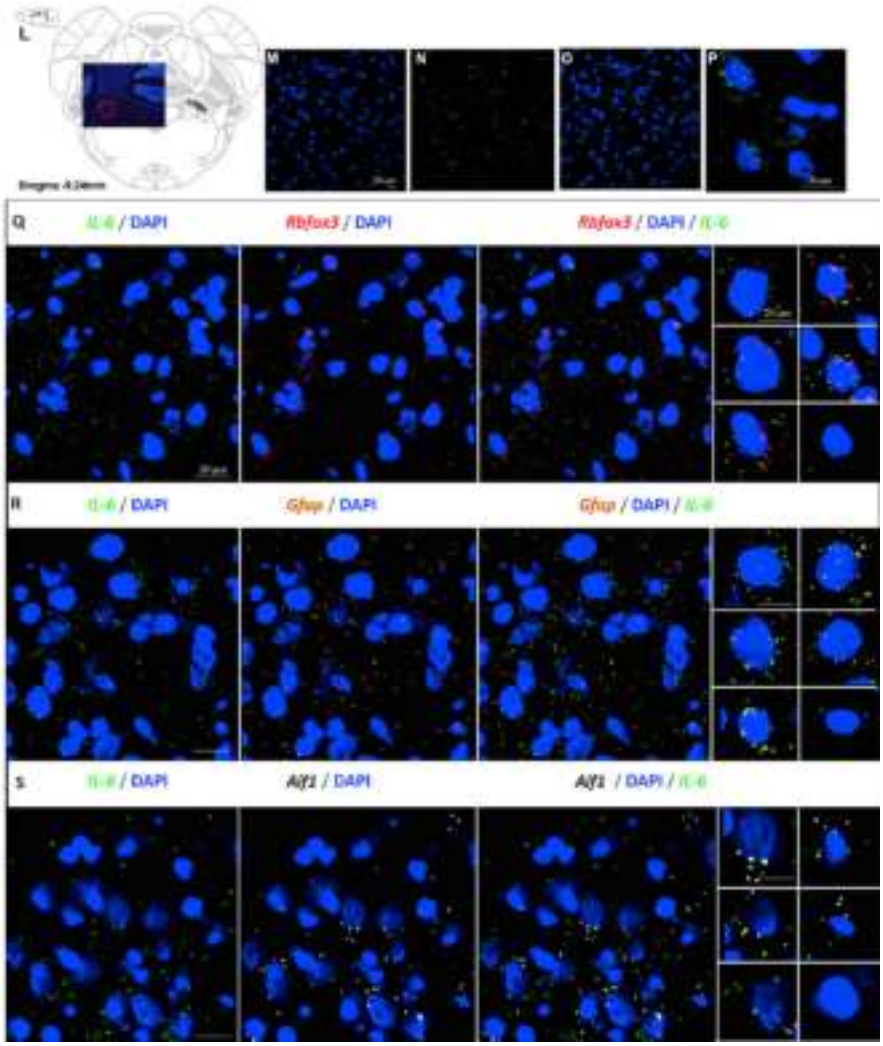

FIGURE 20. Multiplex Fluorescent RNAscope assay was used to co-localize *Il-6* mRNA with neuronal (*Rbfox3*; red; Q), glial (*Gfap*; orange; R), or microglial (*Aif1*; gray; S) mRNA markers in lPBN. Images from Mishra *et al., Cell Reports,* 2019.

Detection of RNA in post-mortem human brain samples

Studies on the post-mortem human brain are a very important tool for understanding the neurobiology of neurodegenerative diseases or psychiatric disorders. Histological stains, IHC, and traditional ISH are often challenging due to technical limitations and the sub-optimal mRNA in these samples, as RNA is rapidly degraded after death.

Consequently, molecular markers specifically expressed by a given neuronal population often cannot be assessed in human post-mortem brain, demanding the generation of novel techniques to address this limitation.

With their high sensitivity and specificity, the RNAscope and BaseScope assays now enable the investigation of gene expression at the RNA level in post-mortem human brain tissues.

Related publications

Below are a few examples of recent peer-reviewed publications illustrating how researchers have taken advantage of the RNAscope technology to detect gene expression in post-mortem human brain samples.

Integrative single-cell analysis of transcriptional and epigenetic states in the human adult brain[21]

Reported by Lake et al., Nature Biotechnology, 2016

Lake *et al.* developed a scalable approach to sequence and quantify RNA molecules in isolated neuronal nuclei from post-mortem human brain, generating 3,227 sets of single neuron data from six distinct regions of the cerebral cortex. They then used the RNAscope assay (Figure 21) for a set of selected markers to confirm subtype- and layer-specific expression patterns in the cortex as revealed by single-nucleus RNA sequencing (snRNA-seq) of the human post-mortem brain.

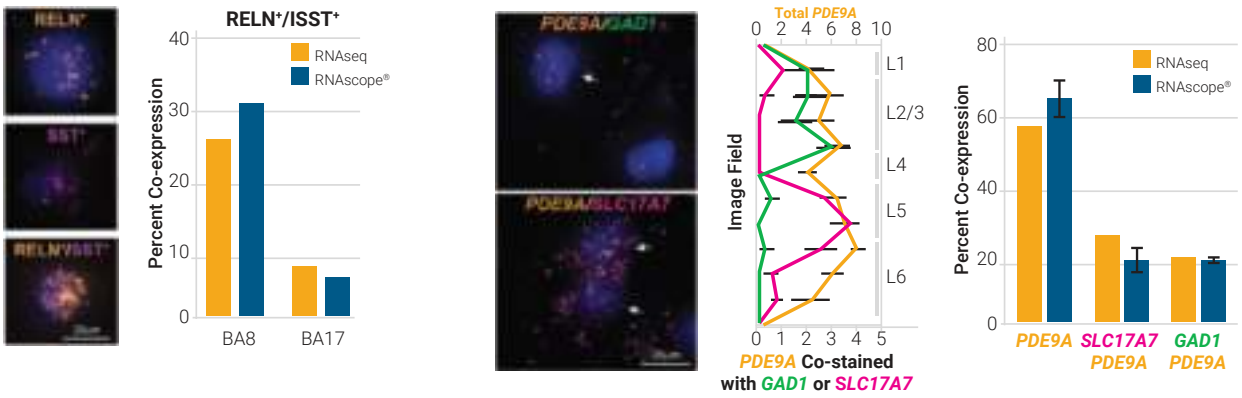

FIGURE 21. A. RNAscope co-staining of *RELN* and *SST* in human brain areas BA8B and BA17 shows positive cell distribution that are consistent with snRNA-seq data. B. *PDE9A*-positive expression in inhibitory and excitatory neuronal subtypes was confirmed by RNAscope co-staining with *GAD1* (double positive restricted to layers 2/3) and *SLC17A7* (double positive restricted to layers 5/6). The RNAscope data is consistent with snRNA-seq data. Images from Lake *et al., Nature Biotechnology*, 2016.

Unique RNA signature of different lesion types in the brain white matter in progressive multiple sclerosis [22]

Reported by Elkjaer et al., Acta Neuropathol Commun, 2019

Heterogeneity in multiple sclerosis (MS) is a result of dynamic changes of various lesion types in brain white matter (WM). Elkjaer *et al.* identified potential drivers of MS lesions using a comprehensive unbiased approach that included RNAseq, bioinformatics, IHC, and RNAscope performed on the WM from MS and control patients (Figure 22). The MS biomarker *CHI3L1* was identified as one of the top ten upregulated genes in chronic active lesions expressed by astrocytes in the rim.

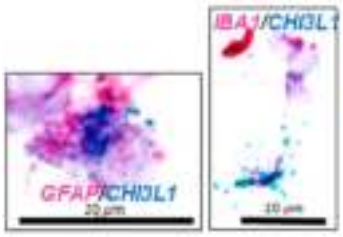

FIGURE 22. Chitinase-3-like protein 1 (*CHI3L1*) in the rim of chronic active lesions. Detection of *CHI3L1* mRNA (green) and *IBA1* or *GFAP* mRNA (red) using the RNAscope 2.5 HD Duplex Chromogenic assay on human brain post-mortem FFPE samples. Image from Elkjaer M. *et al., Acta Neuropathol Commun*, 2019.

C9ORF72 repeat expansion causes vulnerability of motor neurons to Ca2+-permeable AMPA receptor-mediated excitotoxicity[23]

Reported by Selvaraj et al. Nature Communications, 2018

Mutations in *C9ORF72* are the most common cause of familial amyotrophic lateral sclerosis (ALS), as expansion of a GGGGCC repeat in the *C9ORF72* gene accounts for 10% of sporadic ALS cases and increased expression of *GluA1* AMPA receptor (AMPAR) subunit occurs in MNs with *C9ORF72* mutations.

The precise mechanisms of motor neuron death in ALS is unknown, but excitotoxicity mediated by glutamate and AMPAR (*GluA1*) subunits has been implicated. Selvaraj *et al.* showed that upregulation of AMPAR (*GluA1*) subunits in human motor neurons with the *C9ORF72* repeat expansion could be the pathogenic mechanism in ALS patients.

The BaseScope ISH assay was used to analyze the expression of AMPAR subunits (*GluA1-4*) in post-mortem human brain samples of control and ALS patients carrying the *C9ORF72* repeat expansion mutation (Figure 23). The BaseScope assay revealed elevated *GluA1* expression in the spinal cord of ALS patients compared to control and mutant *C9ORF72* spinal cord (but not cortical) neurons show selective upregulation of the *GluA1* transcript.

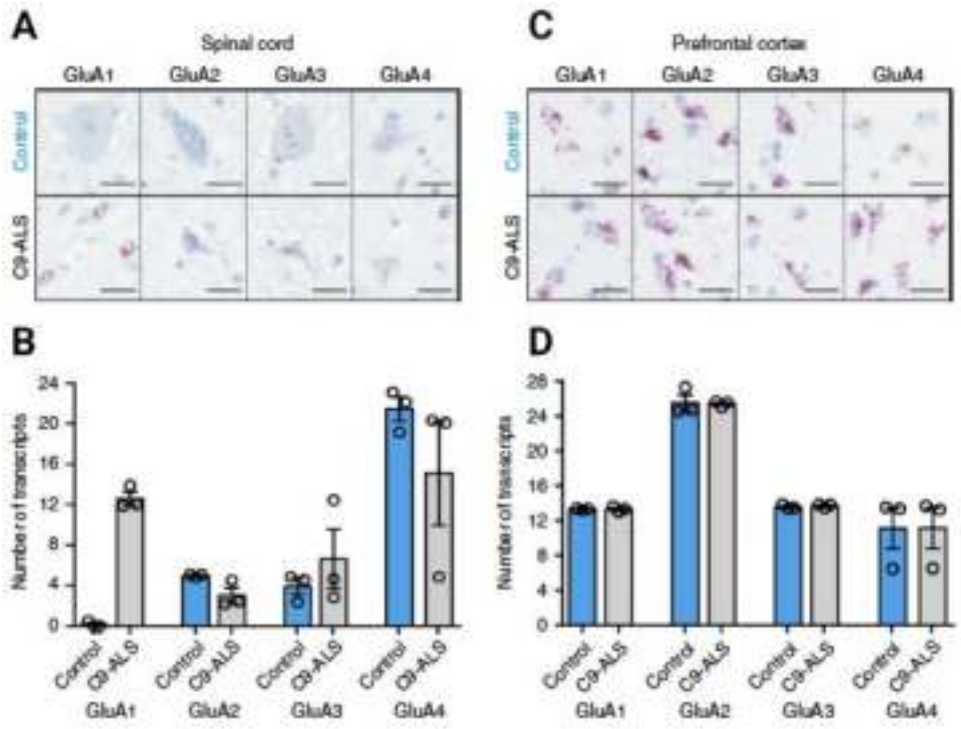

FIGURE 23. AMPAR subunit expression in post-mortem spinal cord of healthy patients and ALS patients with *C9ORF72* repeat expansion. A. Representative RNAscope images showing the expression of AMPAR *GluA1*—four transcripts in the anterior horn of cervical spinal cord sections from an ALS patient (*C9ORF72*) and an age-matched healthy patient and reveals increased expression of *GluA1* in ALS patient sample. B. Quantification of the mean ± s.e.m. expression levels of AMPAR transcripts in spinal cord samples from three independent patients and controls. C. Representative RNAscope images showing the expression of AMPAR *GluA1*—four transcripts in the prefrontal cortex from an ALS patient (*C9ORF72*) and an age-matched healthy patient. D. Quantification of the mean ± s.e.m. expression levels of AMPAR transcripts in prefrontal cortex samples from three independent patients and controls showing equivalent expression of all transcripts. Images from Selvaraj *et al., Nature Communications*, 2018.

Utilization of the RNAscope assay on whole mount samples

Whole mount *in situ* hybridization (WISH) is a critical tool in neuroscience for studying the expression and localization of RNA molecules in intact embryos and tissues. The current technologies available to detect mRNAs in whole mount embryos can be challenging due to low signal to noise ratio and methods that are very time-consuming. It is, however, possible to perform the RNAscope assay on whole mount tissue samples with high specificity and sensitivity (Figure 24).

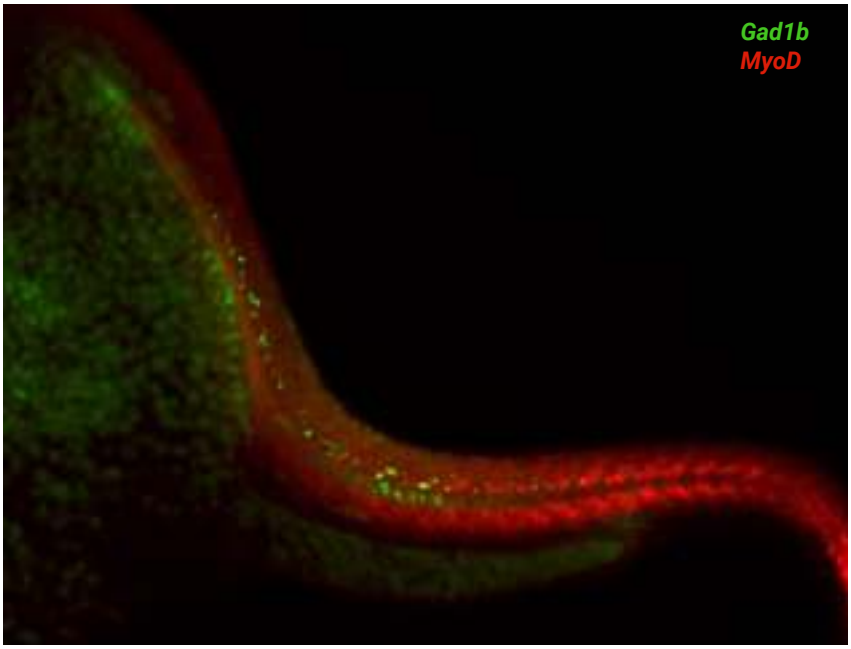

FIGURE 24. Detection of *Gad1b* (green) and *MyoD* (red) in 24 hpf zebrafish whole mount embryos with the RNAscope Multiplex Fluorescent v2 assay.

Related publications

Below is an example of a recent peer-reviewed publication illustrating how researchers have taken advantage of the RNAscope to detect gene expression in whole mount tissues.

The HisCl1 histamine receptor acts in photoreceptors to synchronize Drosophila behavioral rhythms with light-dark cycles[24]

Reported by Alejevski et al., Cell Rep, 2019

In *Drosophila*, the clock that controls rest-activity rhythms synchronizes with light-dark cycles through either the blue-light sensitive cryptochrome (*Cry*), located in most clock neurons, or rhodopsin-expressing histaminergic photoreceptors. Alejevski *et al.* showed that, in the absence of *Cry*, each of the two histamine receptors *Ort* and *HisCl1* contribute to synchronize, or "entrain" the *Drosophila* clock, whereas no entrainment occurs in the absence of the two receptors (Figure 25).

These results show that both *Ort* and *HisCl1* define two different pathways for circadian entrainment:

- *Ort* contributes through its expression in the interneurons of the optic lobe
- *HisCl1* mostly contributes through its expression in retinal photoreceptors

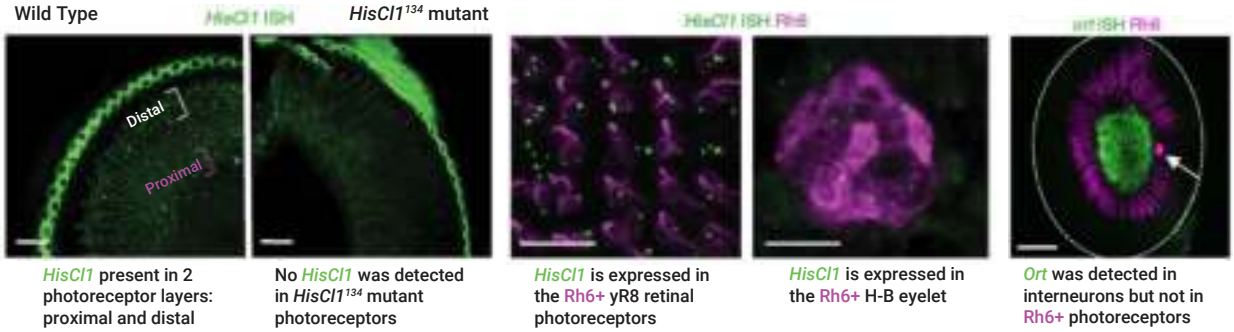

FIGURE 25. *HisCl1* but not *Ort* is expressed in photoreceptors. Detection of *HisCl1* (green) but not *Ort* (green) with the Multiplex Fluorescent v2 assay combined with IF for *Rh6* (pink) on whole-mount Drosophila retina. Images from Alejevski *et al., Cell Rep,* 2019.

Detection of Targets in the Nervous System when No (Reliable) Antibodies Are Available

In situ detection of GPCRs in the nervous system using the RNAscope ISH Assay

While IHC has proven to be a well-established method for a broad range of applications from discovery to diagnostics and prognostics, raising antibodies to G-protein coupled receptors (GPCRs) can be challenging due to difficulties in obtaining suitable antigen accessibility, amongst other reasons, as GPCRs are transmembrane proteins that can be expressed at low levels and tend to be unstable when purified[26]. Alternatively, one can interrogate the RNA as a way to specifically detect GPCRs in the tissue context. Here we show examples for the detection of numerous GPCRs, including dopaminergic, cannabinoid, cholinergic, and opioid receptors, using the highly specific RNAscope ISH assay.

Figures 25–29 provide both fluorescent and chromogenic images for four types of GPCRs — readily detected as mRNA targets by the RNAscope assay — in hippocampal and striatal normal mouse brain areas: Dopaminergic Receptors D1 and D2 (*Drd1* and *Drd2*), Cannabinoid Receptor 1 (*Cnr1*), Opioid Receptor μ (*Oprm1*), δ (*Oprd1*), and κ (*Oprk1*), and Cholinergic Receptor Muscarinic 3 (*Chrm3*).

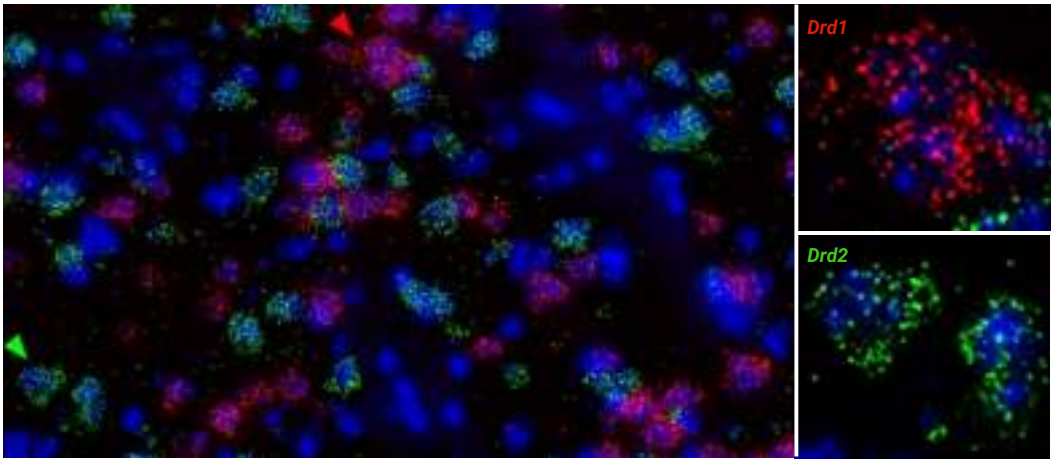

FIGURE 26. Detection of two distinct striatal neuronal populations expressing either Dopamine Receptor D1 (*Drd1*, Red) or Dopamine Receptor D2 (*Drd2*, Green) using the RNAscope Multiplex Fluorescent assay on fresh frozen mouse brain tissue samples. Areas indicated by green and red arrows are shown as higher magnification images in the right panels. Cells are counterstained with DAPI.

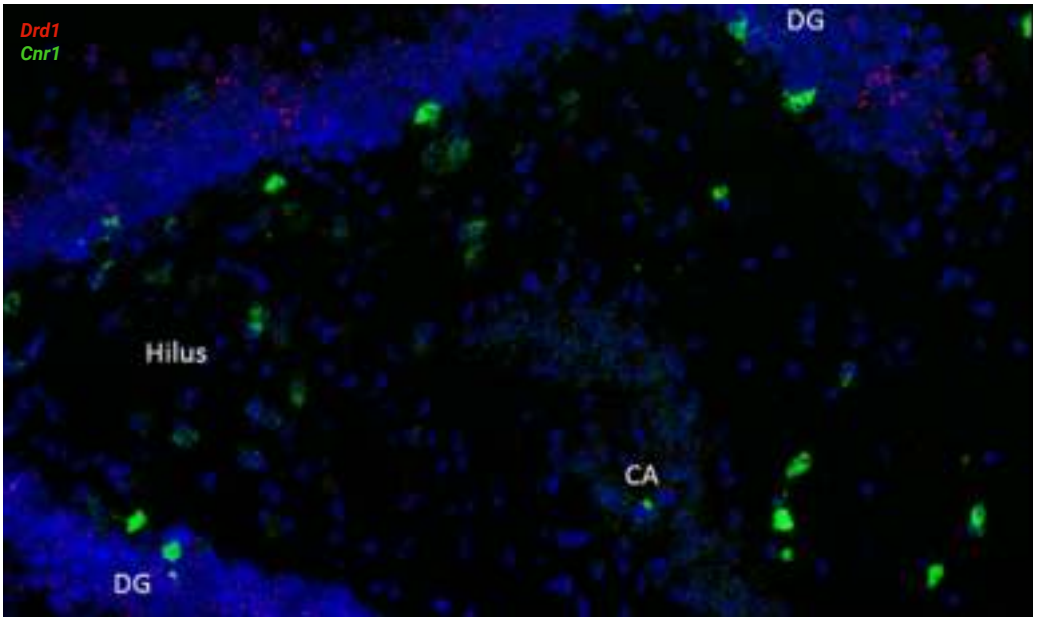

FIGURE 27. Duplex detection of GPCRs in normal mouse brain hippocampus using the RNAscope Multiplex Fluorescent assay on fresh frozen mouse brain tissue samples: Cannabinoid Receptor 1 (*Cnr1*, green) and Dopaminergic Receptor D1 (*Drd1*, red). Cells are counterstained with DAPI. CA = Cornu Ammonis. DG = Dentate Gyrus.

Further information about GPCR detection with the RNAscope assay:
acdbio.com/science/applications/research-areas/g-protein-coupled-receptors-ion-channels

Watch the video:
youtube.com/watch?v=SFjUVZGdToc&feature=youtu.be

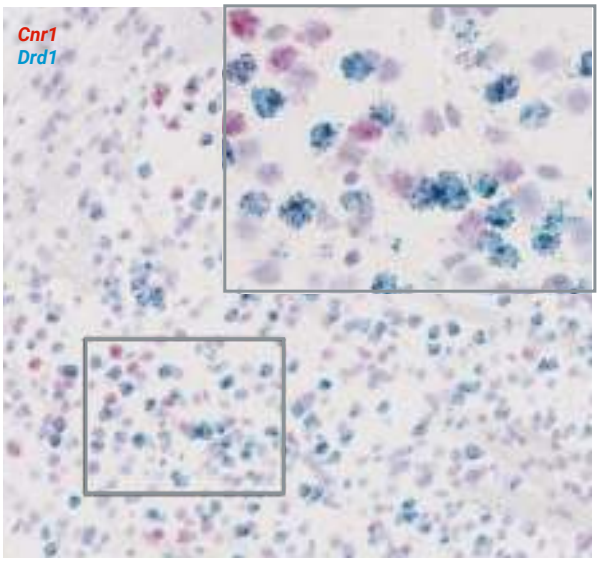

FIGURE 28. Detection of GPCRs in normal mouse brain striatum using the RNAscope 2.5 HD Duplex Chromogenic assay on FFPE mouse brain tissue samples: Cannabinoid receptor 1 (*Cnr1*, red) and Dopaminergic receptor D1 (*Drd1*, green). Cells are counterstained with Hematoxylin. The area indicated by the box is shown as higher magnification inset.

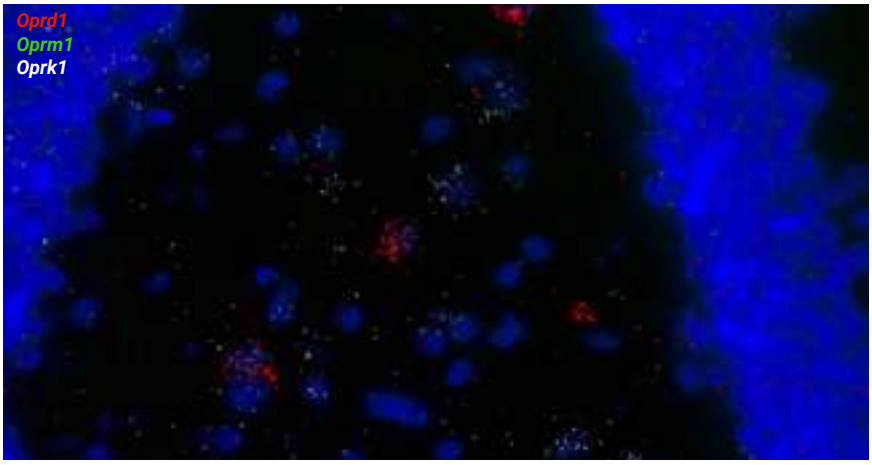

FIGURE 29. Detection of three distinct opioid receptors in normal mouse brain hippocampus using the RNAscope Multiplex Fluorescent assay on fresh frozen mouse brain tissue samples: Opioid Receptor μ (*Oprm1*, green), δ (*Oprd1*, red), and κ (*Oprk1*, white). Cells are counterstained with DAPI.

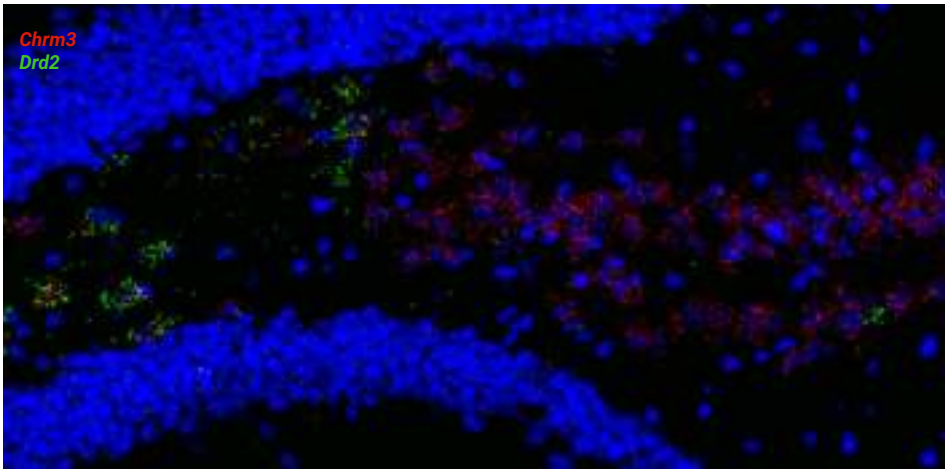

FIGURE 30. Detection of Cholinergic Receptor Muscarinic 3 (*Chrm3*, red) and Dopamine Receptor D2 (*Drd2*, green) in normal mouse brain hippocampus using the RNAscope Multiplex Fluorescent assay on fresh frozen tissue samples. Cells are counterstained with DAPI.

Related publications

Below are a few examples of recent peer-reviewed publications illustrating how researchers have taken advantage of the RNAscope technology as an alternative assay to specifically detect GPCRs in the morphological context of the brain.

GPR88 in A2AR Neurons Enhances Anxiety-Like Behaviors[26]

Reported by Meirsman et al., eNeuro, 2016

In their study investigating the influence of the orphan GPCR Gpr88 in A2AR-expressing Drd2 neurons on anxiety-like behaviors, Meirsman *et al.* used Multiplex Fluorescent RNAscope ISH for *Gpr88*, *Drd1* and *Drd2* to verify the specific excision of *Gpr88* in striatal Drd2-medium spiny neurons of the conditional A2AR-driven *Gpr88* knock-out (Figure 31).

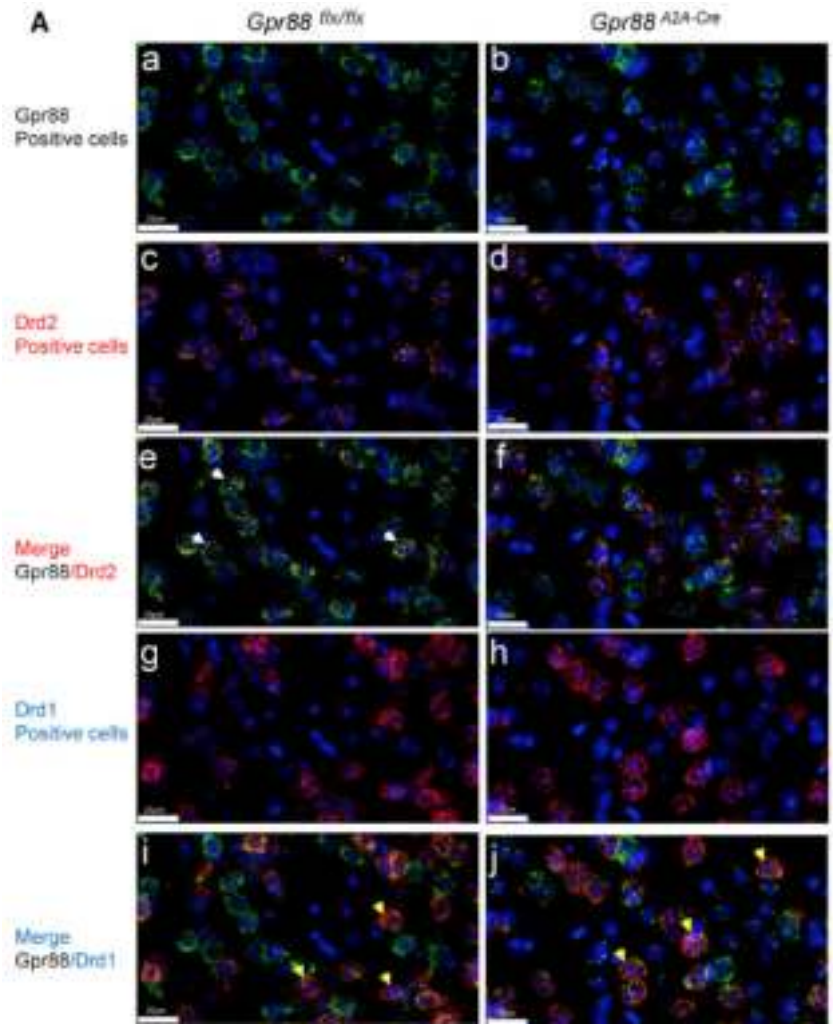

FIGURE 31. A. Molecular characterization of conditional A2AR-Gpr88 KO mice. A, Triple-fluorescent *in situ* hybridization probing *Gpr88* (Aa, Ab, Ae, Af, Ai, and Aj; probe labeled in green), *Drd2* (Ac–Af; probe labeled in orange), and *Drd1* (Ag–Aj; probe labeled in red). Representative images are shown. In Gpr88flx/flx control animals, *Gpr88* mRNA colocalizes with both *Drd2* (Ae: merge *GPR88/Drd2*, white arrows) and *Drd1* mRNA (Ai: merge *GPR88/Drd1*, yellow arrows). In contrast, Gpr88A2A-Cre conditional mice show almost no colocalization with *Drd2* (Af: merge *GPR88/D2R*), while colocalization with *Drd1* remains (Aj: merge *GPR88/Drd1*, yellow arrows). DAPI staining (blue) was used to label all cell nuclei. Images from Meirsman *et al., eNeuro*, 2016.

GPR139 and dopamine D2 Receptor co-express in the same cells of the brain and may functionally interact[27]

Reported by Wang et al., Frontiers in Neuroscience, 2019

The physiological function of the Gq-coupled receptor GPR139 remains elusive, but may play a role in addiction, Parkinson's disease, and schizophrenia. Sequencing data suggests similar expression patterns between GPR139 and the GPCR DRD2. In this study, Wang *et al.* have used ACD's Pharma Assay Services to perform RNAscope Multiplex Fluorescent assays for assessment of *Gpr139* and *Drd2* in the mouse brain (Figure 32). The results showed co-expression in multiple regions, including the portions of the telencephalon, diencephalon, midbrain, and pituitary. Previous IHC results showed GPR139 expression only in the medial habenula (diencephalon) and lateral septum (telencephalon), indicating variation in the sensitivity between

methods detecting mRNA and protein expression. Furthermore, co-expression of *Gpr139* and *Drd2*, along with other data, suggests that the two receptors functionally interact.

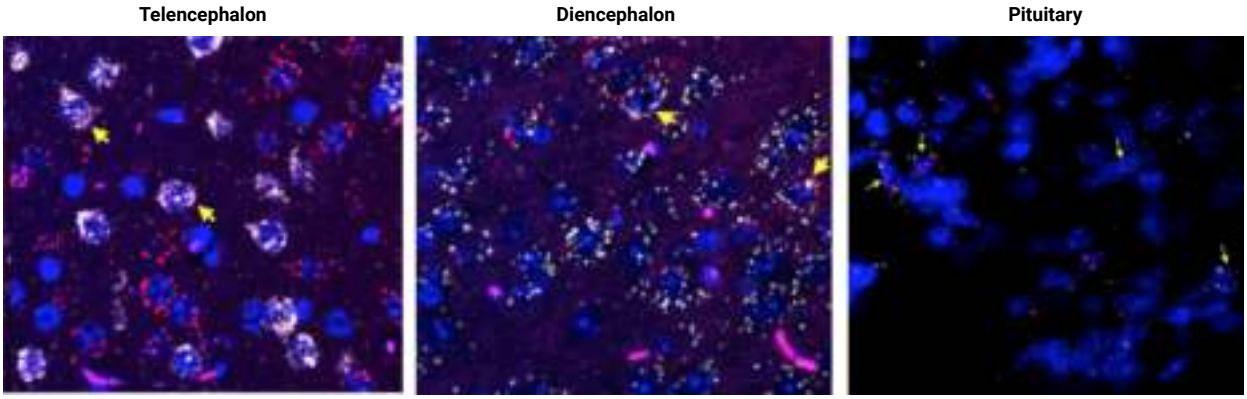

FIGURE 32. RNAscope ISH analysis of *Gpr139* (red) and *Drd2* (white) mRNA in mouse mid brain. Yellow arrows indicate colocalization of *Gpr139* and *Drd2* mRNA in the same cells. The nuclei of cells were stained with DAPI. Images from Wang *et al.*, *Frontiers in Neuroscience,* 2019.

Kappa opioid receptors drive a tonic aversive component of chronic pain[28]

Reported by Liu et al., J Neurosci, 2019

Pain is a multidimensional experience and how much the pain is "bothersome" significantly impacts the sufferers' quality of life. The kappa opioid system, functioning through kappa opioid receptors (KORs), contributes to depressive and dysphoric states but whether it contributes to the emotional component of chronic pain remains tenuous. Liu *et al.* showed that KORs are enough to drive the emotional part of chronic pain that is argued to significantly impact a patient's quality of life. Antagonists to KORs can act as therapeutic adjuvants to alleviate the emotional component of pain. The RNAscope Multiplex Fluorescent assay was used to examine KOR expression in a mouse model of chronic pain (PNI, peripheral nerve injury) and connect expression to function (Figure 33).

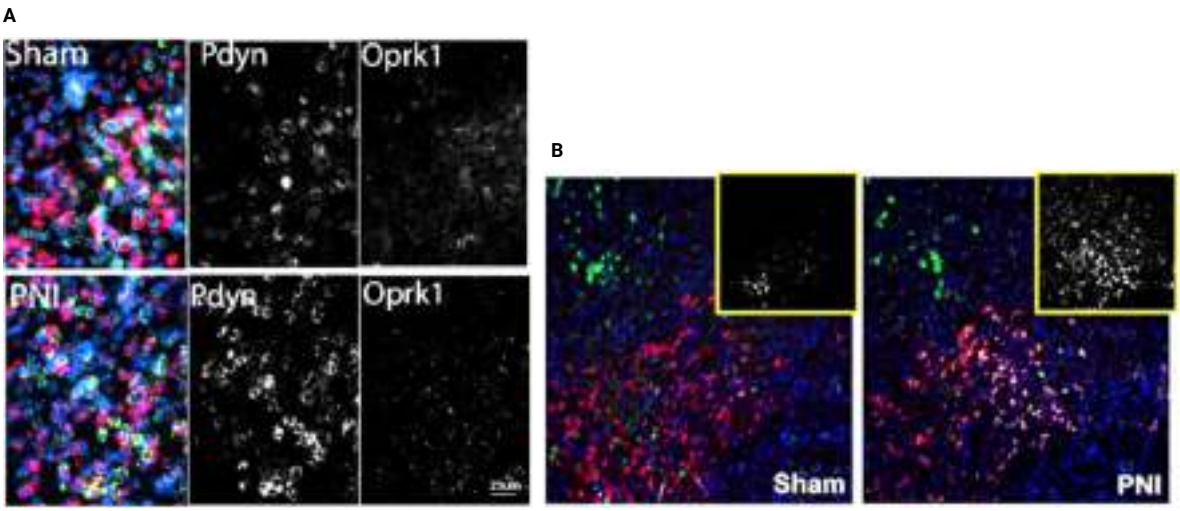

FIGURE 33. A. Detection of the kappa opioid receptor (*Oprk1*, white), pro-dynorphin (*Pdyn*, green) and pro enkephalin (*Penk,* pink) using with RNAscope Multiplex Florescent assay in the nucleus accumbens (NAc) of pain-naive, sham and PNI mice. Scale bar 25 µm. B. Detection of the kappa opioid receptor (*Oprk1*, white) with the RNAscope Multiplex Florescent assay in both GABA+ (green, identified by *Gad*) and tyrosine hydroxylase+ (*TH*, red) neurons in the ventral tegmental area (VTA) of male mice. Images from *Liu et al. J Neurosci*, 2019.

In situ detection of ion channels in the nervous system using the RNAscope Assay

Ion channels, which are another class of membrane protein, also constitute a challenging class of targets for antibody development since they must remain membrane-associated to maintain their native conformation. Examples for the detection of ion channels can be found in Figure 34. Altogether, the RNAscope technology is an ideal method to visualize these targets within their morphological context in the central and peripheral nervous system.

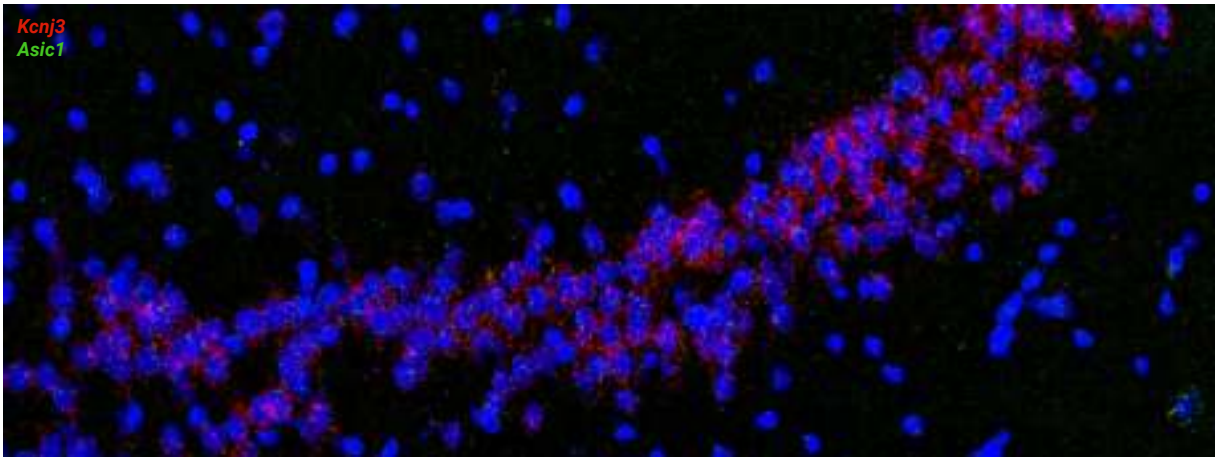

FIGURE 34. Fluorescent detection of ion channels. Detection of Sodium Acid- Sensing Ion Channel 1 (*Asic1*, green) and Inwardly Rectifying Potassium Channel 3 (*Kcnj3*, red) in normal mouse brain hippocampus using the RNAscope Multiplex Fluorescent assay on fresh frozen tissue samples.

Related publications

Below are a few examples of recent peer-reviewed publications illustrating how researchers have taken advantage of the RNAscope technology as an alternative assay to specifically detect ion channels in the morphological context of the brain.

Near-Perfect Synaptic Integration by Nav1.7 in Hypothalamic Neurons Regulates Body Weight[29]

Reported by Branco et al., Cell, 2016

The loss of Nav1.7 in hypothalamic neurons disrupts the regulation of body weight. The necessity of Nav1.7–dependent synaptic integration for the control of body weight was shown by body weight differences between control mice and mice depleted for Nav1.7 in AGRP (POMC and PVH) neurons after 8 weeks on a regular mouse diet. Through colocalization of *Scn9a* (or Nav1.7 channel) mRNA with both *Agrp* or *Pomc* mRNA, Branco *et al.* showed that this sodium channel is expressed in both AGRP and POMC neurons (Figure 35).

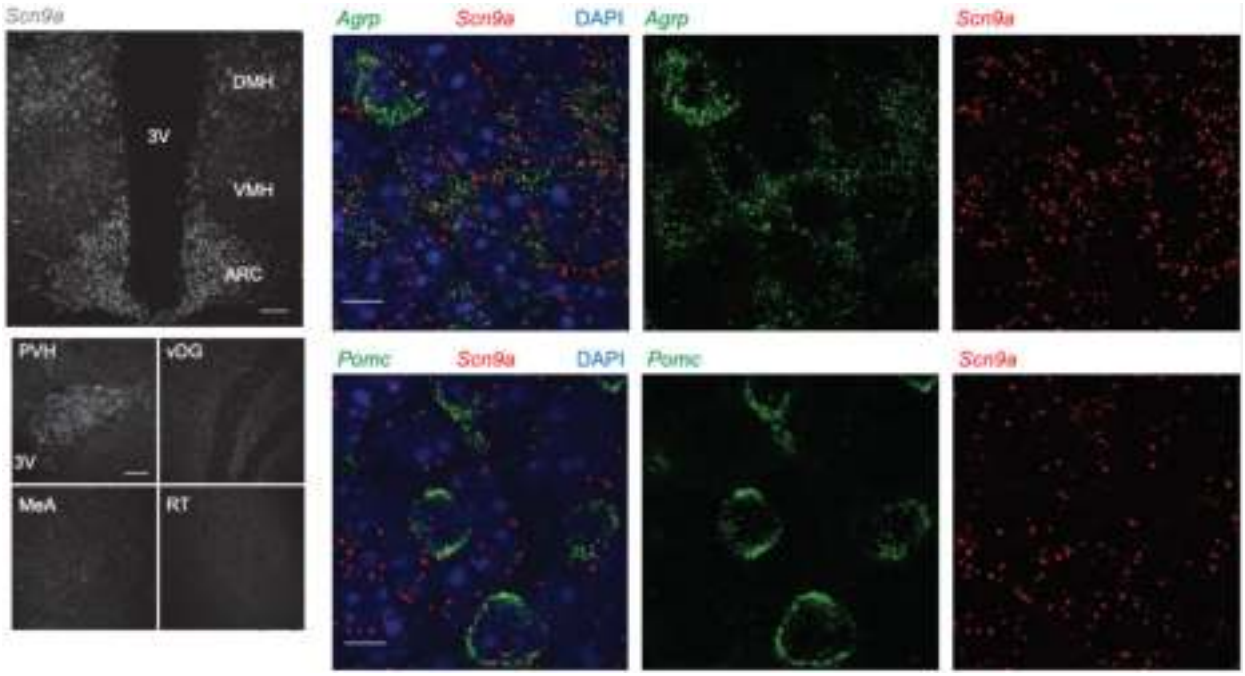

FIGURE 35. Detection of Nav1.7 in AGRP and POMC Neurons. Left: RNAscope detection of *Scn9a* (white) in the ARC and DMH, but not in the VMH. 3V, third ventricle. Scale, 100 mm. Right: RNAscope Multiplex Fluorescent detection of *Agrp* (green) and *Scn9a* (red) or *Pomc* (green) and *Scn9a* showing extensive colocalization. Blue, DAPI. Images from Branco *et al., Cell*, 2016.

Shedding light on human cerebral cortical folding and channelopathies[30]

Reported by Smith et al., Neuron, 2018

Channelopathies are responsible for a range of brain disorders and are caused by abnormal ion channel function. There is a need for better understanding of the underlying pathophysiology of these channel-based disorders, as individuals presenting with clinical phenotypes are difficult to diagnose and treat.

Smith *et al.*, discovered an unexpected association between one channelopathy, connecting sodium channels to cortical folding and brain development. They described an abnormal developmental disorder of the brain, polymicrogyria (PMG), that is associated with pathogenic variants in the sodium channel gene *SCN3A*. They showed that *SCN3A* is robustly expressed in cerebral cortex during foetal gestation but downregulated after birth. Conversely, *SCN1A* is lower during gestation and upregulated postnatally.

They used the RNAscope Multiplex Fluorescent Assay in foetal human brain and revealed the highest *SCN3A* expression in the cortical plate (CP), which contains immature neurons whereas the adult human cortex showed very low *SCN3A* expression across all cortical layers (Figure 36).

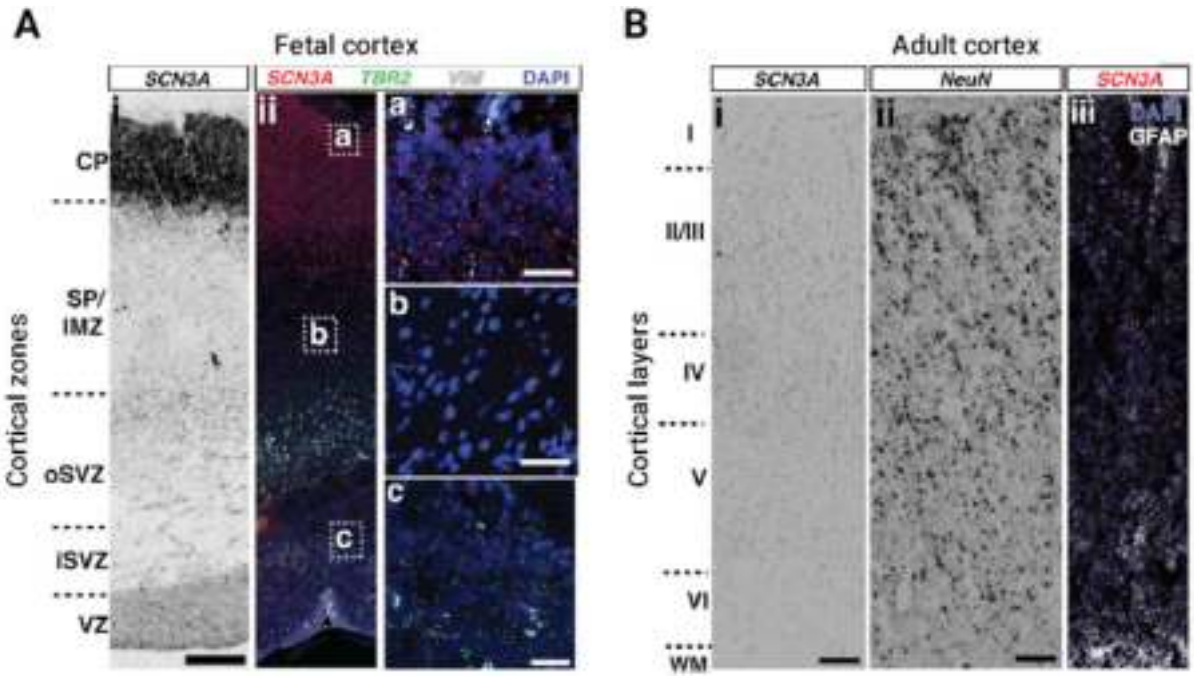

FIGURE 36. A. The RNAscope Multiplex Fluorescent assay shows the specific cortical layer and cell type expression pattern of *SCN3A* in human fetal brain. Most highly expressed in progenitor cells located in the CP, oSVZ, and iSVZ cortical zones. *TBR2* (green) intermediate progenitor marker, *VIM* (white) neural progenitor marker. B. RNAscope Multiplex Fluorescent assay showed very low *SCN3A* expression across all cortical layers in adult human brain. *NeuN* (*RBFOX3*): neuronal marker *GFAP*: astrocytes. Images from Smith *et al., Neuron*, 2018.

Listen to the interview :
acdbio.com/science/applications/research-areas/neural-development

Listen to the interview from Dr Richard S. Smith, Postdoctoral Research Fellow, Department of Genetics and Genomics, Boston Children's Hospital and Harvard Medical School.

Detection of Long Non-Coding RNAs (lncRNA) in the Brain

Long non-coding RNAs (lncRNAs) are a large and diverse class of RNA transcripts with a length of more than 200 nucleotides and no protein-coding potential. Most recent statistics from GENCODE3 (v31, March 2019) show that the human genome contains 23,025 non-coding genes, surpassing the number of protein-coding genes (19,950). About 70% (15,767) of these non-coding genes code for long non-coding RNAs (lncRNAs). Recent studies have suggested the involvement of lncRNAs in neurodevelopment and brain function. Despite their functional importance, the mechanisms by which lncRNAs control cellular processes are still elusive. The RNAscope technology can shed light on the brain-enriched lncRNA functionality by visualizing tissue-restricted expression patterns, localization of lncRNAs to distinct subcellular structures, and expression regulation. Figure 37 depicts the expression for two lncRNAs, *Neat1* and *Malat1*, in the mouse hippocampus.

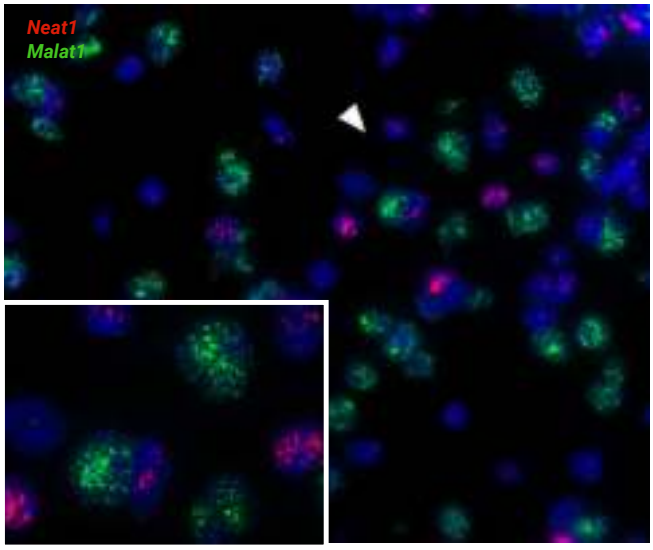

FIGURE 37. Detection of lncRNA in normal mouse brain hippocampus using the RNAscope Multiplex Fluorescent assay on fresh frozen tissue samples: *Neat1* (red) and *Malat1* (green). Cells are counterstained with DAPI.

Further information about lncRNA detection using the RNAscope assay:
acdbio.com/science/applications/research-solutions/long-non-coding-rna

Related publications

Below are a few examples of recent peer-reviewed publications illustrating how researchers have taken advantage of the RNAscope visualize lncRNAs in the tissue context.

The long noncoding RNA Pnky regulates neuronal differentiation of embryonic and postnatal neural stem cells[31]

Reported by Ramos et al., Cell Stem Cell, 2015

Ramos *et al*. identified a novel neural-specific lncRNA, Pinky (*Pnky*), which regulates neurogenesis from neural stem cells (NSCs) in the embryonic and postnatal brain. Using the RNAscope assay, they demonstrated the mostly nuclear expression of *Pnky* in ventricular-subventricular zone (V-SVZ) of NSC cultures and in the V-SVZ of the adult mouse brain (Figure 38).

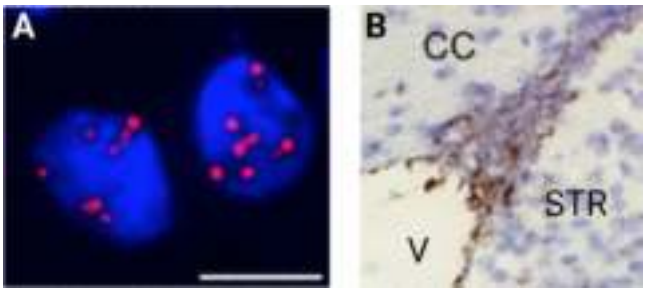

FIGURE 38. A. Detection of *Pnky* lncRNA in V-SVZ NSC cultured cells using the RNAscope Fluorescent Multiplex Assay. Nuclei are counterstained with DAPI. B. Detection of *Pkny* lncRNA in adult mouse coronal brain sections using RNAscope HD Reagent Kit-BROWN. Nuclei are counterstained with hematoxylin. V: ventricle, CC: corpus collosum, STR: striatum. Images from Ramos *et al., Cell Stem Cell*, 2015.

ALS-linked FUS mutations confer loss and gain of function in the nucleus by promoting excessive formation of dysfunctional paraspeckles[32]

Reported by An et al., Acta Neuropathologica Communications, 2019

FUS is an essential component of paraspeckles, which are subnuclear bodies assembled on the lncRNA *NEAT1*. Paraspeckle functions include sequestration of RNAs and transcription factors and thus regulation of gene expression. Dysfunction of paraspeckle components has been identified as a pathological marker in many diseases, including cancer, autoimmune, and neurodegenerative diseases such as amyotrophic lateral sclerosis (ALS). Mutations in FUS cause ALS, however it is still unknown how endogenous levels of mutant FUS would affect *NEAT1*+ paraspeckles. In this study, An *et al*. identified excessive assembly of dysfunctional paraspeckles as a novel nuclear pathology caused by FUS mutations. They used the RNAscope assay in combination with the Hs-NEAT1_2 probe, which detects both the long and short forms of *NEAT1*, to visualize the accumulation of paraspeckles in ALS human spinal cord cells as compared to low expression in healthy cells (Figure 39).

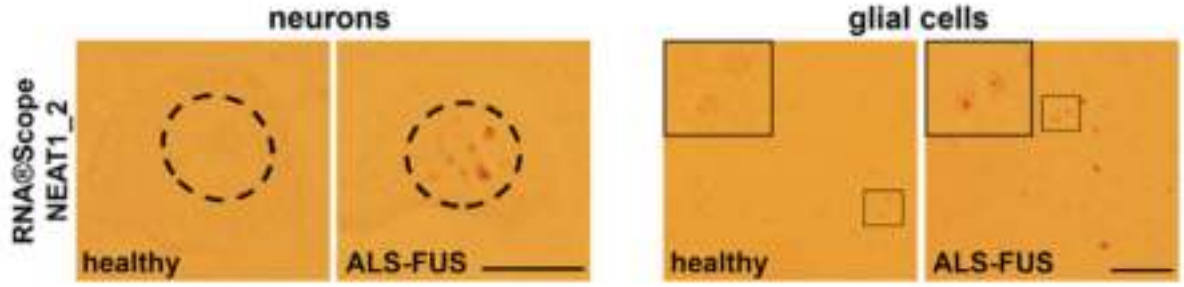

FIGURE 39. Accumulation of paraspeckles in spinal neurons and glial cells from healthy or ALS patients with mutant FUS. Examples of paraspeckles in spinal neurons (left panels) and glial cells (right panels) in an ALS-FUS patient visualised with the RNAscope assay using Hs-NEAT1_2 probe. Neuronal nuclei are circled. Images from An *et al.*, *Acta Neuropathologica Communications*, 2019.

Visualization of Neuronal Network Activity and Plasticity

During learning and memory formation, gene expression is dynamically regulated in response to experience-dependent neuronal activity. In particular, the expression of immediate-early genes (IEGs) such as *c-fos* and *Arc* is rapidly and transiently altered in specific neurons or neuronal ensembles in brain areas involved in the learning and memory processing of a certain task/activity. Therefore, the visualization of IEG mRNA expression patterns have widely been used as a molecular readout for neuronal populations that are engaged in generating and encoding long-term memories.

The multiplexing capability of the RNAscope assay enables IEG mRNA detection in combination with other targets or cell type markers, providing further characterization of activated neuronal cell populations. The detection of neuronal activity in the mouse brain hippocampus is shown by using a probe for *c-fos*, which is a proto-oncogene and transcription factor that is induced within 15 minutes of stimulation (Figure 40). To detect neuronal plasticity, the expression of the effector immediate early gene Activity-Regulated Cytoskeleton-associated protein *Arc* (also known as *Arg3.1*) is visualized in Figure 41.

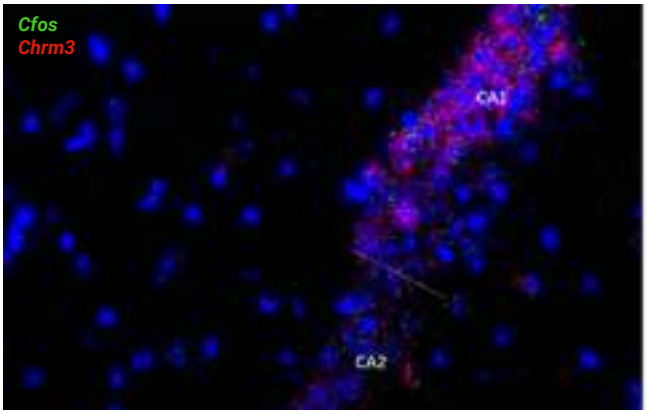

FIGURE 40. Detection of the transcription factor immediate early gene and activity marker *c-fos* (green) in combination with the GPCR Cholinergic Receptor Muscarinic 3 (*Chrm3*, red) in normal mouse brain hippocampus using the RNAscope Multiplex Fluorescent assay on fresh frozen tissue samples. Cells are counterstained with DAPI. CA = Cornu Ammonis.

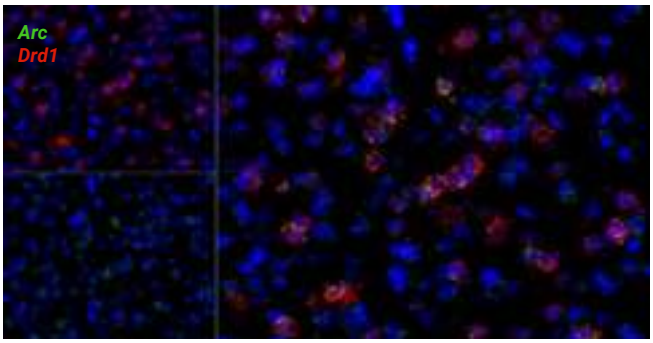

FIGURE 41. Detection of the effector immediate early gene and plasticity marker *Arc* (green) in combination with the G protein-coupled Dopamine Receptor D1 (*Drd1*, red) in normal mouse brain striatum using the RNAscope Multiplex Fluorescent assay on fresh frozen tissue samples.

Related publications

Below are a few examples of recent peer-reviewed publications illustrating how researchers have taken advantage of the RNAscope technology to visualize neuronal activity and plasticity.

Reactivation of recall-induced neurons in the infralimbic cortex and the basolateral amygdala after remote fear memory attenuation[33]

Reported by Khalaf et al., Front. Mol. Neurosci., 2019

Post-traumatic stress and other anxiety disorders lead to long-lasting memories that can be recalled for months in mice and for years in humans. Due to the persistent nature of traumatic memories, it has been shown that early interventions are of prime importance, with the most effective treatments for traumatic memories being exposure-based therapies. The areas of the brain that are involved in remote fear memory storage include basal lateral amygdala (BLA) but not adjacent central amygdala (CeA). Khalaf *et al.* used the RNAscope assay to reveal that cytoplasmic *Homer1a* and nuclear *c-Fos* were upregulated only in the BLA upon memory recall. The RNAscope Multiplex Fluorescent assay allowed the subcellular visualization of immediate early genes (IEGs) enabling detection of (re)activation of various brain regions (Figure 42).

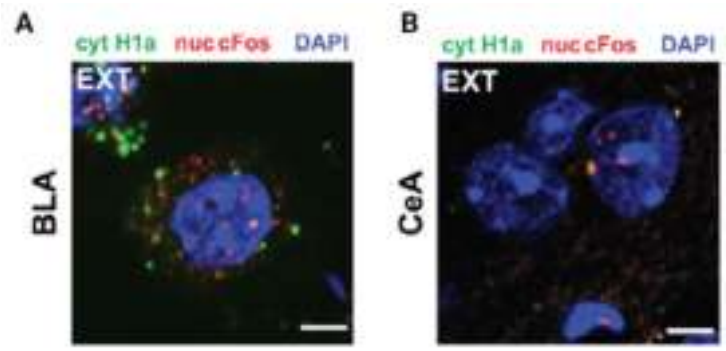

FIGURE 42. Detection of *Homer1a* and *c-Fos* mRNA in the BLA (A) and CeA (B) upon remote fear memory attenuation (A) using the RNAscope Multiplex Fluorescent assay. Images from Khalaf *et al., Front. Mol. Neurosci.*, 2019.

Massively parallel single nucleus transcriptional profiling defines spinal cord neurons and their activity during behavior[34]

Reported by Sathyamurthy et al., Cell Reports, 2018

Sathyamurthy *et al.* developed an atlas of adult mouse spinal cord cell types and molecularly characterized 43 neuronal populations that can be used to identify activated populations following behavior. They used the RNAscope Multiplex Fluorescent assay for the validation of neuronal populations (Figure 43, labeled by key markers in red) that were activated (upregulated *c-fos* expression in green) by formalin injection induced pain (sensory).

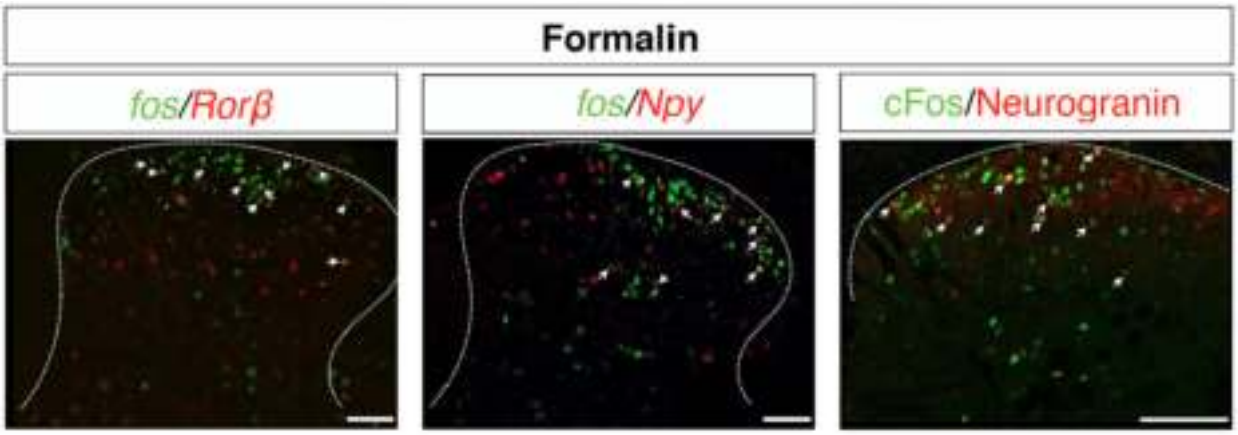

FIGURE 43. Experimental validation of clusters associated with formalin injection induced pain (sensory), as detected by snRNA-seq. For each cluster, a marker protein (Npy or Neurogranin) was compared with *c-fos* RNA expression using the RNAscope Multiplex Fluorescent assay (scale bars, 100 mm). Images from Sathyamurthy *et al., Cell Reports*, 2018.

Validation and Spatial Mapping of Gene Signatures Identified by Single Cell RNA Sequencing Analysis

Characterizing the transcriptomic profiles of individual cells by single-cell RNA sequencing (scRNA-seq) has become a universal tool to identify both known and novel cell populations and to understand tissue structure and function, ushering in a new era of single cell biology. This has proven to be especially true in complex organs with high cellular heterogeneity, such as the mammalian brain. However, scRNA-seq utilizes dissociated cells and results in the loss of spatial organization of the cell population being analyzed. Confirmation and spatial mapping of scRNA-seq results can be obtained using assays that retain spatial organization, such as the RNAscope ISH technology.

The multiplexing capabilities of the RNAscope Multiplex Fluorescent assay, with simultaneous detection of up to 4 targets, and the new RNAscope HiPlex assay, with simultaneous detection of up to 12 targets in fresh frozen tissue samples, provide pivotal single cell imaging data to confirm and spatially map gene profiles identified by scRNA-seq in complex tissues (Figure 44).

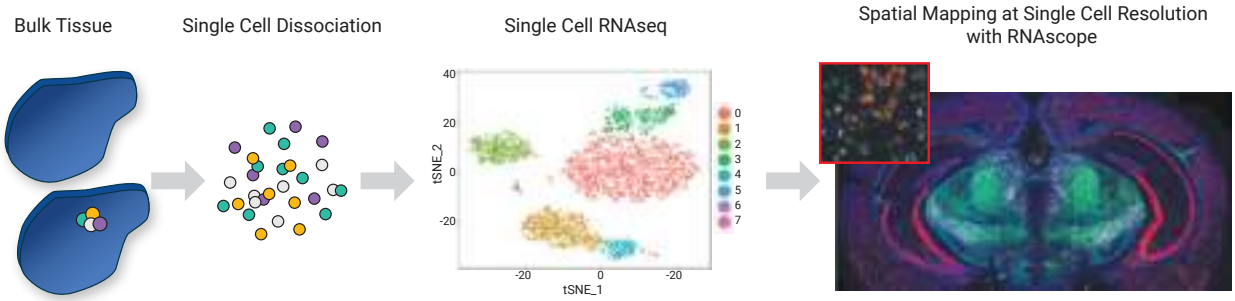

FIGURE 44. Incorporation of spatial mapping into single cell RNA sequencing workflows with the RNAscope technology.

The RNAscope Multiplex Fluorescent Assay and the RNAscope HiPlex Assay were used to confirm and spatially map the diverse cell types in the mouse striatum that have been previously identified by scRNA-seq[35] (Figure 45). The major and minor gene signatures identified by scRNA-seq, including discrete Drd1+ (D1) and Drd2+ (D2) medium spiny neuron (MSN) subtypes, were spatially resolved with the RNAscope assays (Figure 45).

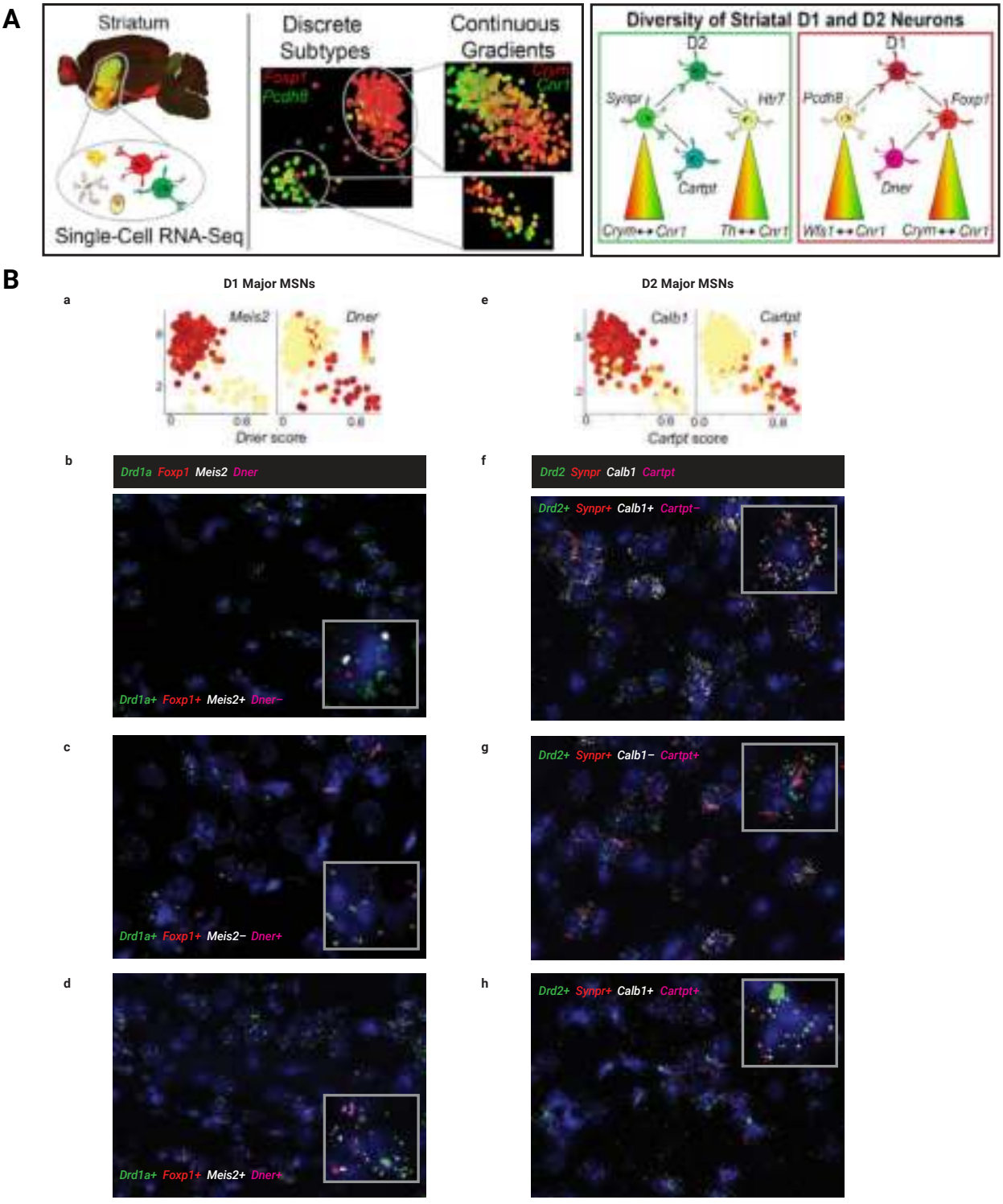

FIGURE 45. A. scRNA-seq reveals discrete striatal medium spiny neuronal (MSN) subtypes. Schematic depicting the striatal neuronal subpopulations identified by scRNAseq. Images from Gokce *et al., Cell Rep.*, 2016. B. Refinement of the major MSN subtypes in the mouse striatum. (a–d) Major Drd1a MSNs identified by scRNA-seq (a) and confirmed by the RNAscope Multiplex Fluorescent assay (b–d) to express *Drd1a* and *Foxp1* in combination with *Meis2* and/or *Dner*. (e–h) Major Drd2 MSNs identified by scRNA-seq (e) and confirmed by the RNAscope Multiplex Fluorescent assay (f–h) to express *Drd2* and *Synpr* in combination with *Calb1* and/or *Cartpt*. (A, a, e) Images from Gokce *et al., Cell Rep.*, 2016.

Further information about scRNAseq validation with the RNAscope assay:
acdbio.com/science/applications/research-solutions/ngsht-transcriptomic-validation-rna-seq

Find out more about the RNAscope HiPlex assay:
acdbio.com/rnascope%C2%AE-hiplex-assay

While multiplexing with 4 probes was sufficient to visualize the individual D1 and D2 subtypes on separate sections, simultaneous detection of both the D1 and D2 subtypes on the same striatal section was needed to fully assess the two populations in the same spatial orientation. To detect all the D1 and D2 subtypes on the same section, we employed the RNAscope HiPlex assay, which provides signal amplification for up to 12 RNA targets on the same tissue section by performing iterative fluorescent imaging in groups of 4 targets at a time (Figure 46).

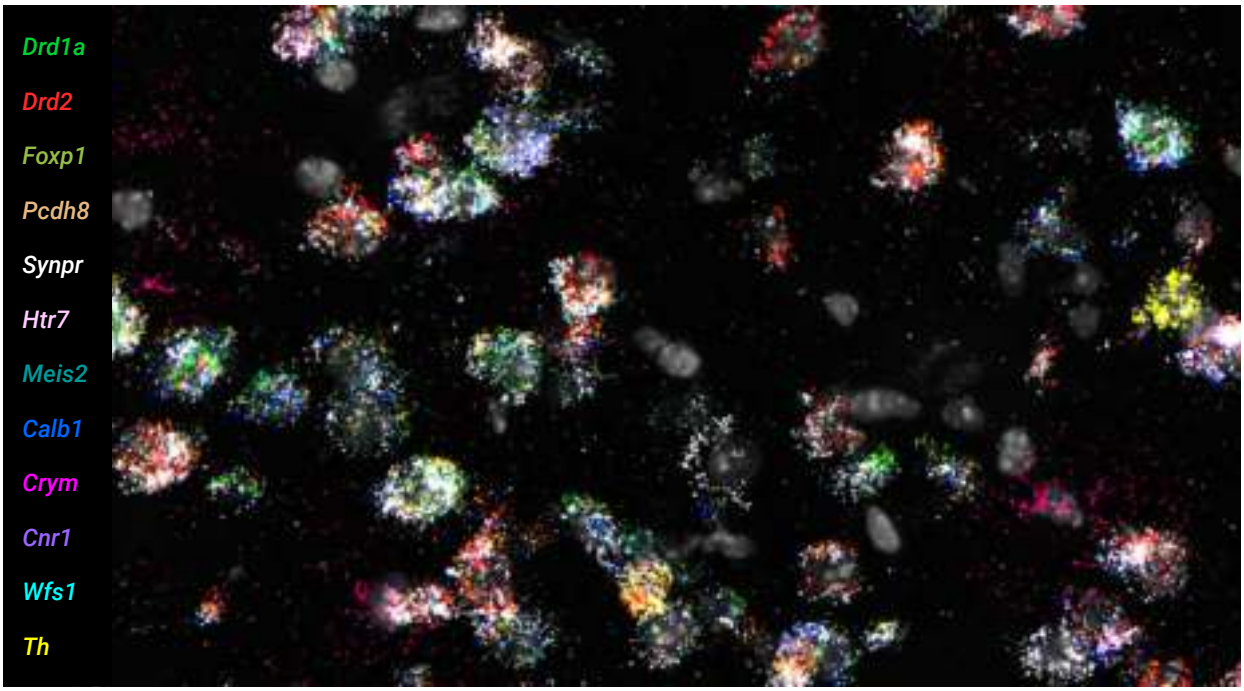

FIGURE 46. The RNAscope HiPlex assay for 12 targets provides comprehensive spatial mapping of the D1/D2 striatal MSN subtypes simultaneously in the tissue context.

Related publications

Below are a few examples of recent peer-reviewed publications illustrating how researchers have taken advantage of the RNAscope technology to complement their scRNAseq analyzes by validating and spatially mapping their transcriptomic results in the tissue context.

Neuronal atlas of the dorsal horn defines its architecture and links sensory input to transcriptional cell types[36]

Reported by Häring et al., Nature Neuroscience, 2018

The dorsal horn of the spinal cord plays a critical role in sensory processing in response to different chemical, thermal or mechanical stimuli. Aberrations in these circuits results in chronic pain. A comprehensive molecular classification and spatial map of dorsal horn neurons is essential for identifying their functional role in normal and pathological sensory processing. Häring *et al.* identified 15 glutamatergic excitatory and 15 GABAergic inhibitory neurons organized in a multilayered pattern defined by cell type. Distinct neurons are activated in response to heat and cold stimuli indicating functionally specialized circuits.

The RNAscope Multiplex Fluorescent assay was used for validation of scRNA-seq results *in vivo*, thus confirming the existence of the 30 total distinct molecular subtypes of neurons in the spinal cord (Figure 47). Spatial analysis with the RNAscope Multiplex assay revealed an organizational pattern of neuronal subtypes in multiple discrete layers.

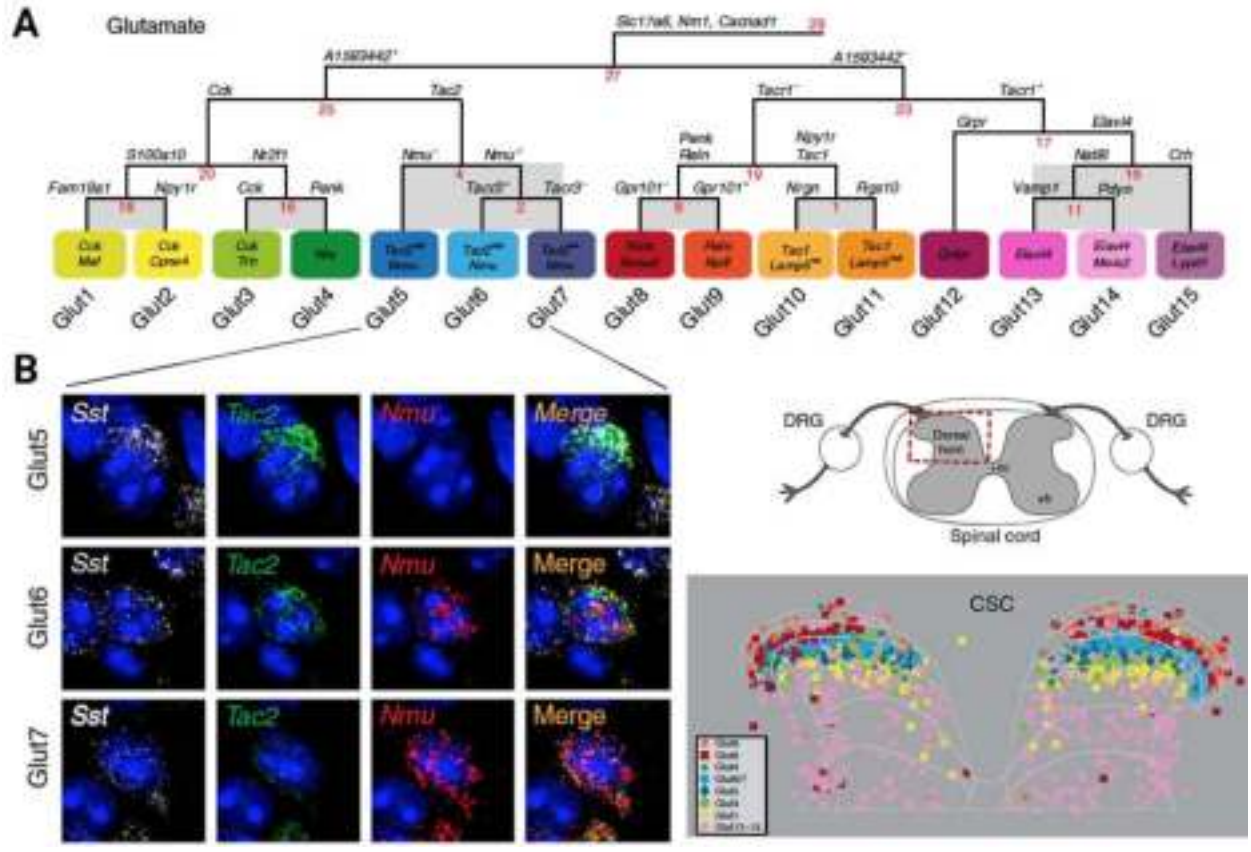

FIGURE 47. A, Identification of 15 molecular subtypes of glutamatergic neurons by single-cell RNA seq. B, RNAscope Multiplex for *in situ* validation of neuronal subtypes in spinal cord tissue. C, Spatial map of glutamatergic neurons in the cervical spinal cord (CSC). Images from Häring *et al.*, *Nature Neuroscience*, 2018.

Single-cell transcriptomics of the developing lateral geniculate nucleus reveals insights into circuit assembly and refinement[37]

Reported by Kalisch et al., PNAS, 2017

Early patterning and cell-type specification of the central nervous system cause changes in gene expression. As not much is known about how changes influence the later stages of circuit assembly and refinement Kalish *et al.* examined the developing dorsal lateral geniculate nucleus (LGN) across four time points by applying single-cell RNA sequencing in a mouse model. Through analysis of all cells across all time points, they identified 29 cell clusters with distinct gene expression signatures with greater than 100 cells per cluster. Based on the expression of markers Stmn2 and Snap25 clusters were divided into 8 neuronal and 19 non-neuronal clusters. Those non-neuronal clusters were then grouped into oligodendrocytes, microglia, astrocytes, endothelial cells, pericytes, and macrophages. They used the RNAscope Multiplex Fluorescent assay to confirm that non-overlapping populations of cells in the LGN expressed those markers (Figure 48).

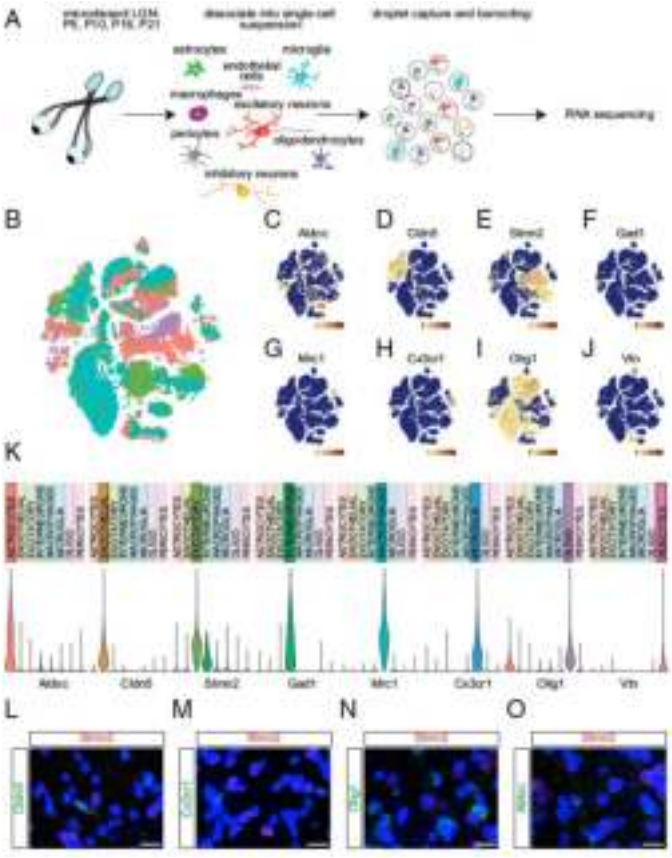

FIGURE 48. Capture, sequencing, and classification of cell types. (A) Schematic of the experimental design. Dorsal LGNs were microdissected from mice at four developmental ages: P5, P10, P16, or P21. Tissue was dissociated into a single-cell suspension, and then cells were captured and barcoded using the in Drops platform. Libraries were prepared and whole-transcriptome RNA sequencing was performed. (B) t-SNE plot of all cell types clustered by principal component analysis. Purple, P5; pink, P10; green, P16; teal, P21. (C) Expression pattern of the astrocyte marker *Aldoc* across cell clusters. (D) Expression pattern of the endothelial cell marker *Cldn5* across cell clusters. (E) Expression pattern of the excitatory neuron marker *Stmn2* across cell clusters. (F) Expression pattern of the inhibitory neuron marker *Gad1* across cell clusters. (G) Expression pattern of the macrophage marker *Mrc1* across cell clusters. (H) Expression pattern of the microglial marker *Cx3cr1* across cell clusters. (I) Expression pattern of the oligodendrocyte marker *Olig1* across cell clusters. (J) Expression pattern of the pericyte marker *Vtn* across cell clusters. (K) Violin plots displaying normalized expression levels of each cell type-specific marker across all cell types. (L–O) Confocal images of coronal LGN sections following FISH, probed for the excitatory neuron marker *Stmn2* (red) and endothelial cell marker *Cldn5* (green; L); microglial marker *Cx3cr1* (green; M); oligodendrocyte marker *Olig1* (green; N); and astrocyte marker *Aldoc* (green; O). Images from Kalisch *et al., PNAS,* 2017.

Molecular Architecture of the Mouse Nervous System[38]

Reported by Zeisel et al., Cell, 2018

Zeisel *et al.* utilized scRNAseq to sequence 500,000 single cells to create a detailed molecular survey of cell types in the mouse nervous system (Figure 49). In addition, they mapped cell types spatially and derived a hierarchical, data-driven taxonomy. They also found neurons to be the most diverse cell type in the nervous system and therefore grouped them by developmental anatomical units and by the expression of neurotransmitters and neuropeptides. They found seven distinct, locally restricted astrocyte types that obeyed developmental boundaries and correlated with the spatial distribution of key glutamate and glycine neurotransmitters. However, oligodendrocytes showed a loss of local identity followed by a secondary diversification.

This study provides a single-cell transcriptional profiling of the adult mouse nervous system and uncovers new cell classes and types across regions, providing a clearer picture of cell diversity by region and a reference atlas for studying the mammalian nervous system. They used the RNAscope Multiplex Fluorescent to validate the identity and spatial distribution of astrocyte cell types (Figure 49).

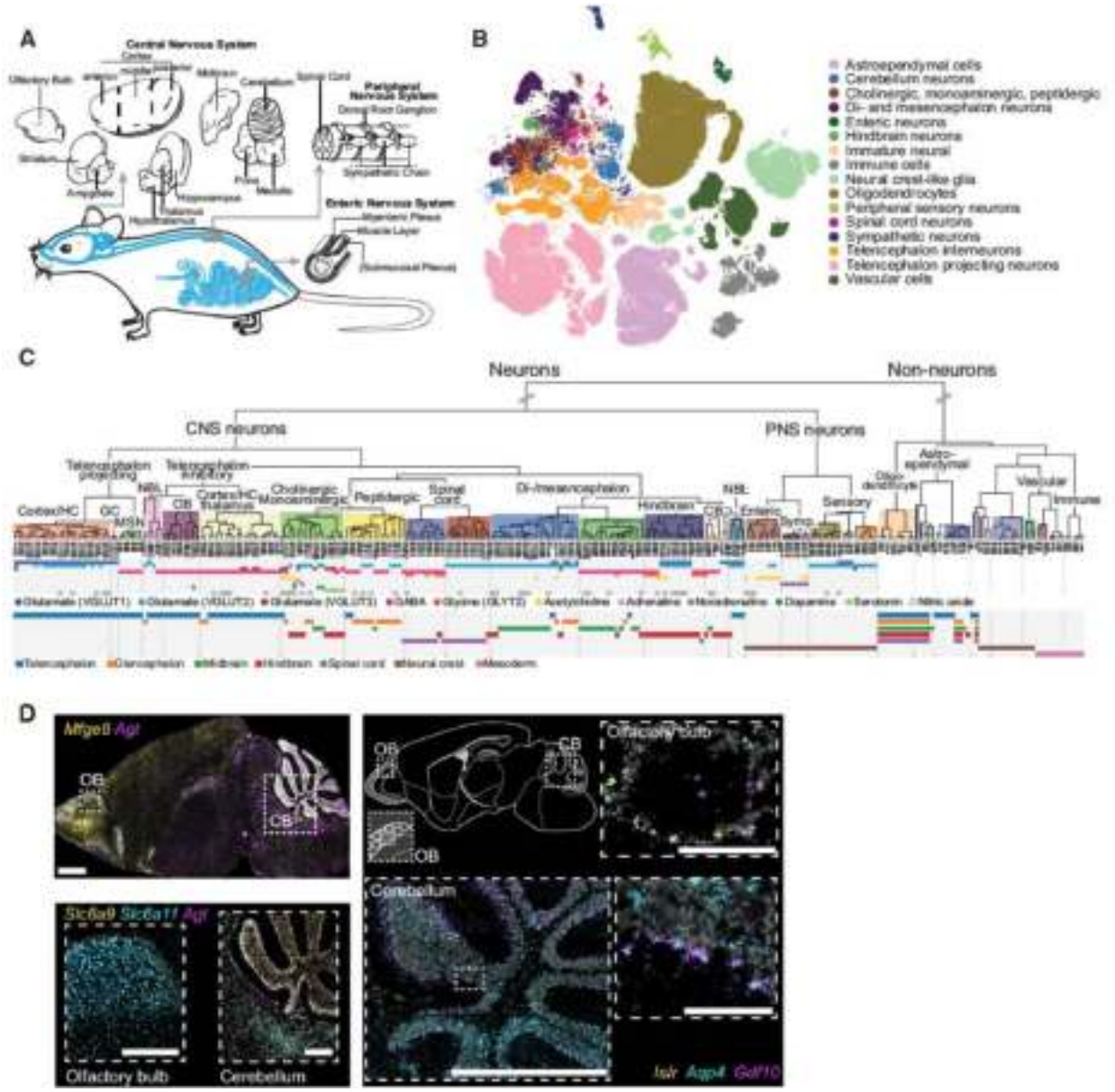

FIGURE 49. Molecular Survey of the Mouse Nervous System Using Single-Cell RNA Sequencing. (A) Schematic illustration of the sampling strategy. The brain was divided into coarse anatomical units, and in addition, we sampled from the spinal cord, dorsal root ganglia, sympathetic ganglion, and enteric nervous system. (B) Visualization of the single-cell data using gt-SNE embedding. Cells are coloured by rank 3 taxonomy units indicated in the legend. (C) Dendrogram describing the taxonomy of all identified cell types. Main branches, corresponding to the taxonomy, are annotated with labels and coloured background. The neurotransmitter used by each cell type is indicated below the leaves as coloured circles. (D) Validation of spatial distribution of astrocytes cell types using multiplex ISH (RNAscope). Images from three consecutive sections were aligned and overlaid to generate a composite with dots representing cells (upper panel). Below, high-magnification images show details of spatial location. Images from Zeisel *et al., Cell,* 2018.

In Situ Visualization of Splice Variants, circRNAs, and Short Targets Using the BaseScope Assay

The BaseScope assay enables the specific detection of exon junctions, splice variants, highly homologous sequences, short targets, and point mutations, with single cell detection sensitivity in a broad range of tissues, samples and species.

Detection and visualization of EGFRvIII splice variant in human glioblastoma

The epidermal growth factor receptor (EGFR) is overexpressed in a variety of human epithelial tumors, often because of gene amplification, including primary glioblastoma (GBM). Tumors with EGFR gene amplification frequently contain EGFR gene rearrangements, with the most common extracellular domain mutation being EGFRvIII, which results from an in-frame deletion of exons 2–7. About 50% of GBM patients with EGFR amplification harbor the EGFRvIII variant. However, EGFRvIII can also be present independently of EGFR amplification.

In this case study, BaseScope probes (Figure 50 and Figure 51) were used to detect expression of EGFR and EGFRvIII in glioblastoma tissue, demonstrating that the BaseScope assay can be used successfully to:

- Analyze exon junction in FFPE sample
- Visualize low to overexpression of a specific target
- Differentiate expression of wild type and splice variant
- Localize co-expression of wild and mutant variant in tissue
- Demonstrate heterogeneous expression of variants within a tissue sample

Four BaseScope probes were designed to detect specific exon junctions, as shown in Figure 47. Probes E1–E2 and E7–E8 are specific to EGFR, while probe E8-E9 detects both EGFR and EGFRvIII and probe E1–E8 will detect specifically EGFRvIII.

Further information about splice variant detection with the BaseScope assay:
acdbio.com/science/applications/research-areas/splice-variant

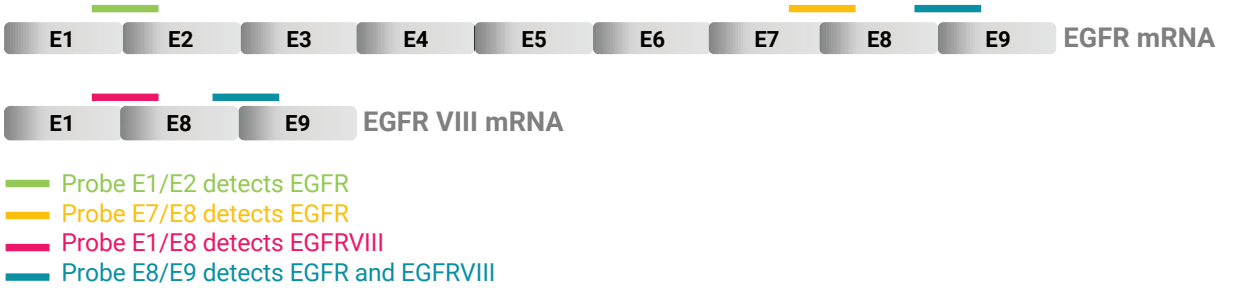

FIGURE 50. Schematic of BaseScope probe design for detection of *EGFR* and *EGFRVIII*.

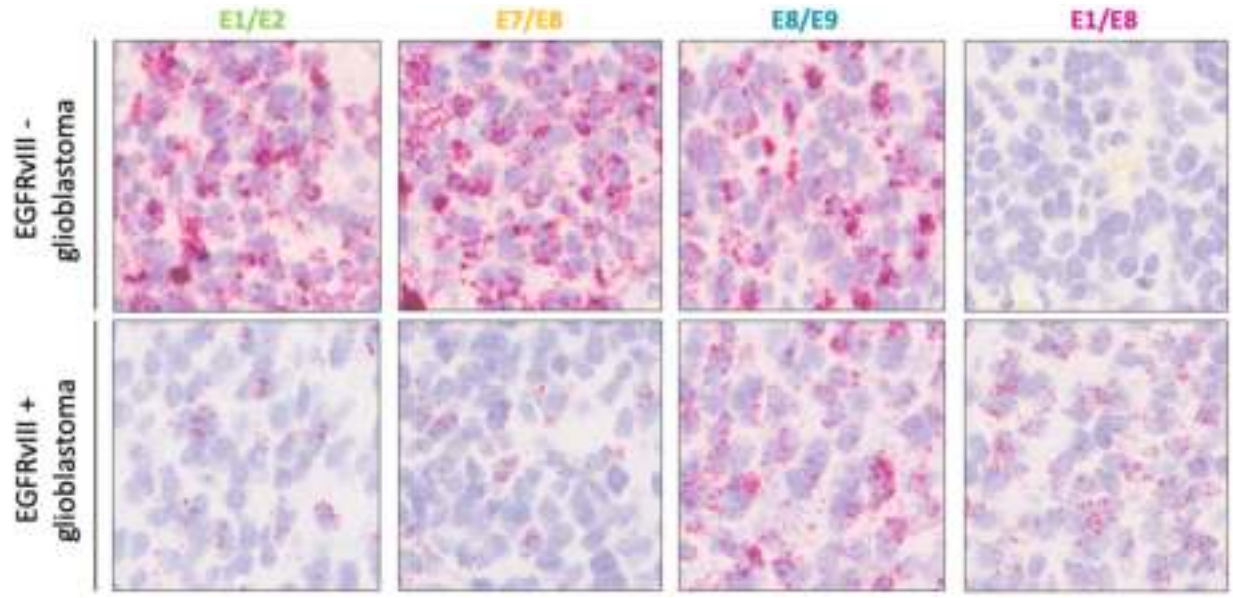

FIGURE 51. Detection of *EGFR* and *EGFRvIII* mRNA using the BaseScope assay on a WHO Grade IV glioblastoma case shows expression of *EGFR* and of the mutant variant *EGFRvIII*.

Related publications

Below are a few examples of recent peer-reviewed publications illustrating how researchers have taken advantage of the BaseScope assay to visualize splice variants and short targets in the tissue context.

A novel ultrasensitive *in situ* hybridization approach to detect short sequences and splice variants with cellular resolution[39]

Reported by Erben et al., Molecular Neurobiology, 2017

Erben *et al.* used the BaseScope assay to investigate the expression of four splice variants encoding four isoforms of the neuregulin (NRG) receptor ErbB4 in the mouse brain with single cell resolution (Figures 52–54). Alternative splicing of exons encoding two juxtamembrane (JMa/JMb) and two cytoplasmic (CYT-1/CYT-2) domains alter receptor stability and signaling modes, respectively (Figure 52). NRG/ErbB4 signaling pathway is reported to be associated with a risk for Schizophrenia (Scz). *ErbB4* transcript levels comprising JMa and CYT-1 exons are increased in the dorsolateral prefrontal cortex of Scz subjects and single nucleotide

polymorphisms in *ErbB4* correlate with changes in receptor isoform expression and risk for Scz. The four *ErbB4* isoforms differ functionally. Because of the different functions imparted by distinct *ErbB4* splice variants, it is critically important to identify the cells that express these distinct isoforms.

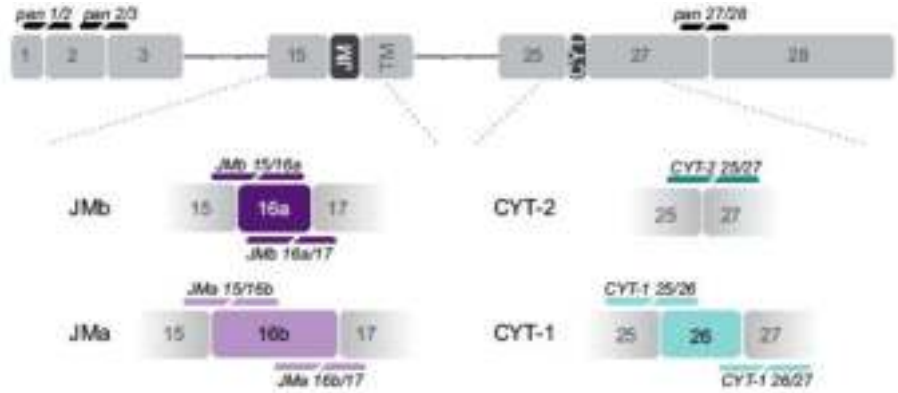

FIGURE 52. Scheme summarizing *ErbB4* isoforms.

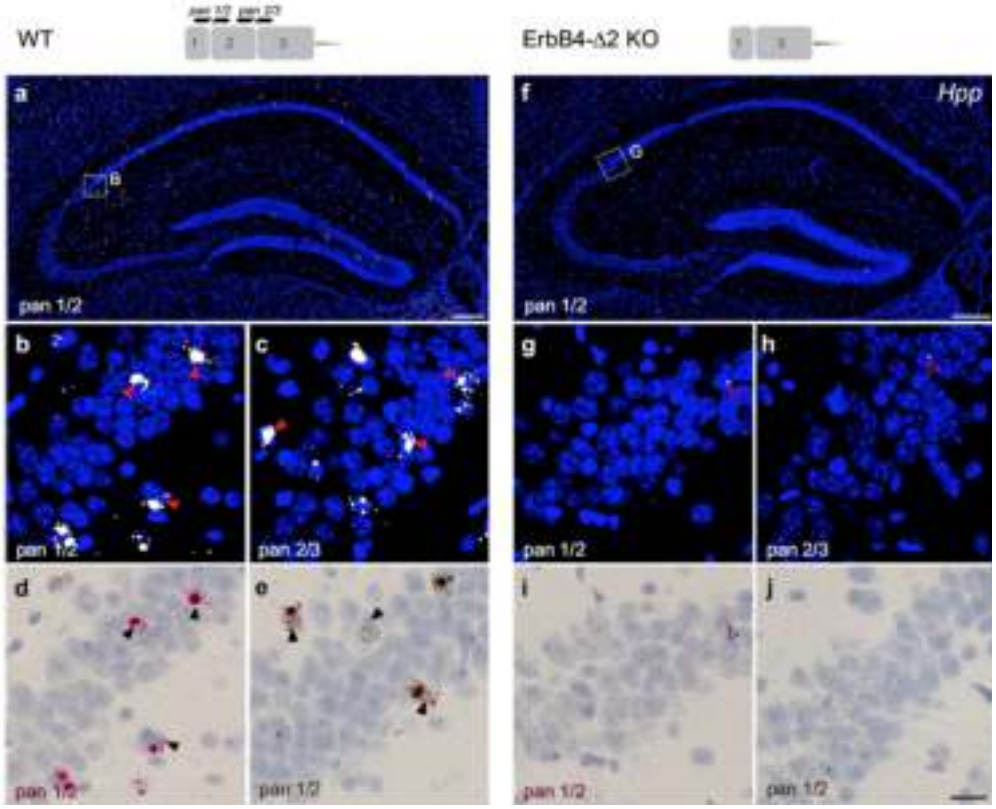

FIGURE 53. The specificity and sensitivity of single-pair probes targeting exon-exon boundaries were determined by hybridizing sections from WT (a-e) and ErbB4-Δ2KOmice (f-j). Probes targeting the exon 1/2 (pan1/2; a,b,d,e) or exon2/3 (pan 2/3; c) junctions—common to all *ErbB4* isoforms—labeled scattered cells in the WT hippocampus (arrowheads). (f-j) By contrast, neither probe generated signals in sections from ErbB4-Δ2 KO mice (background signal marked by open arrowheads). (b, g) Magnified insets in panels (a) and (f) are from area CA2. Signal can be detected by alkaline phosphatase and FastRed visible both in fluorescence (a-c, f-j) and bright field microscopy (d, i) or horseradish peroxidase and diaminobenzidine (e, j). Images from Erben *et al., Molecular Neurobiology*, 2017.

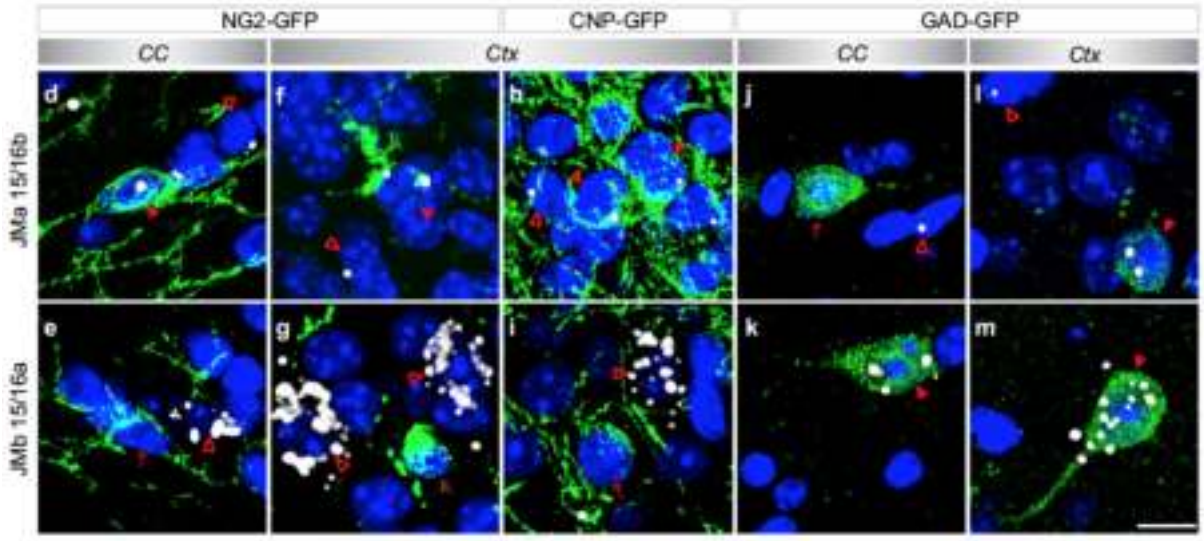

FIGURE 54. Oligodendrocytes and GABAergic neurons in the corpus callosum express different *ErbB4* juxtamembrane isoforms. (d–m) Isoform-specific BaseScope *in situ* hybridization using probes JMa 15/16b (d, f, h, j, l) and JMb 15/16a (e, g, i, k, m) was combined with IF for GFP (green) on sections from NG2-GFP (d– g), CNP-GFP (h, i) and GAD-GFP (j–m) transgenic mice. JM isoforms (white) were detected on GFP+ cells (red arrowheads), as well as on GFP negative cells (open red arrowheads) in the corpus callosum (CC) and the cortex (Ctx). Arrows depict GFP+ cells negative for JM probes. Images from Erben *et al., Molecular Neurobiology,* 2017.

Functional ectopic neuritogenesis by retinal rod bipolar cells (RBCs) is regulated by *miR-125b-5p* during retinal remodeling in RCS rats[40]

Reported by Fu et al., Scientific Reports, 2017

Retinitis pigmentosa (RP) is a form of inherited retinal degeneration that causes blindness in humans. During retinal degeneration, second-order retinal neurons gradually remodel, and this remodeling starts with bipolar cells.

Using Royal College of Surgeon (RCS) rat model to study retinal degeneration and remodeling, Fu *et al.* found that the microRNA *miR-125b-5p* was associated with retinal degeneration, and that it regulated dendritic growth and function in rod bipolar cells (RBCs). This study finding suggests that therapies that reduce *miR-125b-5p* expression could be beneficial in human retinal degenerative disease.

To determine the expression of *miR-125b-5p* in the retinae, the authors used BaseScope probes for the *miR-125b-5p* precursor microRNA *mir-125b* and found that the *mir-125b* signal was present in the outer plexiform layer (OPL), inner nuclear layer (INL) and ganglion cell layer (GCL). Combining the BaseScope assay with IF revealed that *mir-125b* co-localized with the rod bipolar cell (RBC) marker protein kinase C alpha (PKCα), which suggested that RBCs could be *miR-125b-5p* positive (Figure 55).

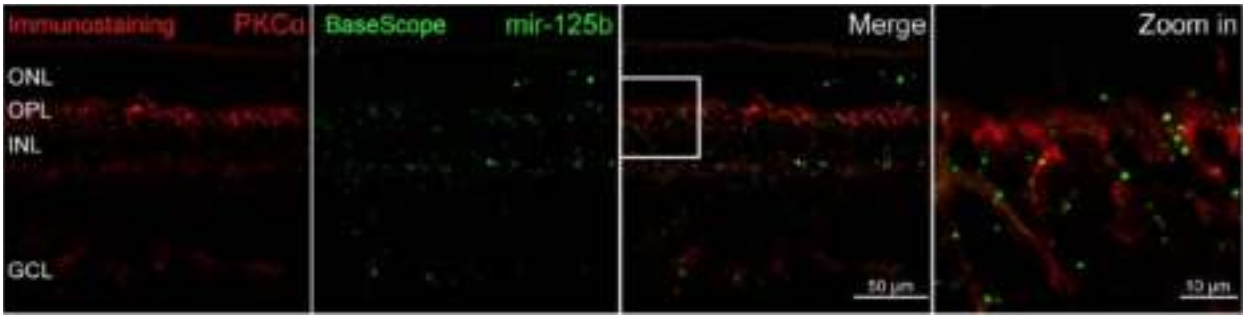

FIGURE 55. Detection of the precursor microRNA *mir-125b* (RNA, green) and PKCα (protein, red) in the retinae of P36 RCS rats using the BaseScope assay in combination with IF staining. Images from Fu *et al., Scientific Reports*, 2017.

In situ detection of circular RNAs using BaseScope Assay

Circular RNAs (circRNAs) are a recently identified class of ncRNAs that are generated by an alternative splicing mechanism that covalently links the 5' end of one exon with the 3' end of another exon. These highly conserved circRNAs are characterized by tissue- and developmental stage-specific expression patterns. More specifically, it was recently shown that circRNAs are particularly enriched in the brain with expression dynamics independent of the linear mRNA transcripts derived from the same gene. Although abundantly expressed in the nervous system, their function remains largely unknown. In addition, evidence has emerged for circRNA involvement in various diseases, including cancer, possibly by regulating gene expression levels through interaction with other molecules. The accurate detection and localization of circRNAs is pivotal to elucidate their biological functions especially given the fact that they could serve as putative clinical biomarkers.

Here, we highlight the anatomical localization and corresponding quantification of the linear mRNA and circRNA splice variant for the brain plasticity-related target *Dlgap1* in the developing mouse brain. Using the BaseScope assay we detected exon junctions specific to either the mRNA- or circRNA form of *Dlgap1* in the hippocampus of P1, P10 and P30 C57Bl/6J mouse brains (Figure 56 and Figure 57).

Further information about circRNA detection with the BaseScope assay:
acdbio.com/science/applications/research-solutions/circular-rna

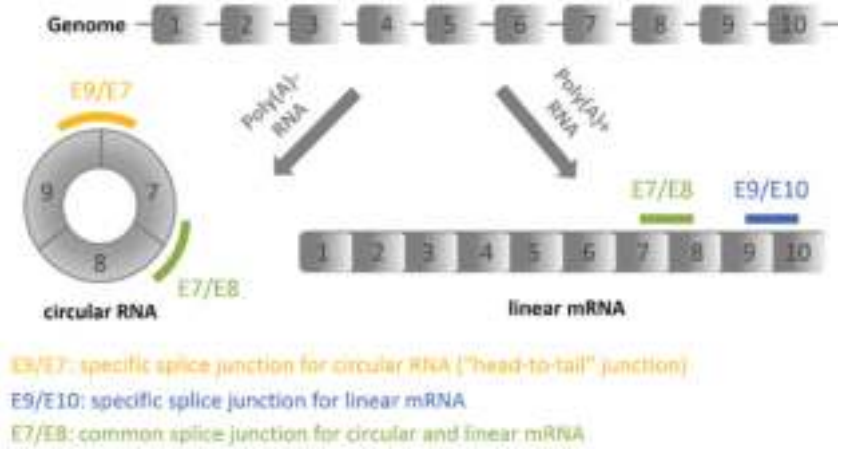

FIGURE 56. BaseScope probe design for *Dlgap1* circular RNA, linear RNA and total RNA detection.

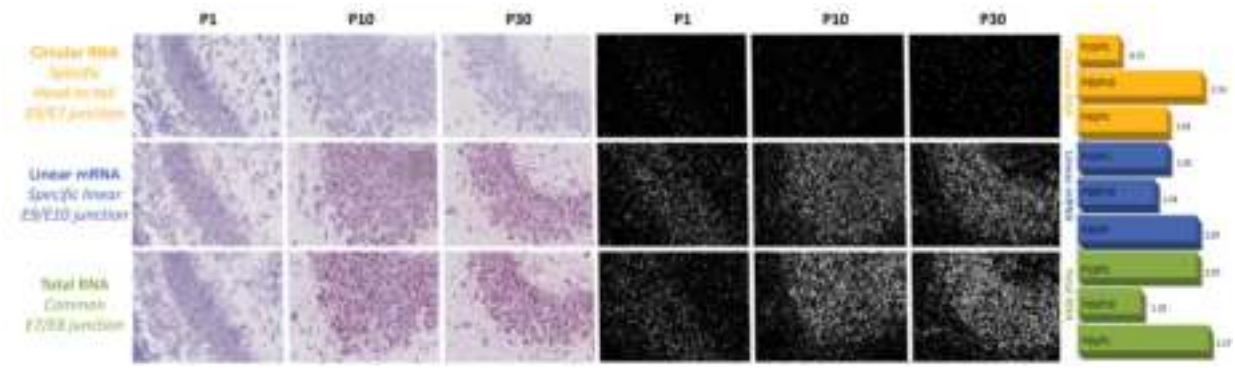

FIGURE 57. Highly sensitive and specific *in situ* detection and quantification of circular RNA, linear mRNA and total RNA for *Dlgap1* in C57Bl/6J developing mouse brain with a focus on the hippocampal CA3 region using the BaseScope assay.

Related publications

Below is an example of a recent peer-reviewed publication illustrating how researchers have taken advantage of the BaseScope assay to visualize and characterize circRNAs in the brain.

Annotation and functional clustering of circRNA expression in rhesus macaque brain during aging[41]

Reported by Xu et al., Cell Discovery, 2019

The expression profile of circRNAs and specific regulatory mechanisms by which they contribute to brain aging in primates is not known. Xu *et al.* show that expression of circRNAs in rhesus macaque brains changes with aging based on spatiotemporal, age and sex-related factors. The BaseScope assay was used to analyze two age-related and calcium channel gene derived circular RNAs: *circCACNA2D1* and *circCACNA1E* (Figure 58). These data validated Northern blot data showing increased expression of both circRNAs with aging and allowed to show spatial expression and nuclear enrichment in different regions of the brain.

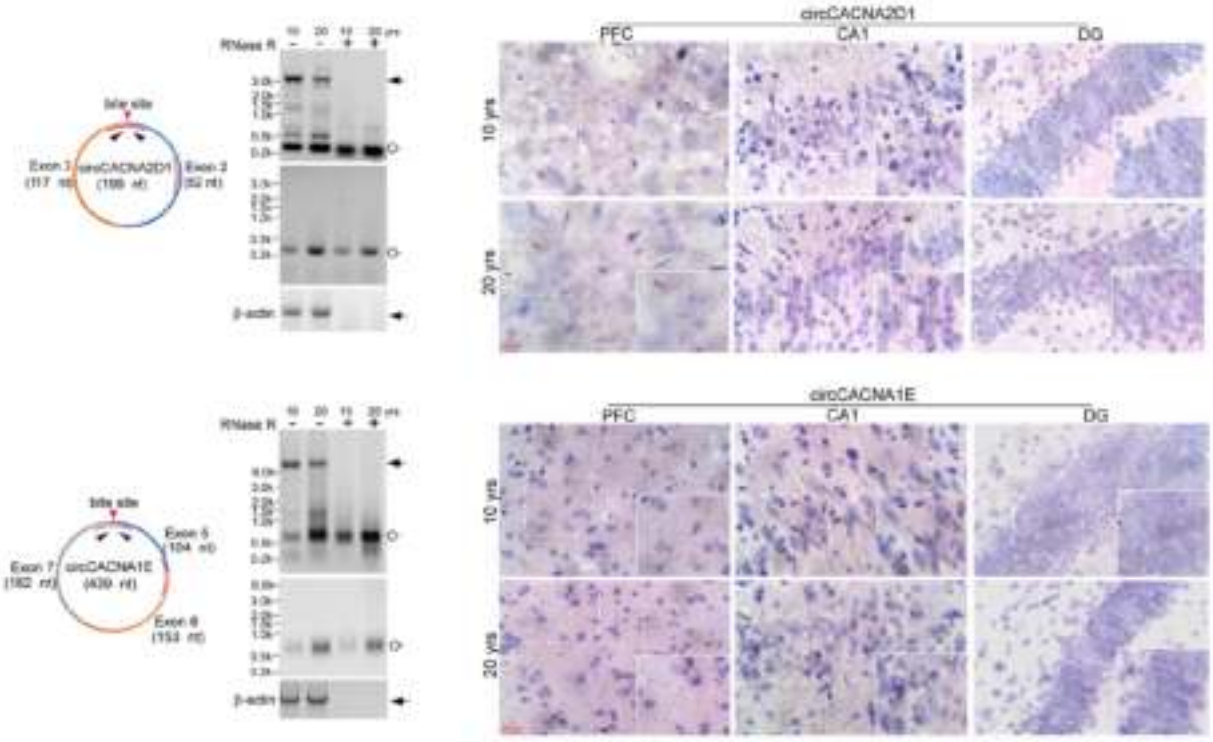

FIGURE 58. *circCACNA2D1* and *circCACNA1E* expression negatively correlated with host mRNA production over the aging states. Left: Representative northern blots of *CACNA2D1* and *CACNA1E* linear and circular transcripts. Total RNAs were extracted from 10 years and 20 years macaque frozen CA1 tissues. Right: Detection of *circCACNA2D1* and *circCACNA1E* using the BaseScope assay and with specific 1zz junction site-targeting probes against *circCACNA2D1* and *circCACNA1E*, respectively (red dots with nuclei counterstaining by Haematoxylin). White squares represent high magnificent images. Images from Xu *et al., Cell Discovery*, 2019.

Get the Most Out of Your RNAscope Experiments

Getting Started with the RNAscope Assay

Before you begin, download the appropriate user manual based on the selection guide table found at acdbio.com/go

Download RNAscope Reference Guide:
acdbio.com/referenceguide

Watch webinars:
acdbio.com/technical-support/learn-more/recorded-webinars

1

Check that all required materials are available
Download the RNAscope Manual Assay Pre-Run Checklist by following this link: acdbio.com/go

2

Always use control probes and slides
Run the RNAscope assay with the control slides to validate the assay workflow and use control probes on your tissue sample to validate the quality of RNA in your samples. The housekeeping gene PPIB (Cyclophilin B), is commonly used as a positive control. The negative control probes target the bacteria dapB gene.

3

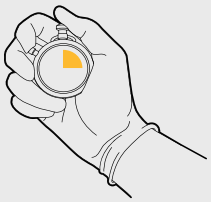

Optimize RNAscope assay conditions for your tissues to obtain optimal data
Target Retrieval and Protease conditions might require optimization depending on tissue samples type. Further optimization might be required if samples are not prepared according to ACD's recommendations: for FFPE samples, for 16-32 hours at room temperature in fresh 10% neutral buffered formalin (NBF) or 4% paraformaldehyde (PFA).

FIGURE 59. Recommended steps to get started with the RNAscope and BaseScope assays.

Pre-run checklist: Check that all required materials are available

Before running your assay, check to ensure that your materials are complete. Select and download the checklist that corresponds to your tissue and assay type. Please read the recommended guidelines to ensure great results.

Tissue and sample preparation essentials

Sample preparation is critical for successful staining of tissue with RNAscope ISH methodology. RNAscope manual assay can be used with FFPE (formalin-fixed, paraffin-embedded) tissue, cultured cells, fresh-frozen & or fixed-frozen tissues, or whole mount samples.

FFPE tissue specimens should be blocked into a thickness of 3–4 mm and fixed for 24 +/- 8 hours in 10% neutral-buffered formalin at room temperature. The fixed tissues should then be dehydrated in a graded series of ethanol and xylene, followed by infiltration by melted paraffin held at no more than 60°C. Specimens should be analyzed within 3 months of sectioning when stored at room in desiccant temperature (20–25 °C). Slides need to be air dried and baked at 60°C for 1–2 hours prior to the RNAscope Assay. FFPE tissue sections should be cut into sections of 5 +/– 1 µm.

Fixed frozen tissue samples should be blocked into a thickness of 3–4 mm and fixed for 24 +/- 8 hours in 10% neutral-buffered formalin or 4% paraformaldehyde at 4°C after intracardial perfusion (optional). The fixed tissues should then be embedded in OCT (Optimal Cutting Temperature) compound and stored at –80°C. Specimens should be analyzed within 3 months of preparation and sectioning when stored at –80°C. Tissue thickness for fixed frozen tissue should be between 7–15 µm.

For free-floating sections, we recommend cutting sections between 30–40 µm, store them at 4°C and use them within 2 days after cutting for optimal results.

Fresh frozen tissue samples should be blocked into a thickness of 3–4 mm and harvested within 5 minutes of sacrifice. The fresh tissues should be embedded as quickly as possible in OCT compound and stored at –80°C. Specimens should be analyzed within 3 months of preparation and sectioning when stored at –80°C. Tissue thickness for fixed frozen tissue should be between 10–20 µm.

Use Fisher Scientific SuperFrost Plus™ Slides for all tissue types to avoid tissue loss.

Whole mount tissue samples should be fixed for 17–24 hours in 10% neutral-buffered formalin or 4% paraformaldehyde at room temperature. The fixed tissues should then be dehydrated in a graded series of methanol and can be stored in 100% methanol for up to two months.

Validate the workflow and the quality of your samples using controls

We recommend you run RNAscope assay with the control slides to validate the assay workflow and test the quality of your samples and the RNA integrity using the ACD control probes. Using control slides will test assay conditions, while using control probes will test the quality of the RNA in your samples. The housekeeping gene PPIB (Cyclophilin B), often used as a reference gene for RT-PCR, can be used as a positive control. The bacterial dapB gene is used as a negative control.

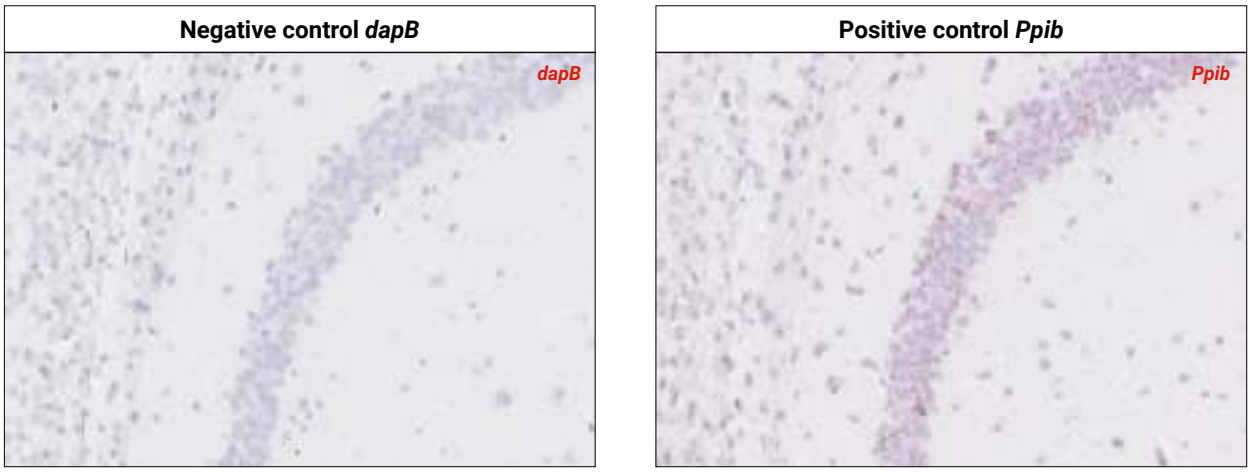

FIGURE 60. Validation of tissue samples using the negative control probe dapB and the positive control Ppib in FFPE mouse brain tissue samples using the RNAscope 2.5 HD Chromogenic Red assay.

Optimizing Your RNAscope Assay

Target retrieval conditions often require optimization and depend on the tissue type and the fixation and handling of the samples. RNAscope Target Retrieval conditions may also need optimization, particularly if tissue samples were not prepared according to our recommended protocols. Always start with the pretreatment guideline recommendations as documented in the RNAscope assay user manual. In situations where information on how the tissue was prepared is not available or if tissues were prepared differently than our recommendations, simple optimization steps can help you obtain excellent results with RNAscope assay (Figure 61).

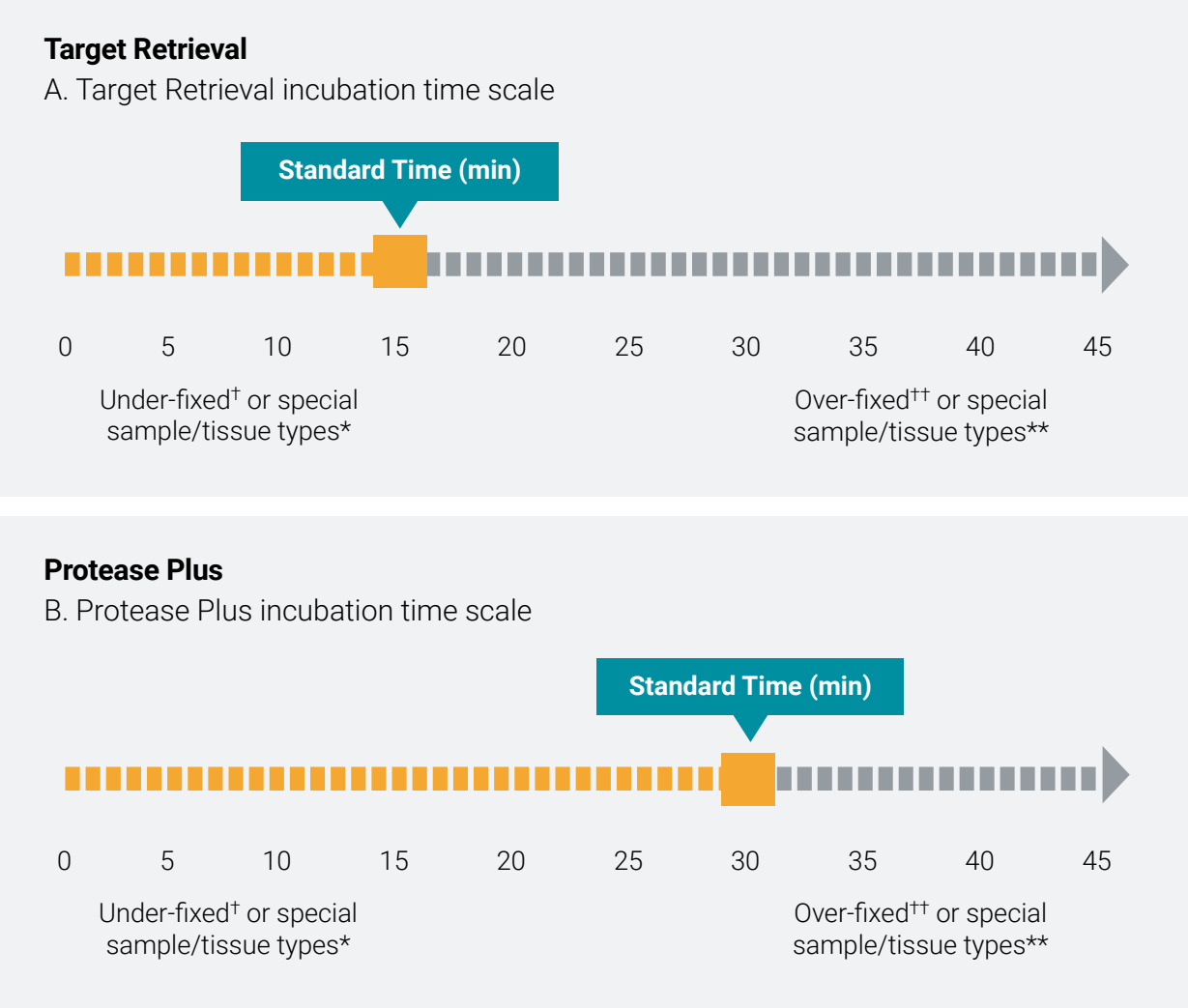

FIGURE 61. Recommendations for RNAscope and BaseScope assays optimization for FFPE samples. For fixed/fresh frozen tissues you may need to vary the protease step.

Troubleshooting Your RNAscope Results

Altered cell morphology and unexpected staining patterns

Unexpected staining patterns are commonly due to suboptimal digestion conditions. Over-fixed or under-digested tissue will have excellent tissue morphology with weak/no signal and low signal/background ratio due to poor probe accessibility to RNA. Under-fixed or over-digested tissue will have poor tissue morphology (tissue appears faded with loss of cell borders) and loss of RNA due to protease over-digestion. Use below examples of unexpected staining patterns to determine if your sample is under- or over-digested (Figure 62).

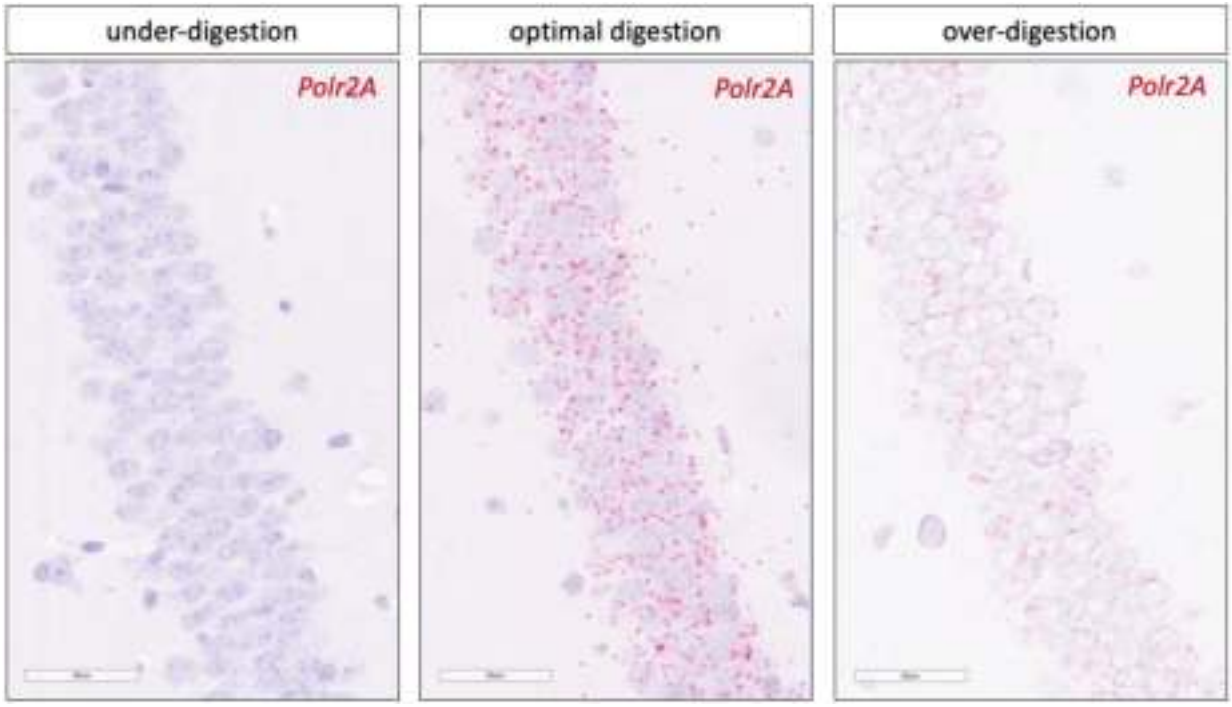

FIGURE 62. Detection of mouse *Polr2a* in FFPE mouse brain tissue samples using the RNAscope 2.5 HD Chromogenic Red assay with different pretreatment conditions.

Unspecific background

It is important to use the ACD EZ-Batch™ Slide Processing System for optimal washing efficiency and stringency.

This accessory facilitates processing of multiple sample slides simultaneously. We designed this product for higher efficiency in running the manual RNAscope assay protocol. The system comprises RNAscope EZ-Batch Slide Holder and EZ-Batch Wash Tray.

The ACD EZ-Batch Slide Holder is designed with an easy locking mechanism to keep slides intact during washing steps. This design eliminates the time-consuming transfer of slides between the slide rack and ensure optimal washing efficiency. When using the EZ-Batch System, use at least 300 mL of RNAscope Wash buffer.

If you still observe unspecific signal with the RNAscope negative control probe(s), you can improve your results by increasing washing steps to 3 times 5 minutes after RNAscope probes and amplifiers incubations.

Watch the video on how to use the EZ-Batch system:
acdbio.com/ez-batch-system

FIGURE 63. ACD EZ-Batch Slide Processing System with the EZ-Batch Slide Holder and the EZ-Batch Wash Tray.

Tissue detachment

Various samples undergo detachment during preparation for the RNAscope assay. Based on the sample type certain steps can be implemented. The following figures illustrate the steps to be adjusted.

FFPE Samples

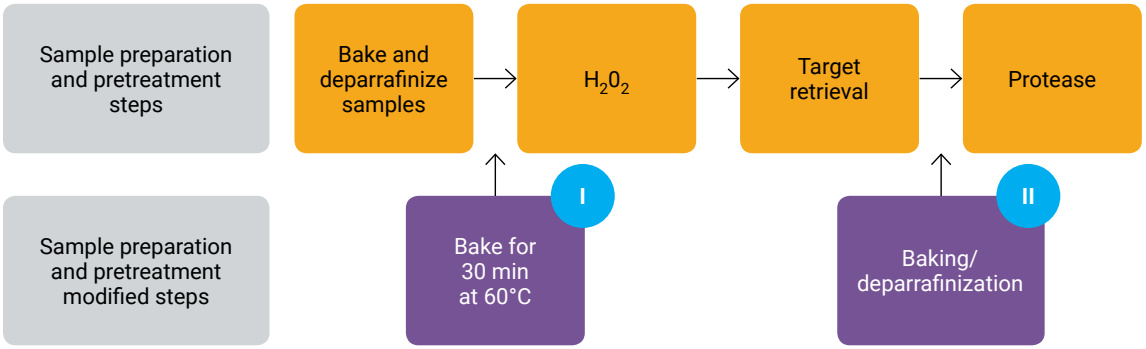

FIGURE 64. FFPE samples. Additional backing steps are added to the sample's preparation workflow. For sample detachment after baking/deparaffinization step or after target retrieval step, a baking step is added for 30 minutes at 60°C (I) or (II), respectively.

Fixed Frozen Samples

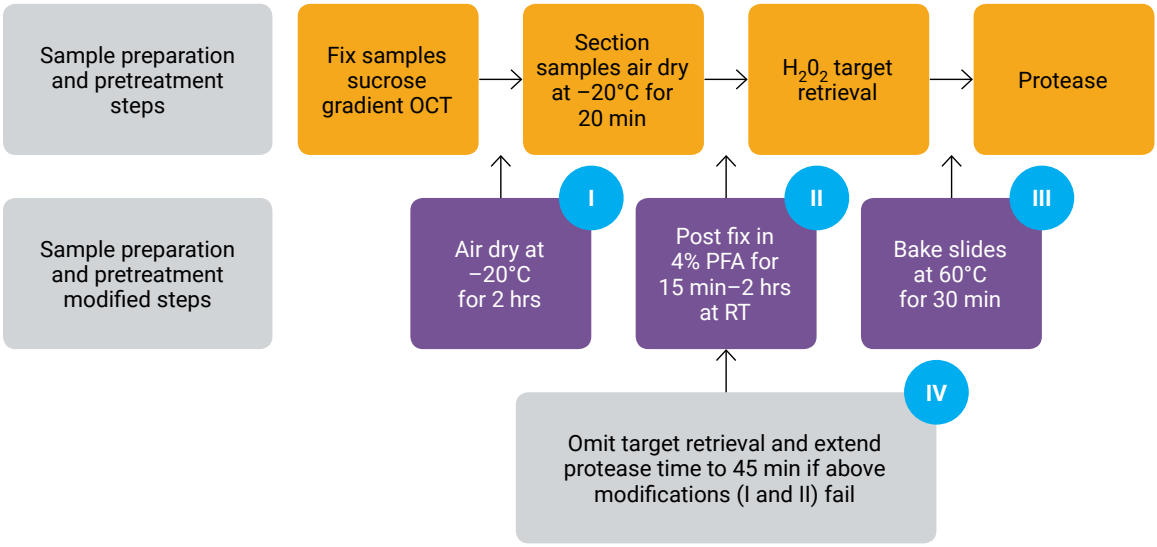

FIGURE 65. Fixed frozen samples. An extended air-drying step is added to the sample preparation protocol at the air dying step (I) to prevent sample detachment. For sample detachment before H_2O_2 step or protease digestion step, a post-fixation protocol is added; 4% PFA for 15 minutes to 2 hours (II) or a baking step at 60°C for 30 minutes (III). Omit Target Retrieval and extend protease time to 45 min if the above modifications fail (IV).

Tips for troubleshooting tissue detachment in fixed frozen samples:

- Recommended section thickness 7–15 µm
- Always use Superfrost Plus™ Slides
- Bake/dry slides in active air circulating oven
- Maintain mild boiling of Target Retrieval at ~100°C

Fresh Frozen Samples

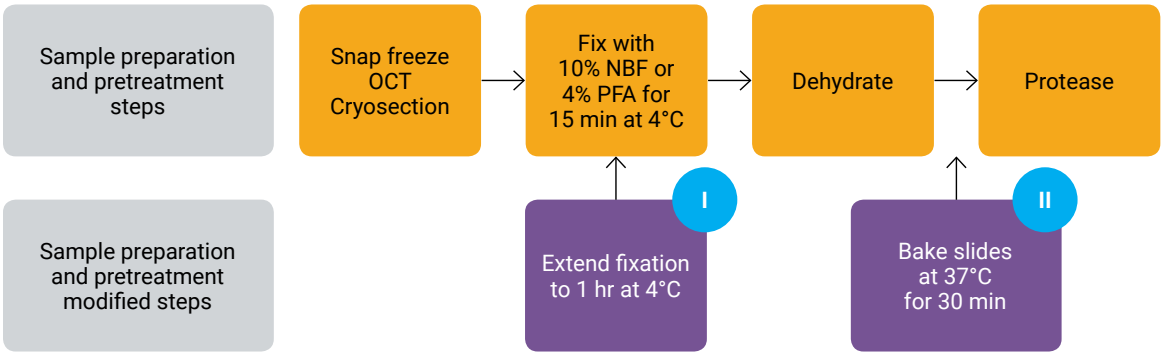

FIGURE 66. Fresh frozen samples. An extended fixation step is added to the sample preparation protocol to prevent sample detachment during fixation (I). For sample detachment after dehydration step and before the protease digestion step, slides are baked at 37°C for 30 minutes (II).

Tips for troubleshooting tissue detachment in fresh frozen samples:

- Recommended section thickness 10–20 µm
- Always use Superfrost Plus™ Slides
- Bake/dry slides in active air circulating oven

For more troubleshooting tricks, visit:
acdbio.com/technical-support/solutions

Watch webinars:
acdbio.com/technical-support/learn-more/recorded-webinars

Autofluorescence

Autofluorescence is most severe in shorter visible fluorescence wavelengths (FITC) and is less visible in red (Cy3), far-red (Cy5), and near-infrared (Cy7).

Tissue samples preparation methods have an influence on the level of autofluorescent background. FFPE tissue samples will present higher autofluorescent background due to the accumulation of fixatives in the samples during the long fixation time and the embedding.

Additionally, different tissue samples will also have different inherent levels of autofluorescence, for example, aged tissues present high accumulation of lipofuscin granules that are highly autofluorescent.

In order to fix autofluorescence issues when running the RNAscope Multiplex Fluorescent or RNAscope HiPlex assays, we recommend following the guidelines below:

- The Multiplex Fluorescent v2 assay will be the optimal assay to use with highly autofluorescent samples due the additional signal amplification step with the horseradish peroxidase (HRP) and the Opal™ dyes.
- Check an unstained slide with short wavelength (10–498 nm).
    - If you see fluorescence, it is likely autofluorescence: choose a fluorescent dye that differs from the autofluorescent background and use a narrow band filter when taking images.
    - If you do not see fluorescence, it is likely unspecific background and you will need to optimize the assay conditions (see section Unspecific Background).

- Increase the fluorescent dye concentrationThe RNAscope Multiplex Fluorescent v2 assays protocol recommends testing 1:1500 dilution of Opal dye for testing. Increasing the Opal dye concentration will increase the signal/noise ratio and the signal will stand out from the autofluorescent background.

Postmortem tissue samples

Postmortem tissue samples are challenging to work with due to the compromised RNA integrity in these samples.

A few parameters need to be taken into consideration when working with postmortem samples:

- **Collection delay:** optimal RNA integrity will be when samples are collected less than 12 hours after death (the shorter the delay is, the better the RNA integrity will be). After 12 hours, RNA integrity will decline, and tissue samples collected after 24 hours will be challenging to work with (with both the RNAscope and BaseScope assays)
- **Fixation time:** post-mortem tissue samples tend to be overfixed. Obviously the ACD recommendations for FFPE tissue samples between 16–32 hours in 10% NBF at room temperature are optimal, but signal can be retrieved from samples fixed for longer period of time, but with with decreased sensitivity.
- **Cohort study:** heterogenous cohort (regarding the collection delay and fixation times and conditions) will be more challenging to work with.
- **Age of the patients and disease study:** tissue samples from older patients and neurodegenerative diseases will have high lipofuscin contents, making RNAscope Multiplex Fluorescent assays challenging.
- **Expression of the target of interest:** both the RNAscope and BaseScope assays will be more successful with medium to high expressed targets

Interpretation of RNAscope Staining

The RNAscope Assay uses a semi-quantitative scoring guideline to evaluate the staining results. When interpreting RNAscope staining we recommend scoring the number of dots per cell rather than the signal intensity. The number of dots correlates to the number of RNA copy numbers, whereas dot intensity reflects the number of probe pairs bound to each molecule. Compare the expression of your target gene with both negative (dapB) and positive controls (PPIB, UBC, or POLR2A). Successful staining should have a PPIB/POLR2A score ≥2 or UBC score ≥3 and a dapB score <1.

Below is an overview of the different methodologies that can be used to quantify the RNAscope signal:

Methodology #1

Semi-quantitative histological assessment of the target expression level within a cell population or area of interest using the ACD scoring criteria.

Score	Criteria
0	No staining or <1 dot/ 10 cells*
1	1–3 dots/cell
2	4–9 dots/cell. None or very few dot clusters
3	10–15 dots/cell and <10% dots are in clusters
4	>15 dots/cell and >10% dots are in clusters

Methodology #2

Quantitative image-based assessment of the target expression level within a cell population or area of interest using quantitative digital image analysis software.

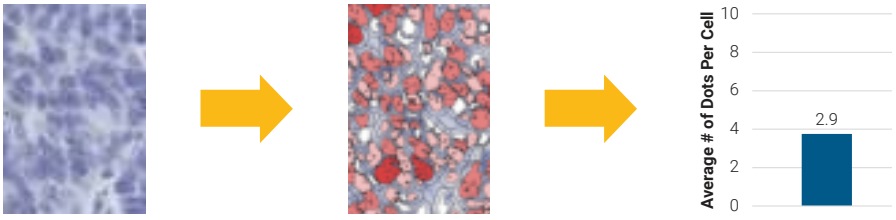

Methodology #3

H score: semi-quantitative or quantitative image-based software analysis to visualize the dynamic expression level by binning the percentage of cells with a certain expression level or number of dots in one bin. The number of bins ranges from 0–4 according to the ACD scoring system. The overall H score can range from 0–400 and is calculated as shown:

$$\text{H-score} = \sum_{\text{Bin } 0 \rightarrow 4} (\text{ACD score or bin number} \times \text{percentage of cells per bin})$$

	% of Cells	Weighted Formula
Bin 0 (0 Dots/Cell)	8	0 * 8
Bin 1 (1–3 Dots/Cell)	46	+ 1 * 46
Bin 2 (4–9 Dots/Cell)	39	+ 2 * 39
Bin 3 (10–15 Dots/Cell)	5	+ 3 * 5
Bin 4 (>15 Dots/Cell)	2	+ 4 * 2
H-Score		**147**

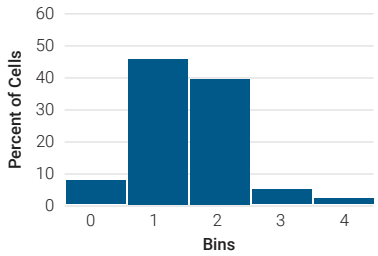

Download RNAscope Data Analysis Guide:
acdbio.com/dataanalysisguide

Watch webinars:
acdbio.com/technical-support/learn-more/recorded-webinars

Support

If you still have questions or need help, please contact the ACD Support team:

US and APAC:
support.ACD@bio-techne.com

EMEA:
info.emea@bio-techne.com

Conclusion

The nervous system consists of numerous specialized cell types that remain to be fully characterized at the molecular level. Due to the high degree of structural and functional heterogeneity and the intricate spatial organization of these cells, it is of utmost importance to analyze gene expression within the morphological and spatial tissue context and at single cell resolution. With its signal amplification and simultaneous background noise suppression the RNAscope technology advances transcriptomic analyses by enabling highly sensitive and specific spatial mapping of gene expression in tissues of the nervous system at the single cell level.

Benefits of the RNAscope Technology

- **High sensitivity:** The serial signal amplification design increases sensitivity such that a single RNA molecule can be detected.
- **High specificity:** Proprietary probe design ensures target-specific binding while the double Z probe design prevents signal amplification of non-specific hybridization.
- **Morphological context:** Spatial resolution of gene expression in the complex tissue environment allows spatial mapping.
- **Single-cell resolution:** High sensitivity combined with morphological context results in single-molecule detection at single-cell resolution and allows for quantification.
- **Universal:** Works for virtually ANY gene from ANY species in ANY tissue.
- **Multiplexing:** Ability to detect up to 12 targets simultaneously in the tissue enables thorough characterization of cell populations.

Download the RNAscope probe list:
acdbio.com/catalog-probes

References

1 Wang, F.F., J.; Su, N.; Wang, L. C.; Bui, S.; Nielson, A.; Wu, X.; Vo, H. T.; Ma, X. J.; Luo, Y. RNAscope: a novel *in situ* RNA analysis platform for formalin-fixed, paraffin-embedded tissues. *The Journal of Molecular Diagnostics* **14**, 22–29 (2012).

2 Carstens, K.E.P., M. L.; Pozzo-Miller, L.; Weinberg, R. J.; Dudek, S. M. Perineuronal Nets Suppress Plasticity of Excitatory Synapses on CA2 Pyramidal Neurons. *The Journal of Neuroscience: The Official Journal of the Society for Neuroscience* **36**, 6312–6320 (2016).

3 Hackett, T.A.C., A. R.; Takahata, T.; Hackett, N. J.; Polley, D. B. Differential maturation of vesicular glutamate and GABA transporter expression in the mouse auditory forebrain during the first weeks of hearing. *Brain Structure & Function* **221**, 2619–2673 (2016).

4 Nectow, A.R.S., Marc; Zhang, Hongxing; Field, Bianca C.; Renier, Nicolas; Azevedo, Estefania; Patel, Bindiben; Liang, Yupu; Mitra, Siddhartha; Tessier-Lavigne, Marc; Han, Ming-Hu; Friedman, Jeffrey M. Identification of a Brainstem Circuit Controlling Feeding. *Cell* **170**, 429–442.e411 (2017).

5 Ruud, J., *et al.* The Fat Mass and Obesity-Associated Protein (FTO) Regulates Locomotor Responses to Novelty via D2R Medium Spiny Neurons. *Cell Reports* **27**, 3182–3198.e3189 (2019).

6 Vanlandewijck, M.H., L.; Mae, M. A.; Andrae, J.; Ando, K.; Del Gaudio, F.; Nahar, K.; Lebouvier, T.; Lavina, B.; Gouveia, L.; Sun, Y.; Raschperger, E.; Rasanen, M.; Zarb, Y.; Mochizuki, N.; Keller, A.; Lendahl, U.; Betsholtz, C. A Molecular Atlas of Cell Types and Zonation in the Brain Vasculature. *Nature* (2018).

7 Stempel, A.J.M., C. W.; Stout, J. T.; Appukuttan, B. Simultaneous visualization and cell-specific confirmation of RNA and protein in the mouse retina. *Molecular Vision* **20**, 1366–1373 (2014).

8 Liou, G.Y.B., L.; Fleming, A.; Doppler, H.; Edenfield, B. H.; Dawson, D. W.; Zhang, L.; Bardeesy, N.; Storz, P. The Presence of Interleukin-13 at Pancreatic ADM/PanIN Lesions Alters Macrophage Populations and Mediates Pancreatic Tumorigenesis. *Cell Reports* **19**, 1322–1333 (2017).

9 Jäkel, S., *et al.* Altered human oligodendrocyte heterogeneity in multiple sclerosis. *Nature* (2019).

10 Petitpré, C.W., Haohao; Sharma, Anil; Tokarska, Anna; Fontanet, Paula; Wang, Yiqiao; Helmbacher, Françoise; Yackle, Kevin; Silberberg, Gilad; Hadjab, Saida; Lallemend, François. Neuronal heterogeneity and stereotyped connectivity in the auditory afferent system. *Nature Communications* **9**, 3691 (2018).

11 Albisetti, G.W., *et al.* Dorsal Horn Gastrin-Releasing Peptide Expressing Neurons Transmit Spinal Itch But Not Pain Signals. *The Journal of Neuroscience : the Official Journal of the Society for Neuroscience* (2019).

12 Holly, E.N., *et al.* Striatal Low-Threshold Spiking Interneurons Regulate Goal-Directed Learning. *Neuron* (2019).

13 Davies, A.J., *et al.* Natural Killer Cells Degenerate Intact Sensory Afferents following Nerve Injury. *Cell* (2019).

14 Fe Lanfranco, M.L., D. J.; Mocchetti, I.; Burns, M. P.; Villapol, S. Combination of Fluorescent *in situ* Hybridization (FISH) and Immunofluorescence Imaging for Detection of Cytokine Expression in Microglia/Macrophage Cells. *Bio-protocol* **7**(2017).

15 Zhang, M., Wang, Y., Geng, J., Zhou, S. & Xiao, B. Mechanically Activated Piezo Channels Mediate Touch and Suppress Acute Mechanical Pain Response in Mice. *Cell Reports* **26**, 1419–1431.e1414 (2019).

16 Rotem, N.M., I.; Ionescu, A.; Gershoni-Emek, N.; Altman, T.; Costa, C. J.; Gradus, T.; Pasmanik-Chor, M.; Willis, D. E.; Ben-Dov, I. Z.; Hornstein, E.; Perlson, E. ALS Along the Axons — Expression of Coding and Noncoding RNA Differs in Axons of ALS models. *Scientific Reports* **7**, 44500 (2017).

17 Boulay, A.-C.S., Bruno; Adam, Nicolas; Chasseigneaux, Stéphanie; Mazaré, Noémie; Gilbert, Alice; Bahin, Mathieu; Bastianelli, Leïla; Blugeon, Corinne; Perrin, Sandrine; Pouch, Juliette; Ducos, Bertrand; Le Crom, Stéphane; Genovesio, Auguste; Chrétien, Fabrice; Declèves, Xavier; Laplanche, Jean-Louis; Cohen-Salmon, Martine. Translation in astrocyte distal processes sets molecular heterogeneity at the gliovascular interface. *Cell Discovery* **3**, 17005 (2017).

18 Poulopoulos, A., *et al.* Subcellular transcriptomes and proteomes of developing axon projections in the cerebral cortex. *Nature* (2019).

19 Geraghty, A.C., *et al.* Loss of Adaptive Myelination Contributes to Methotrexate Chemotherapy-Related Cognitive Impairment. *Neuron* (2019).

20 Mishra, D., *et al.* Parabrachial Interleukin-6 Reduces Body Weight and Food Intake and Increases Thermogenesis to Regulate Energy Metabolism. *Cell Reports* **26**, 3011–3026.e3015 (2019).

21 Lake, B.B.A., R.; Kaeser, G. E.; Salathia, N. S.; Yung, Y. C.; Liu, R.; Wildberg, A.; Gao, D.; Fung, H. L.; Chen, S.; Vijayaraghavan, R.; Wong, J.; Chen, A.; Sheng, X.; Kaper, F.; Shen, R.; Ronaghi, M.; Fan, J. B.; Wang, W.; Chun, J.; Zhang, K. Neuronal subtypes and diversity revealed by single-nucleus RNA sequencing of the human brain. *Science* **352**, 1586–1590 (2016).

22 Elkjaer, M.L., *et al.* Unique RNA signature of different lesion types in the brain white matter in progressive multiple sclerosis. *Acta Neuropathologica Communications* **7**, 58 (2019).

23 Selvaraj, B.T.L., M. R.; Zhao, C.; Gregory, J. M.; James, O. T.; Cleary, E. M.; Chouhan, A. K.; Gane, A. B.; Perkins, E. M.; Dando, O.; Lillico, S. G.; Lee, Y. B.; Nishimura, A. L.; Poreci, U.; Thankamony, S.; Pray, M.; Vasistha, N. A.; Magnani, D.; Borooah, S.; Burr, K.; Story, D.; McCampbell, A.; Shaw, C. E.; Kind, P. C.; Aitman, T. J.; Whitelaw, C. B. A.; Wilmut, I.; Smith, C.; Miles, G. B.; Hardingham, G. E.; Wyllie, D. J. A.; Chandran, S. C9ORF72 repeat expansion causes vulnerability of motor neurons to Ca(2+)-permeable AMPA receptor-mediated excitotoxicity. *Nature Communications* **9**, 347 (2018).

24 Alejevski, F., *et al.* The *HisCl1* histamine receptor acts in photoreceptors to synchronize Drosophila behavioral rhythms with light-dark cycles. *Nature Communications* **10**, 252 (2019).

25 Hutchings, C.J., Koglin, M. & Marshall, F.H. Therapeutic antibodies directed at G protein-coupled receptors. *MAbs 2*, 594–606 (2010).

26 Meirsman, A.C.R., A.; de Kerchove d'Exaerde, A.; Kieffer, B. L. GPR88 in A2AR Neurons Enhances Anxiety-Like Behaviors. *eNeuro* 3(2016).

27 Wang, L., *et al*. GPR139 and Dopamine D2 Receptor Co-express in the Same Cells of the Brain and May Functionally Interact. *Frontiers in Neuroscience* 13 (2019).

28 Liu, S.S., *et al.* Kappa Opioid Receptors Drive a Tonic Aversive Component of Chronic Pain. *The Journal of Neuroscience: The Official Journal of the Society for Neuroscience* (2019).

29 Branco, T.T., A.; Magnus, C. J.; Sugino, K.; Tanaka, S.; Lee, A. K.; Wood, J. N.; Sternson, S. M. Near-Perfect Synaptic Integration by Nav1.7 in Hypothalamic Neurons Regulates Body Weight. *Cell* 165, 1749–1761 (2016).

30 Smith, R.S.K., Connor J.; Ganesh, Vijay; Jang, Ahram; Borges-Monroy, Rebeca; Partlow, Jennifer N.; Hill, R. Sean; Shin, Taehwan; Chen, Allen Y.; Doan, Ryan N.; Anttonen, Anna-Kaisa; Ignatius, Jaakko; Medne, Livija; Bönnemann, Carsten G.; Hecht, Jonathan L.; Salonen, Oili; Barkovich, A. James; Poduri, Annapurna; Wilke, Martina; de Wit, Marie Claire Y.; Mancini, Grazia M. S.; Sztriha, Laszlo; Im, Kiho; Amrom, Dina; Andermann, Eva; Paetau, Ritva; Lehesjoki, Anna-Elina; Walsh, Christopher A.; Lehtinen, Maria K. Sodium Channel *SCN3A* ($Na_V1.3$) Regulation of Human Cerebral Cortical Folding and Oral Motor Development. *Neuron* (2018).

31 Ramos, A.D.A., R. E.; Liu, S. J.; Nowakowski, T. J.; Hong, S. J.; Gertz, C. C.; Salinas, R. D.; Zarabi, H.; Kriegstein, A. R.; Lim, D. A. The long noncoding RNA Pnky regulates neuronal differentiation of embryonic and postnatal neural stem cells. *Cell Stem Cell* **16**, 439–447 (2015).

32 An, H., *et al.* ALS-linked FUS mutations confer loss and gain of function in the nucleus by promoting excessive formation of dysfunctional paraspeckles. *Acta Neuropathologica Communications* **7**, 7 (2019).

33 Khalaf, O.R., S.; Dixsaut, L.; Gorden, V.; Glauser, L.; Graff, J. Reactivation of recall-induced neurons contributes to remote fear memory attenuation. *Science* **360**, 1239–1242 (2018).

34 Sathyamurthy, A.J., K. R.; Matson, K. J. E.; Dobrott, C. I.; Li, L.; Ryba, A. R.; Bergman, T. B.; Kelly, M. C.; Kelley, M. W.; Levine, A. J. Massively Parallel Single Nucleus Transcriptional Profiling Defines Spinal Cord Neurons and Their Activity during Behavior. *Cell Reports* **22**, 2216–2225 (2018).

35 Gokce, O., *et al*. Cellular taxonomy of the mouse striatum as revealed by single-cell RNA-seq. 16, 1126–1137 (2016).

36 Haring, M.Z., A.; Hochgerner, H.; Rinwa, P.; Jakobsson, J. E. T.; Lonnerberg, P.; La Manno, G.; Sharma, N.; Borgius, L.; Kiehn, O.; Lagerstrom, M. C.; Linnarsson, S.; Ernfors, P. Neuronal atlas of the dorsal horn defines its architecture and links sensory input to transcriptional cell types. *Nature neuroscience* (2018).

37 Kalish, B.T.C., L.; Hrvatin, S.; Nagy, M. A.; Rivera, S.; Crow, M.; Gillis, J.; Kirchner, R.; Greenberg, M. E. Single-cell transcriptomics of the developing lateral geniculate nucleus reveals insights into circuit assembly and refinement. *Proceedings of the National Academy of Sciences of the United States of America* (2018).

38 Zeisel, A.H., Hannah; Lönnerberg, Peter; Johnsson, Anna; Memic, Fatima; van der Zwan, Job; Häring, Martin; Braun, Emelie; Borm, Lars E.; La Manno, Gioele; Codeluppi, Simone; Furlan, Alessandro; Lee, Kawai; Skene, Nathan; Harris, Kenneth D.; Hjerling-Leffler, Jens; Arenas, Ernest; Ernfors, Patrik; Marklund, Ulrika; Linnarsson, Sten. Molecular Architecture of the Mouse Nervous System. *Cell* 174, 999–1014.e1022 (2018).

39 Erben, L.H., M. X.; Laeremans, A.; Park, E.; Buonanno, A. A Novel Ultrasensitive *In Situ* Hybridization Approach to Detect Short Sequences and Splice Variants with Cellular Resolution. *Molecular neurobiology* (2017).

40 Fu, Y.H., B.; Weng, C.; Liu, W.; Dai, J.; Zhao, C.; Yin, Z. Q. Functional ectopic neuritogenesis by retinal rod bipolar cells is regulated by miR-125b-5p during retinal remodeling in RCS rats. *Scientific reports* 7, 1011 (2017).

41 Xu, K.C., Dong; Wang, Zhengbo; Ma, Jian; Zhou, Jian; Chen, Nanhui; Lv, Longbao; Zheng, Yongtang; Hu, Xintian; Zhang, Yi; Li, Jiali. Annotation and functional clustering of circRNA expression in rhesus macaque brain during aging. *Cell Discovery* 4, 48 (2018).

Authors: Morgane Rouault, PhD and Courtney Anderson, PhD.

Acknowledgments: The authors would like to thank the ACD R&D and Applications teams for their support and contributions specifically, Ming Xu, PhD, Han Lu, PhD, Li-chong Wang, PhD, Anushka Dikshit and Jyoti Phatak for data collection as well as Nidhi Vashistha, PhD and Bingqing Zhang, PhD for proofreading and advices.

Notes

Notes

Notes

a bio-techne brand

California, USA